Characterization and quantification of hydrodynamic exchange processes in a tidal channel (East Frisian Wadden Sea)

Anne-Christin Schulz

Characterization and quantification of hydrodynamic exchange processes in a tidal channel (East Frisian Wadden Sea)

Von der Fakultät für Mathematik und Naturwissenschaften

der Carl von Ossietzky Universität Oldenburg

zur Erlangung des Grades und Titels eines

Doktors der Naturwissenschaften

- Dr. rer. nat. -

angenommene Dissertation von

Anne-Christin Schulz

geboren am 07.07.1983 in Varel.

Erklärung

Hiermit versichere ich, dass ich diese Arbeit selbstständig verfasst und keine anderen als die angegebenen Quellen und Hilfsmittel benutzt habe. Außerdem versichere ich, dass ich die allgemeinen Prinzipien wissenschaftlicher Arbeit und Veröffentlichung, wie sie in den Leitlinien guter wissenschaftlicher Praxis der Carl von Ossietzky Universität Oldenburg festgelegt sind, befolgt habe.

Declaration of authorship

I hereby declare that I wrote this work independently and that I did not use others as the indicated sources and auxiliary means. Additionally, I declare that I have followed the general principles of scientific work and publication, as stated in the guidelines of good scientific practice of Carl von Ossietzky University of Oldenburg.

Bockhorn, 28.02.2018

Abstract

Coastal regions are subject to constant change due to the strong dynamics of tidal currents. The effects of the tides on the amphibious areas in the UNESCO World Heritage Wadden Sea and the resulting transport of sediments are of particular interest. Naturally occurring flows are exclusively turbulent. Therefore, sediment transport is directly related to turbulent mixing in the water column. To investigate vertical and horizontal as well as turbulent exchange processes, it is necessary to obtain a high number of field observations of mixed variables and their interactions with other processes and dynamics.

The objective of this thesis is the characterization and quantification of hydrodynamic exchange processes in one of the inlets between two islands (tidal channel) within the German Wadden Sea area. Particular focus lies on the complex interactions between tidal currents, their turbulence and the sediment transport within the water column and the quantification of the possibility to measure them. The used approaches are based on operational physical oceanography procedures and field measurements. Namely an Acoustic Doppler Current Profiler (ADCP), a Conductivity-Temperature-Depth probe, radiometers and a turbidity sensor were used. Turbidity and water transparency were chosen as useful and easy to measure proxies of sediment content within the water column. Key points of this thesis were (i) the assessment of turbulence patterns via post-processing of pre-existing current velocity data sets, (ii) the investigation of the impact of these measured currents and turbulence on turbidity dynamics, (iii) and the derivation of acoustic and optical methods to infer water transparency.

The results indicated that turbulence could be estimated from non-high resolution data sets of current velocity. Despite some shortcomings, such as the limited applicability for extreme events such as storm surges, the method can provide valuable

insights into general patterns of turbulence under natural and undisturbed conditions. This is particularly helpful when studying turbulence e.g. under environmental conditions where direct measurements of turbulence are not feasible.

Investigations showed furthermore that during slack water the remaining turbulence is sufficiently strong to keep particles within the water column. Although the research area is an ebb dominated system, an opposite behavior of the turbidity and backscatter signals was observed. At times with high current speeds the velocity shear and, therefore, the current velocities are responsible for the turbidity dynamics.

Further, significant correlations between turbidity measured by the submerged turbidity sensor, values derived from above-water radiometer observations and the backscatter signal derived from the acoustic measurements were recognized. These findings suggested that both optical and acoustic measurements are reasonable proxies of water transparency with the potential to mitigate gaps and increase data quality of long-time observations of marine environments. In addition, the results of this thesis showed that bio-fouling decreases the data quality of in-water optical measurements of turbidity within short time periods. Hence, it was important to find an approach to improve the monitoring over time and increase the robustness of the turbidity results. The Forel-Ule index, derived from radiometer measurements, is a powerful tool for exchangeable estimations of water transparency as much as data sets (acoustic backscatter signals) derived from ADCP measurements. Both measurement methods are hardly influenced by bio-fouling, and therefore suitable alternatives to overcome this problem. Finally, the combination of data sets from different measurement principles (optical and acoustic) is an effective tool for monitoring and verification of complex interactions of different environmental parameters and exchange processes.

Zusammenfassung

Küstengebiete sind durch die starke Dynamik der Gezeitenströme ständigen Veränderungen unterworfen. Die Auswirkungen der Gezeiten auf die amphibischen Gebiete im UNESCO Weltnaturerbe Wattenmeer und der dadurch resultierende Transport von Sedimenten sind dabei von besonderem Interesse. Natürlich vorkommende Strömungen sind ausschließlich turbulent. Daher steht der Sedimenttransport in direktem Zusammenhang zu der turbulenten Vermischung innerhalb der Wassersäule. Um die vertikalen, horizontalen, sowie turbulenten Austauschprozesse zu untersuchen, ist es notwendig eine Vielzahl von Messdaten der sich vermischenden Variabeln, sowie zu deren Wechselwirkungen und Dynamiken, zu erheben.

Das Ziel dieser Arbeit ist die Charakterisierung und Quantifizierung von hydrodynamischen Austauschprozessen in einem Seegatt (Gezeitenkanal) im deutschen Wattenmeer. Ein besonderes Augenmerk liegt dabei auf den komplexen Wechselwirkungen zwischen den Gezeitenströmungen, deren Turbulenz und dem Sedimenttransport, sowie auf deren Messung. Die verwendeten Ansätze basieren auf Verfahren der operationellen, physikalischen Ozeanographie. Es wurde ein Acoustic Doppler Current Profiler (ADCP), eine Conductivity-Temperature-Depth Sonde, Radiometer und ein Trübungssensor verwendet. Trübung und Wassertransparenz wurden als nützliche und einfach zu messende Ersatzgrößen für den Sedimentgehalt gewählt. Kernpunkte dieser Arbeit waren (i) die Bewertung von Turbulenzmustern durch Nachbearbeitung von Strömungsgeschwindigkeitsdatensätzen, (ii) die Untersuchung des Einflusses dieser gemessenen Strömungen und Turbulenzen im Bezug auf die Trübungsdynamik, (iii) und die Herleitung von akustischen und optischen Methoden um auf die Wassertransparenz Rückschlüsse ziehen zu können.

Die Ergebnisse zeigten, dass Turbulenz aus nicht hoch aufgelösten Datensätzen von Strömungsgeschwindigkeiten bestimmt werden konnte. Trotz einiger Schwächen, wie

der begrenzten Anwendbarkeit auf Extremereignisse wie Sturmfluten, kann die Methode wertvolle Einblicke in allgemeine Turbulenzmuster liefern. Dies ist besonders hilfreich bei der Untersuchung von Turbulenzen z.B. unter Umweltbedingungen, bei denen keine direkten Turbulenzmessungen möglich sind.

Außerdem ergab die Untersuchung, dass verbleibenden Turbulenzen während der Stauwasserzeiten ausreichend stark sind, um Partikel in der Wassersäule zu halten. Obwohl das Forschungsgebiet ein Ebb-dominiertes System ist, wurde ein entgegengesetztes Verhalten der Trübungs- und Rückstreusignale beobachtet. Bei Strömungsmaxima sind die Scher- und daher die Strömungsgeschwindigkeiten für die Trübungsdynamik verantwortlich. Ferner wurden signifikante Korrelationen zwischen der Trübung, gemessen mittels Trübungssensor und Radiometern, sowie der akustischen Rückstreusignale gefunden. Diese Ergebnisse deuten darauf hin, dass sowohl Daten aus optischen als auch aus akustischen Messungen vernünftige Indikatoren für die Wassertransparenz sind. Diese Daten haben das Potenzial, Lücken zu schließen und die Datenqualität bei Langzeitbeobachtungen zu verbessern. Darüber hinaus zeigen die Ergebnisse dieser Arbeit, dass Biofouling die Datenqualität von optischen Messungen innerhalb der Wassersäule im Laufe kürzester Zeit verringert. Daher war es wichtig, einen Ansatz zu finden, um die Robustheit der Trübungsergebnisse zu erhöhen. Der Forel-Ule Index (ermittelt aus Radiometerdaten), zusammen mit den akustischen Rückstreusignalen sind leistungsfähige und austauschbare Werkzeug zur Bestimmung der Wassertransparenz. Beide Messmethoden werden kaum durch Biofouling beeinflusst, und daher geeignete Alternativen. Schlußendlich sind daher Kombinationen aus Datensätzen verschiedener Messprinzipien (optisch und akustisch) effektive Werkzeuge zur Überwachung und Verifizierung der komplexen Wechselwirkungen verschiedener Umweltparameter und deren Austauschprozesse.

Contents

CONTENTS

1 Introduction

Turbulence is important for mixing processes in aquatic ecosystems, particularly in shallow water regions with high current velocities such as tidal channels. Here, turbulence may be responsible for most of the exchange and transport processes, such as remobilization of sediments, their transport and dynamics. Therefore, transport and exchange of water masses and contained substances are essential influencing factors of marine ecosystems. In particular, tidal channels are of high relevance because of their morphology. To investigate vertical and horizontal as well as turbulent exchange processes, it is necessary to obtain a high number of field observations of mixed variables and their interactions with other processes and dynamics.

The dynamics of turbulent motion in a fluid can be described by the equation of turbulent kinetic energy. To determine the energy available for turbulent mixing of the water column one needs to know the production rate of turbulent kinetic energy P (see e.g. Hinze (1975) and Rippeth et al. (2002)). Turbulent kinetic energy can also be linked to other processes such as sediment dynamics in coastal seas (e.g. Bowers, 2003; Garaba et al., 2014; Schulz et al., 2015).

The composition and concentration of suspended material is highly variable in coastal and estuarine regions (Winter et al., 2007; Fugate and Friedrichs, 2002). Fragile flocculants change their characteristics over short and over long timescales due to hydrodynamic forces such as currents, turbulence and tides (Vousdoukas et al., 2011; Burchard and Badewien, 2015).

The UNESCO World Heritage Wadden Sea (southern North Sea) is the largest contiguous area of mud and sand flats in the world (UNESCO World Heritage Center, 2009). This ecosystem is under constant change due to the strong dynamics of tidal currents. The effects of tides on the amphibious areas and the resulting transport of sediments are of particular interest. Thus, sediment transport is directly related

to vertical turbulent mixing in the water column. To gather more information on this highly dynamic ecosystem, the Institute for Chemistry and Biology of the Marine Environment (ICBM) is operating a permanent research platform (Time Series Station Spiekeroog) in a tidal inlet of the East Frisian Wadden Sea since 2002.

1.1   Wadden Sea - a tidal inlet system

The UNESCO World Heritage Wadden Sea (southern North Sea) is a typical tidal-inlet / backbarrier-basin system (de Swart and Zimmerman, 2009). This system is characterized by a common pattern of different geomorphologic elements (figure 1.1). An idealized tidal inlet system mainly consists of barrier islands, which separate the coastline from the open ocean (backbarrier-basin). Tidal inlets are located between the barrier islands. Tidal current is the dominant physical process at these tidal inlets (blue arrows in figure 1.1). At the ocean-side of the tidal inlet an ebb tidal delta evolved. Accordingly, a flood delta occurred shore-side of the tidal inlet. This flood delta and other tidal flats are amphibious areas. Amphibious areas are flooded and falling dry during one tidal cycle (intertidal flats). Therefore, backbarrier-basins are traversed by tidal channels and tideways. Morphodynamics within these tidal inlet systems are mostly affected by tidal currents and wind waves. Hence, the magnitude and direction of sediment transport (red arrows in figure 1.1), and with it erosion and deposition are strongly influenced by these physical processes. However, the morphology itself modifies tidal currents and waves and, thereby, sediment transport (de Swart and Zimmerman, 2009). This schematic of a tidal inlet system can even be seen from a satellite picture of the Wadden Sea at every tidal inlet (cf. figure 1.2).

The tidal-inlet / backbarrier-basin system is characterized by complex and highly interdisciplinary natural processes across several time- and length scales. These pro-

cesses can be physical, biogeochemical, ecological or even anthropogenic.

The Wadden Sea as an UNESCO World Heritage Site holds a special protection status. The guiding principle of the trilateral governmental cooperation is to achieve a natural and self-sustaining ecosystem in which natural processes can proceed undisturbed. This requires appropriate measuring approaches.
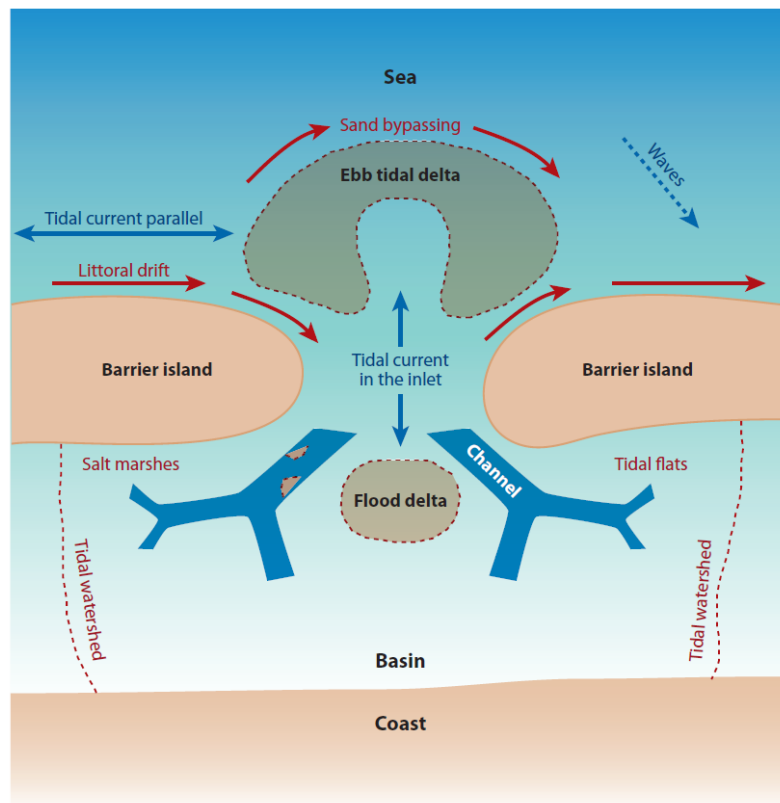

Figure 1.1: Sketch of tidal inlet system showing different geomorphologic elements and dominant physical processes from de Swart and Zimmerman (2009).

Figure 1.2: Satellite picture of the German part of the UNESCO Wadden Sea (Eurimage, 2008).

1.2   Operational oceanography

The role of operational oceanography is the accurate description of the present state of the sea, or in this case the coastal sea, by using advanced technologies of different disciplines.

Since 2002 the ICBM is operating the Time Series Station Spiekeroog (a permanent research platform) in the tidal inlet called Otzumer Balje. It is located between the islands Langeoog and Spiekeroog within the German Wadden Sea area. As part of the COSYNA (Coastal Observing System for Northern and Arctic Seas) project this Time Series Station helps to further improve the understanding of the interdis-

ciplinary interactions between physics, biogeochemistry, and the ecology of coastal seas (Baschek et al., 2017). Especially since the German Bight and, therefore, also the Wadden Sea in the North Sea is a heavily used coastal area. It is a constantly changing environment under strong influence of global change.

Gathering data within a UNESCO Word Heritage Site is a challenging task. Measuring principles were selected, which collect data without jeopardizing the surrounding area. It must also be avoided that the instruments influence one another which could reflect in the measured variables. The instruments of operational, physical and bio-optical oceanography used in this thesis are listed in table 1.1.

Table 1.1: List of used instruments of operational, physical and bio-optical oceanography. Small overview of instrument specifications see table C.1.

Instrument	Measured or estimated variable
Acoustic Doppler Current Profiler, 1200 kHz, Teledyne RD Instruments Workhorse Sentinel.	Current velocity, velocity shear, Reynolds stress, production rate and dissipation of turbulent kinetic energy, acoustic backscatter.
Conductivity-Temperature-Depth-probe, CTD48M, Sea & Sun Technology.	Conductivity, temperature, depth, salinity, density.
Radiometer, TriOS RAMSES-ACC hyperspectral cosine irradiance meter, TriOS RAMSES-ARC hyperspectral radiance meters.	Hyperspectral cosine irradiance, hyperspectral radiance meters, remote sensing reflectance, Forel-Ule color index.
Turbidity sensor, ECO FLNTU sensor, WETlabs.	Turbidity (optical backscattering at a wavelength of 700 nm).

All of these sensors are installed at the Time Series Station Spiekeroog. A continuous recording of various parameters enables insights into the natural processes of the intertidal ecosystem under various environmental conditions such as storm surges or algae blooms. This Time Series Station offers a unique opportunity to study the influence of exchange and mixing processes on sediment transport and water turbidity.

Particularly with regard to future challenges like climate change and related consequences, the development of measuring technologies and the application of methods to uncommon purposes is an ongoing process in operational oceanography. Additionally, the availability of reliable data sets with high resolutions in time and space is crucial. This thesis will contribute to these aims.

1.3 Dissertation objectives and research questions

The aim of this thesis is the characterization and quantification of hydrodynamic exchange processes in one of the inlets between the islands (tidal channel) within the Wadden Sea area. The key points of interest in this dissertation are (i) to develop and deploy in-situ measurements and instrument setup for estimating parameters like current velocity, velocity shear and resulting turbulence and its producing processes, and also to assess turbulence patterns via post-processing of pre-existing data sets, (ii) to investigate the impact of these measured currents and turbulence on turbidity dynamics, (iii) to derive acoustic and optical methods to infer water transparency and to verify interactions of different environmental parameters and exchange processes and quantify the possibility to measure them. Galileo Galilei is credited with having said, "Measure what can be measured, and make measurable what cannot be measured" (Galileo principle - see Cournot (1847); Martin (1868); Dilthey (1894)) .

The following research questions will be answered:

- How can current velocities for long-term turbulence estimations be measured properly?

- How can turbulence or rather the production rate of turbulent kinetic energy be estimated from pre-existing data sets of current velocities via post-processing these data sets?

- How much impact do currents and turbulence have on turbidity dynamics?

- Lead different measuring methods to the same results of e.g. water transparency or sediment content?

- In general, is it possible to measure interactions of different environmental parameters and exchange processes and quantify them?

1.4   List of publications and author's contribution

The cumulative thesis is based upon the following publications and manuscripts:

1. **A.-C. Schulz, T. H. Badewien and O. Zielinski, 2018. Assessment of turbulence patterns from non-high resolution data sets of current velocities. Ocean Dynamics, submitted.**
   I wrote the paper, developed the main concept and performed the data analysis. Oliver Zielinski and Thomas Badewien are both chief scientists on the Time Series Station Spiekeroog. All authors contributed to proofreading and scientific discussions of the manuscript.

2. **A.-C. Schulz, T. H. Badewien, S. P. Garaba and O. Zielinski, 2016. Acoustic and optical methods to infer water transparency at Time**

Series Station Spiekeroog, Wadden Sea. Ocean Sci., 12(6): 1155-1163. DOI: 10.5194/os-12-1155-2016.

I wrote the paper and performed the acoustic data analysis. Shungudzemwoyo Pascal Garaba provided the turbidity sensor and radiometer data (optical data). Oliver Zielinski, Shungudzemwoyo Pascal Garaba and I developed the main concept of this paper. Oliver Zielinski and Thomas Badewien are both chief scientists on the Time Series Station Spiekeroog. All authors contributed to proofreading and scientific discussions of the manuscript.

3. **A.-C. Schulz, T. H. Badewien and O. Zielinski, 2015. Impact of currents and turbulence on turbidity dynamics at the Time Series Station Spiekeroog (Wadden Sea, southern North Sea). 2015 IEEE/OES Eleventh Current, Waves and Turbulence Measurement (CWTM). DOI: 10.1109/CWTM.2015.7098095.**

I wrote the paper and performed the data analysis. Oliver Zielinski and I developed the main concept of this paper. Oliver Zielinski and Thomas Badewien are both chief scientists on the Time Series Station Spiekeroog. All authors contributed to proofreading and scientific discussions of the manuscript.

A list of my publications and conference contributions is attached in appendix A.

1.5 Outline of the thesis

This thesis is structured as follows:
As an experimental study chapter 2 shows different approaches to measure environmental variables which can be used for the estimation of turbulence. These variables are e.g. current velocities or the water density. Measures of turbulent

currents are the production rate P and dissipation rate ε of turbulent kinetic energy. Both production rate P and dissipation rate ε were estimated using current velocity measurements from an Acoustic Doppler Current Profiler. In addition, the dissipation rate ε was also estimated from density data sets which were obtained by a Conductivity-Temperature-Depth probe. Both measurements were conducted aboard the Research Vessel Senckenberg, positioned next to the Time Series Station in an East Frisian tidal channel in the southern North Sea.

Chapter 3 looks at the turbulence producing processes within this tidal channel. In particular the Reynolds Stress τ and the velocity shear S were investigated. The measurement was conducted at the Time Series Station Spiekeroog by using current velocity measurements from a bottom-mounted high-frequency Acoustic Doppler Current Profiler.

Chapter 4 presents a method to assess turbulence patterns from non-high resolution data sets of current velocities (publication 1, Schulz et al. (2018)). This method increases the amount of data sets, which can be used for turbulence investigations based on estimates of current speed and velocity shear.

The thesis will proceed with the research of the complex interactions between tidal currents, the resulting turbulence and the sediment transport within the water column. Chapter 5 starts with the impact of currents and turbulence on turbidity dynamics at the Time Series Station Spiekeroog (publication 3, Schulz et al. (2015)). Data from an optical sensor (turbidity sensor) and an acoustic sensor (Acoustic Doppler Current Profiler) were compared for this analysis.

Further, chapter 6 uses acoustic and optical methods to infer water transparency at the Time Series Station Spiekeroog (publication 2, Schulz et al. (2016)). Additional to data obtained from an Acoustic Doppler Current Profiler data sets from radiometers were used to compare the methods.

Finally, chapter 7 summarizes the findings and perspectives for future work.

2   Estimation of turbulence in an East Frisian tidal channel

2.1   Introduction

Turbulence is important for mixing processes in the ocean. Especially in shallow water regions with high current velocities, e.g. in a tidal channel, vertical mixing is strong. Determination of the available energy for turbulent mixing of the water column requires the turbulent kinetic energy (TKE) equation, with its production rate P and its dissipation rate ε.

In this work, the production rate P and the dissipation rate ε were estimated using current measurements from an Acoustic Doppler Current Profiler (ADCP). In addition, the dissipation rate ε was also estimated from parameters which were obtained by a Conductivity Temperature Depth probe (CTD). Both measurements were conducted aboard the Research Vessel Senckenberg, positioned next to a Time Series Station Spiekeroog in the East Frisian tidal channel (Otzumer Balje) in the southern North Sea (see figure 2.1).

2.2   Methods

The dynamics of turbulent motion in a fluid can be described by the equation of turbulent kinetic energy (Tennekes and Lumley, 1972; Ivey and Imberger, 1990). Together with the Navier-Stokes-Equation and a simplification of Rippeth et al. (2003) (production rate and the dissipation rate of turbulent kinetic energy are the leading factors for this environmental conditions) the equation of turbulent kinetic
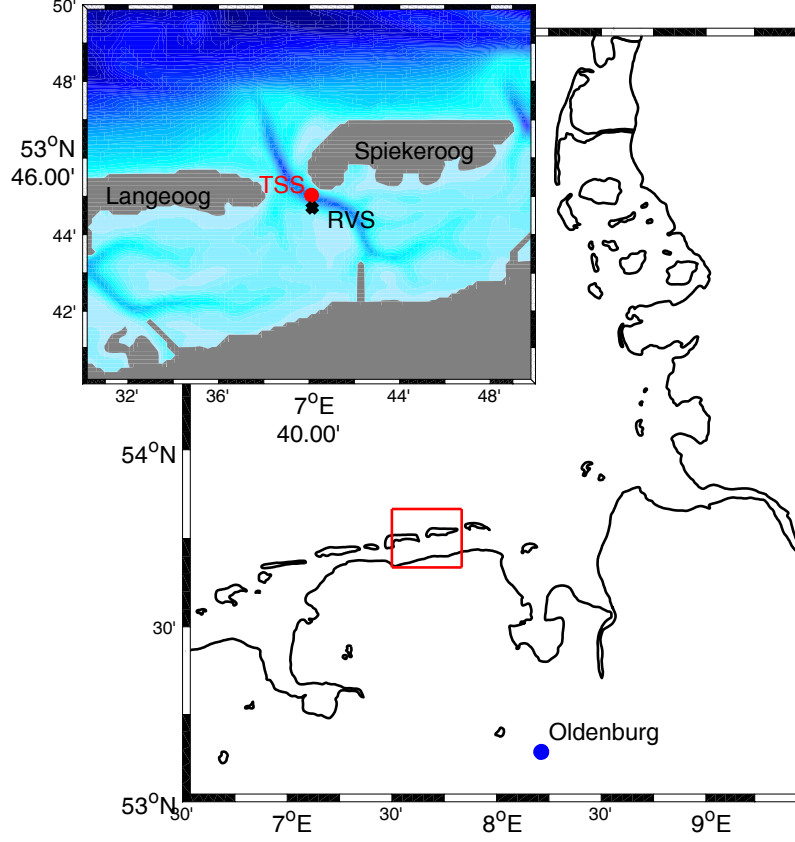
Figure 2.1: Research area in the German Bight; red dot: Time Series Station Spiekeroog (TSS); black cross: Research Vessel Senckenberg (RVS).

energy results to:

$$\frac{\partial}{\partial t}\underbrace{\frac{\rho}{2}\overline{u_i'^2}}_{E^*_{turbulent}} = \underbrace{\rho\overline{u_i'u_j'}\frac{\partial}{\partial x_j}\overline{u_i}}_{P} - \underbrace{\mu\overline{\frac{\partial u_i'}{\partial x_j}\frac{\partial u_i'}{\partial x_j}}}_{\varepsilon}, \quad \text{also} \quad \frac{\partial}{\partial t}E^*_{turbulent} = P - \varepsilon.$$

The velocity fluctuations and the spacial derivatives of the mean velocity in accordance to the Reynolds decomposition are needed to estimate the rate of production of TKE (see e.g. Hinze, 1975).

There are two different methods to estimate the rate of dissipation of the TKE. First, by using the spacial derivatives of velocity fluctuations. With the simplifying assumption of isotropy of the turbulence (Hinze, 1975), the dissipation rate can be

estimated by the ADCP-measurement via

$$\varepsilon_{ADCP} = \frac{15}{2}\mu \overline{\left(\frac{\partial u'}{\partial z}\right)^2}. \tag{2.1}$$

The second method uses the vertical displacements in density profiles and the buoyancy frequency (e.g. Ferron et al., 1998), which are measured by a CTD,

$$\varepsilon_{CTD} = c_1 \; L_T^2 \; N^3. \tag{2.2}$$

The units of dissipation rates ε of TKE estimated via ADCP and CTD differs:

$$[\varepsilon_{ADCP}] = \frac{W}{m^3} = 10^3 \frac{kg}{m^3}\frac{W}{kg} = [\rho\varepsilon_{CTD}].$$

With $E^*_{turbulent}$ the TKE, P being the production rate of TKE, ε the dissipation rate of TKE, t the time, ρ the density, u' the velocity fluctuation of any direction (indicated with i or j), x horizontal direction, μ the dynamic viscosity, z the vertical component of direction, c_1 the proportionality factor, L_T the Thorpe-Scale (root-mean-square of the vertical density replacements) and N the buoyancy frequency.

2.3   Measurements and data processing

Measurements were conducted on-board the Research Vessel Senckenberg with an ADCP and a CTD during one flood and one ebb tide from November 9, 2010 at 7:00 pm until November 10, 2010 at 8:40 am. In the measurement region (see figure 2.1), the magnitude of the current velocity reaches values up 2 $m\ s^{-1}$ (Reuter et al., 2009).

ADCP measures frequency shifts of an acoustic signal caused by the motion of the fluid (Doppler effect). The velocity and direction of the current are estimated on the basis of this frequency shift, resulting in a three-dimensional velocity-field. A ship-mounted, downward looking ADCP (RD Instruments Workhorse Sentinel,

1200 kHz) was used. The ADCP measures with a pinging rate of 5 Hz. The water column is divided in 0.25 m depth-cells (bins) for the depth-dependence of the signal. The CTD measures conductivity, temperature and depth. The CTD (Sea & Sun Technology, CTD48M) was used for yoyo-measurements, this means that every 20 minutes 10 vertical profiles (yoyo) of the water column were measured. The CTD samples with a frequency of 2 Hz.

Data processing   For simplification, data sets measured from ADCP were transformed into the main flow directions. These are at the measuring position of the RV Senckenberg for the inflow 80 ° (approximately eastwards) and 340 ° (approximately north-northwest) for the outflow. These main flow directions differs from them at the Time Series Station Spiekeroog (inflow: 120 ° and outflow: 300 °). The reason for this is the morphology of the tidal channel and the appropriate measuring position.

The production rate P and dissipation rate ε of TKE were estimated from the current velocities of the ADCP measurements. To made these results comparable to the CTD data sets the results from the ADCP were averaged into the burst times of the CTD measurements. CTD data sets were also averaged into depth-cells of 0.25 m like the depth-cells of the ADCP.

2.4   Results

Figures 2.2 and 2.3 show the production rates of TKE P_{ADCP} and dissipation rates of TKE ε_{ADCP} which were estimated from the ADCP measurements. The values of the production rate P_{ADCP} are between -4.43 $log_{10}(W\ m^{-3})$ and -0.02 $log_{10}(W\ m^{-3})$. Conspicuities are near the surface (up to 0.05 $log_{10}(W\ m^{-3})$ at burst 5 (circa 8:20 pm) and up to -0.31 $log_{10}(W\ m^{-3})$ at burst 17 (circa 0:45 am)). The production rate

shows values of -0.62 $log_{10}(W\ m^{-3})$ at flood and ebb. Figure 2.2, however, shows a stronger ebb signal. The values of the dissipation rate ε_{ADCP} (figure 2.3) vary be-
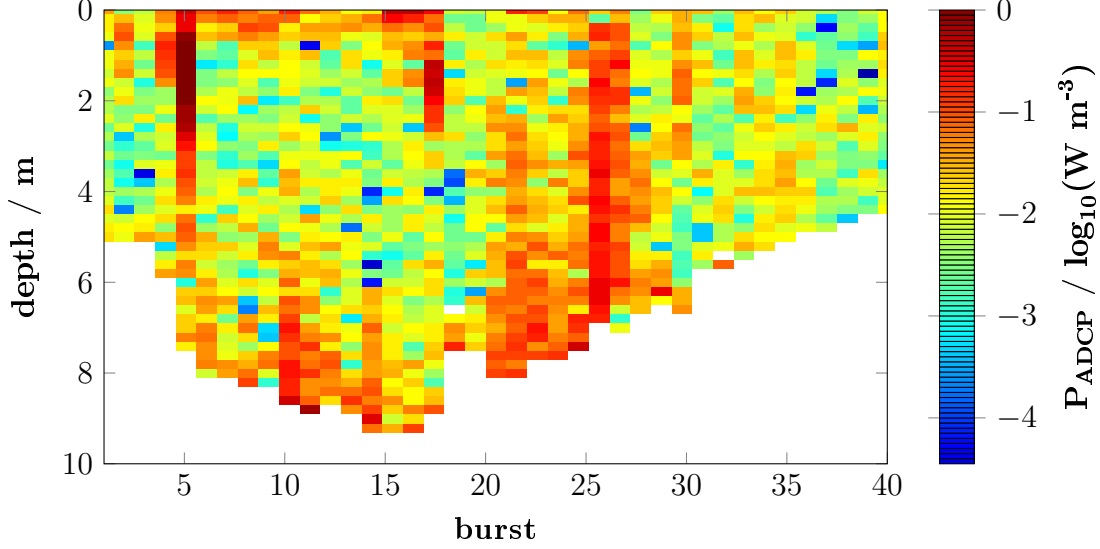

Figure 2.2: Production rate of TKE P_{ADCP} in $log_{10}(W\ m^{-3})$ estimated via ADCP.

tween -4.59 $log_{10}(W\ m^{-3})$ and -2.90 $log_{10}(W\ m^{-3})$. The highest rates of dissipation are with -2.9 $log_{10}(W\ m^{-3})$ at burst 10 (10:15 pm) and with -3.08 $log_{10}(W\ m^{-3})$ at burst 27 (circa 4:00 am). At slack water, the values of the dissipation rate are around -3.8 $log_{10}(W\ m^{-3})$. At flood and ebb, results show values up to -3.27 $log_{10}(W\ m^{-3})$. Besides the flood is stronger and has conspicuities near the surface with values up to -3.16 $log_{10}(W\ m^{-3})$. Figure 2.4 displays the dissipation rate ε_{CTD} which was estimated via the CTD measurements. Values are in the range between -6.47 $log_{10}(W\ m^{-3})$ and -0.61 $log_{10}(W\ m^{-3})$. The dissipation rate shows a clear ebb-dominated tidal signal. At low and high tide the dissipation rate ε_{CTD} is relatively small (up to -2.64 $log_{10}(W\ m^{-3})$) compared to the values at the current cores (-1.43 $log_{10}(W\ m^{-3})$). Therefore, an accordance with the ADCP-data is discernible. The slack water times should be in the bursts 1 (low tide, at circa 6:50 pm), in burst 17 (high tide, at circa 0:45 am) and in the bursts 38 (low tide, at circa 7:10 am). But figure 2.4 lets assume that slack water times occur later (circa 2 bursts later, this

corresponds to a nearly 40 minutes delay).

So, the results of dissipation rate are in the same order of magnitude, but differ in range. The dissipation rate ε_{ADCP} depends on the shear and the stress within the velocity field in the water column. Therefore, maximum values are located near the seabed. However, highest values of ε_{CTD} are seen in the middle of the water column. Results of the ADCP measurements reveal a stronger flood-phase, whereas the results of the CTD measurements show ebb dominance.
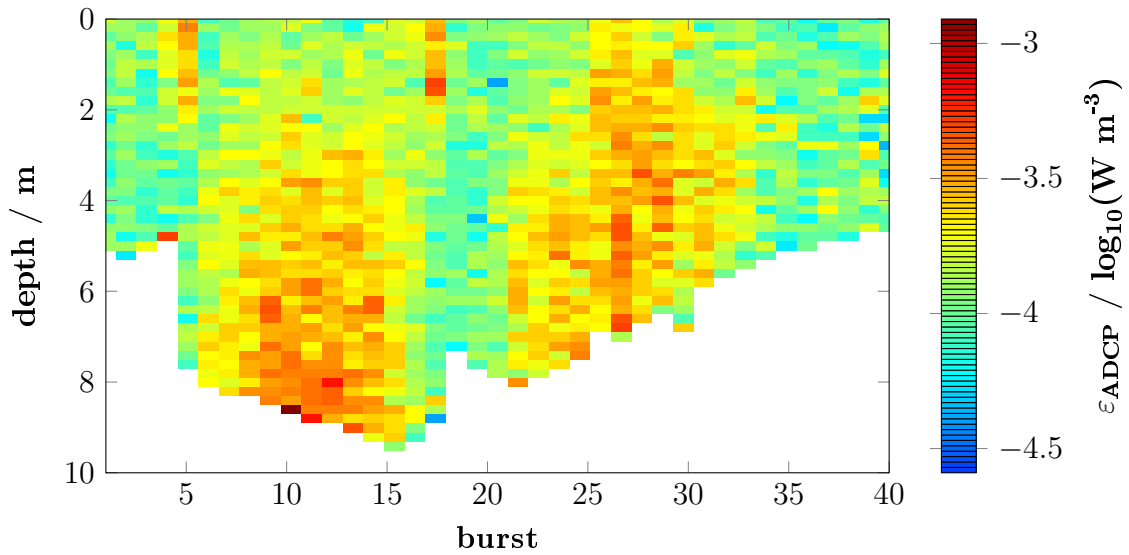
Figure 2.3: Dissipation rate of TKE ε_{ADCP} in $log_{10}(W\ m^{-3})$ estimated via ADCP.

2.5   Conclusion

These results of the production rates and dissipation rates of turbulent kinetic energy over depth (see figures 2.2 to 2.4) are comparable to those from Rippeth et al. (2002, 2003) and Wiles et al. (2006) because the measurements were conducted in similar research areas. Their results have similar patterns over time and the values have the same order.
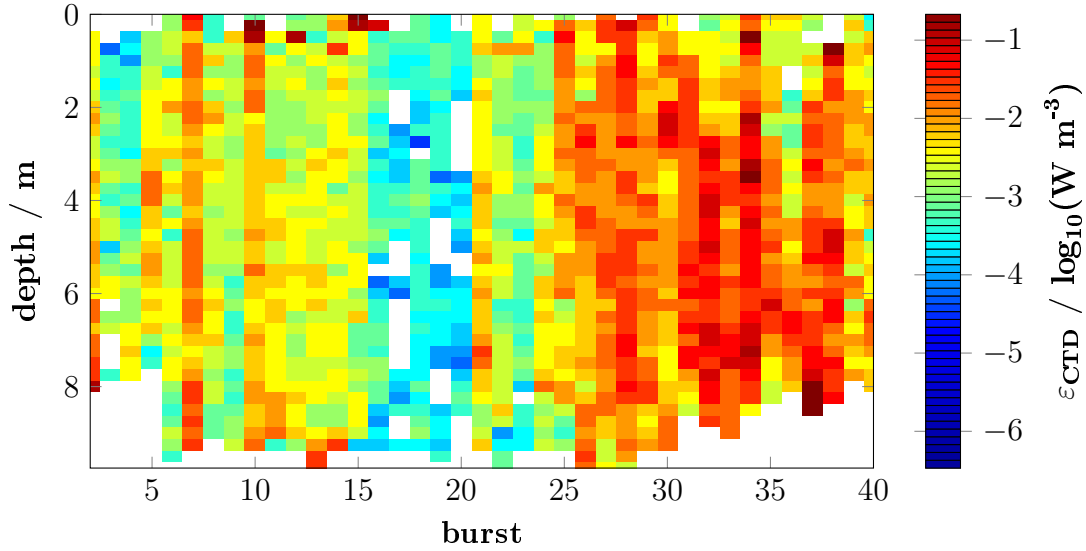
Figure 2.4: Dissipation rate of TKE ε_{CTD} in $log_{10}(W\ m^{-3})$ estimated via CTD.

Figure 2.5 shows the comparison between depth-averaged production rate P_{ADCP} and dissipation rate ε_{ADCP} from the ADCP measurements. The production rate shows no obvious tidal signal in contrast to the dissipation rate. Values range from -2.3 $log_{10}(W\ m^{-3})$ to -0.80 $log_{10}(W\ m^{-3})$ for the production rate and from -3.81 $log_{10}(W\ m^{-3})$ to -3.42 $log_{10}(W\ m^{-3})$ for the dissipation rate. Comparison between the estimated rates of production and dissipation shows that more kinetic energy is supplied than dissipated to the turbulent current, i.e. residual kinetic energy in the turbulent current is used for mixing. Therefore production rate is a source and the dissipation rate is a sink of TKE. Figure 2.6 displays the depth-averaged results of the two different methods for the estimation of the dissipation rate.

The values range from -2.97 $log_{10}(W\ m^{-3})$ to -1.86 $log_{10}(W\ m^{-3})$ for ε_{CTD} and from -3.81 $log_{10}(W\ m^{-3})$ to -3.42 $log_{10}(W\ m^{-3})$ for ε_{ADCP}. The CTD-estimated dissipation rate varies much stronger. In both dissipation rates, the tidal signal can be clearly seen. The highest values occur at times of the strongest current, but magnitudes are different. The course of the dissipation rate exhibits a period, which is related to the quarter-diurnal pattern M_4.
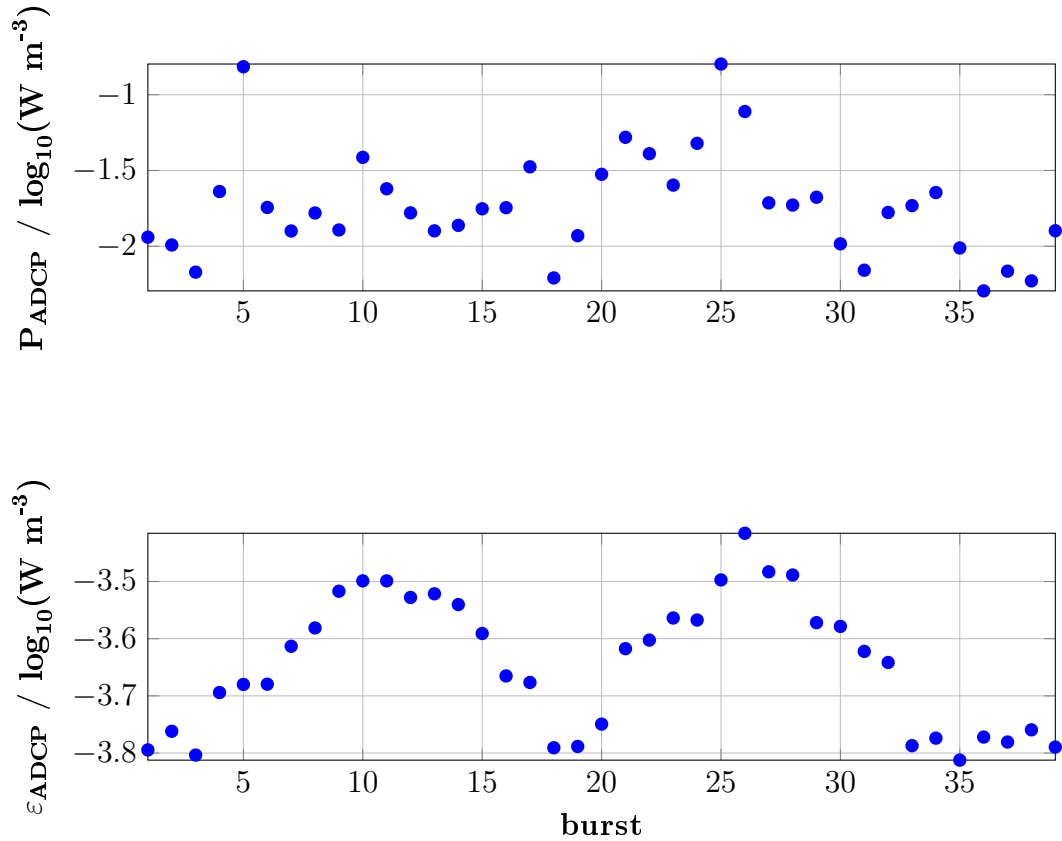
Figure 2.5: Comparison of the depth-averaged production rate P_{ADCP} and the depth-averaged dissipation rate ε_{ADCP}.

The Reynolds number $Re = u \cdot L/\nu$ is an important criterion for the existence of turbulence. Figure 2.7 displays their results which show a continuity of turbulence. A direct comparison of the results for the dissipation of TKE as estimated by the different methods is difficult, because of significant differences in dissipation rate ε. Resulting from the different characteristics of the measures, i.e. the different methods show different mixing processes or due to the special environmental conditions higher sampling rates are needed. Since the CTD sampling rate is the smaller one, the ADCP measurements are more reliable.
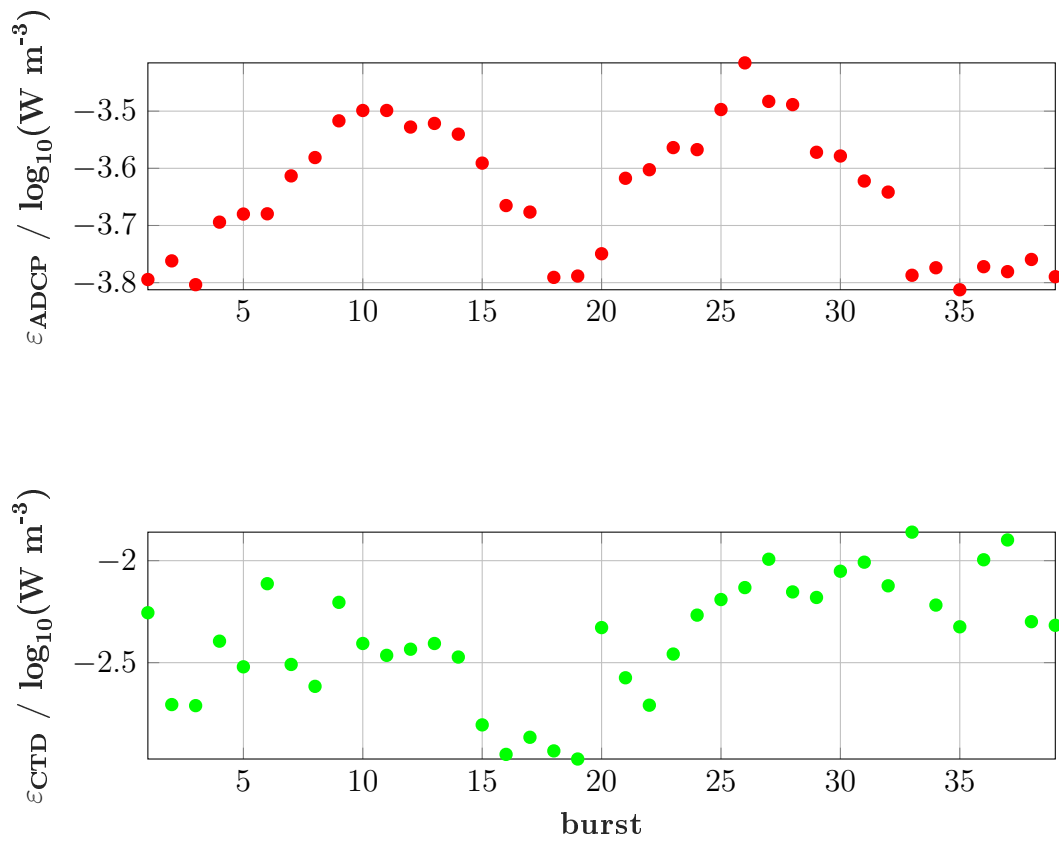
Figure 2.6: Depth-averaged bursts of the dissipation rate ε; top: dissipation rate ε_{ADCP} estimated via ADCP; bottom: dissipation rate ε_{CTD} estimated via CTD.
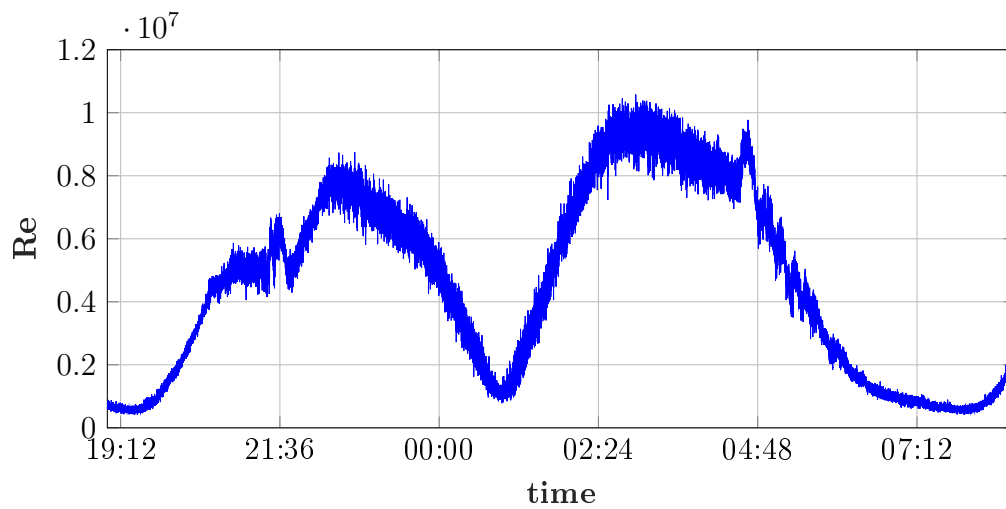
Figure 2.7: Reynolds number Re during the measurement period in November 2010.

3 Turbulence producing processes in a tidal channel

3.1 Introduction

Turbulence is important for mixing processes in the ocean. Especially in shallow water regions with high current velocities, e.g. in a tidal channel, vertical mixing is strong. The origin and continuity of turbulence depends strongly on Reynolds stress τ and velocity shear S. Therefore, Reynolds stress τ and velocity shear S were estimated using current measurements from a bottom-mounted high-frequency Acoustic Doppler Current Profiler (ADCP). The measurement was conducted at the Time Series Station Spiekeroog in an East Frisian tidal channel in the southern North Sea.

3.2 Measurements

The research area in the southern North Sea (German Bight) is part of the UNESCO World Heritage Wadden Sea. It is the largest contiguous area of mud and sand flats in the world (UNESCO World Heritage Center, 2009) with natural dynamic processes that take place in a largely undisturbed natural state. The strong dynamics of the tidal currents are constantly changing particularly in the inlets between the islands.

Measurements were conducted with an ADCP during one flood and one ebb tide from November 9, 2010 7:00 pm until November 10, 2010 8:40 am. A bottom-mounted, upward looking ADCP (RD Instruments Workhorse Sentinel, 1200 kHz) was used. The ADCP measured with a pinging rate of 5 Hz. The water column was divided in 0.25 m depth-cells (bins) for the depth-dependence of the signal.

3.3   Methods

Natural flows are described by a mean and a fluctuating part $u_i = \overline{u_i} + u_i'$ (Reynolds decomposition). Turbulence is generated by the interaction of this fluctuating and mean parts of the flow. To separate these parts the measured velocities were averaged over a period of 10 minutes (Rippeth et al. (2002), cf. figure 3.1).
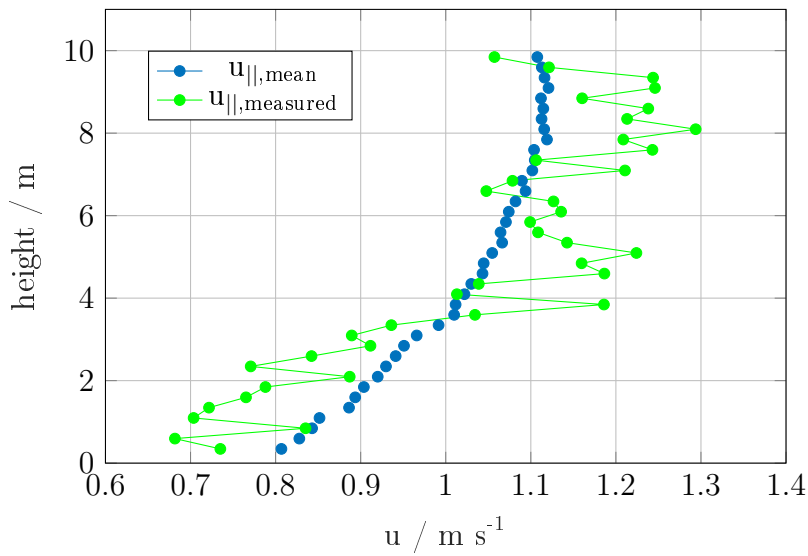

Figure 3.1: Velocity profiles: measured (green) and 10-min-average (blue).

The Reynolds stress τ_{ij} is defined by the means of the fluctuating parts of the flow (e.g. Lu and Lueck, 1999b) as

$$\tau_{ij} = -\overline{u_i' u_j'}. \tag{3.1}$$

The velocity shear S_{ij} results from the mean velocity gradient

$$S_{ij} = \frac{\partial \overline{u_i'}}{\partial x_j} \tag{3.2}$$

with u_i: measured velocity, $\overline{u_i}$: averaged (mean) part of the flow, u_i': fluctuating part of the flow, x_i: direction (along, across, up) and i, j are different components.
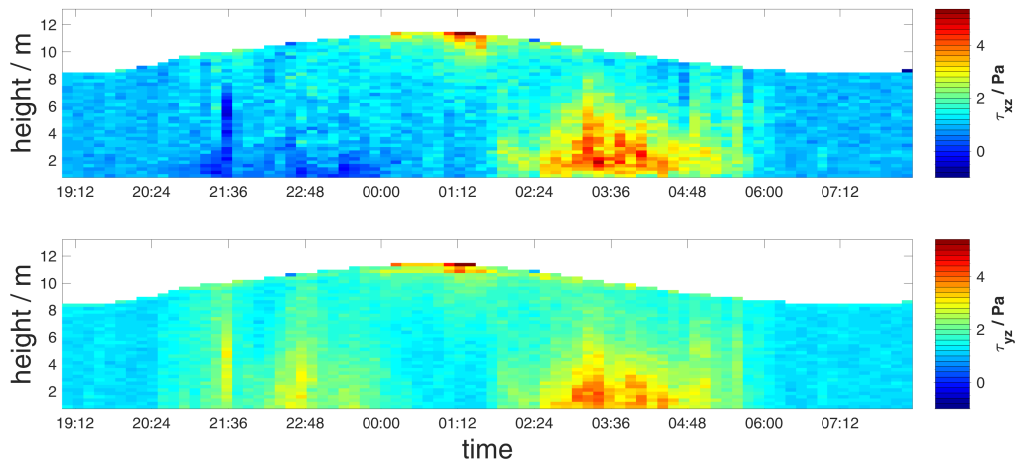
Figure 3.2: Reynolds stress τ estimated via equation 3.1; top: along channel component τ_{xz}; bottom: across channel component τ_{yz} in Pa.

3.4   Results

Figure 3.2 depicts the along channel (τ_{xz}, top) and the across channel (τ_{yz}, bottom) components of the Reynolds stress τ. The along channel component τ_{xz} (figure 3.2, top) reaches values between -1.94 Pa and 5.5 Pa. The highest values of about 5.5 Pa are at high water at the surface and during ebb with 3.26 Pa. At flood tide the Reynolds stress τ_{xz} acts into the other direction with values between -0.55 Pa and -1.8 Pa. Low water times show smallest values of about 1 Pa. Values of the across channel component of the Reynolds stress τ_{yz} (figure 3.2, bottom) range between -0.58 Pa and 6.12 Pa. Both, ebb and flood tides show positive values with 3.2 Pa (flood) and 4.2 Pa (ebb). During slack water times minimum values between 1 Pa and 1.5 Pa occur with one exception at the surface during high water (6.1 Pa). Both components shows the tidal signal with different magnitudes and directions and with high values at the bottom of the water column (flood and ebb) and at the surface (slack water). The Reynolds stress is within the same order of magnitude during flood and ebb showing stronger signals during the ebb tide.
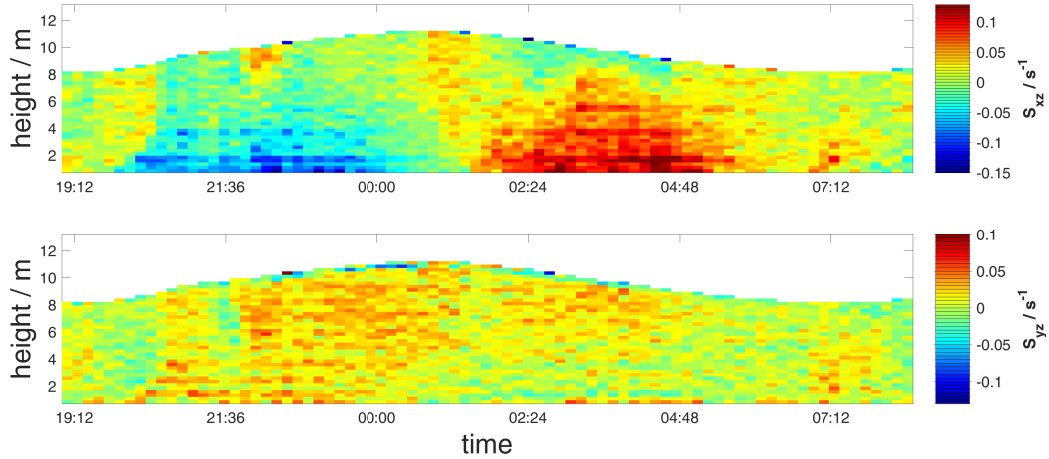
Figure 3.3: Velocity shear S estimated via equation 3.2; top: along channel component S_{xz}; bottom: across channel component S_{yz} in s^{-1}.

Figure 3.3 displays the along channel (S_{xz}, top) and the across channel (S_{yz}, bottom) components of the velocity shear S. The values of the along channel velocity shear S_{xz} vary between -0.26 s^{-1} and 0.17 s^{-1}. These peak values occur during the clearly visible tidal signal with negative values during flood and positive values during ebb. Whereas, the tidal cycle is hardly noticeable at the across channel velocity shear S_{yz}. Their values are between -0.11 s^{-1} and 0.18 s^{-1}. The velocity shear (figure 3.3) shows similarities in the course of the along channel component (top), but is much weaker in the across channel component (bottom).

To demonstrate the tidal cycle figure 3.5 shows the depth-averaged results for the velocity shear (top) and depth-averaged results for the Reynolds stress (bottom). The blue dots show the along channel components and the red dots show the across channel components. In addition, hourly averaged velocity profiles are shown in figure 3.4. These profiles show clearly the tidal cycle of the velocity with the magnitude, direction and the resulting gradient over depth. These have the expected log-profile. At the surface, other influence factors act like e.g. wind or waves. Further, figure

3.4 presents the corresponding profiles of the along channel velocity shear S_{xz} and Reynolds stress τ_{xz} over depth.
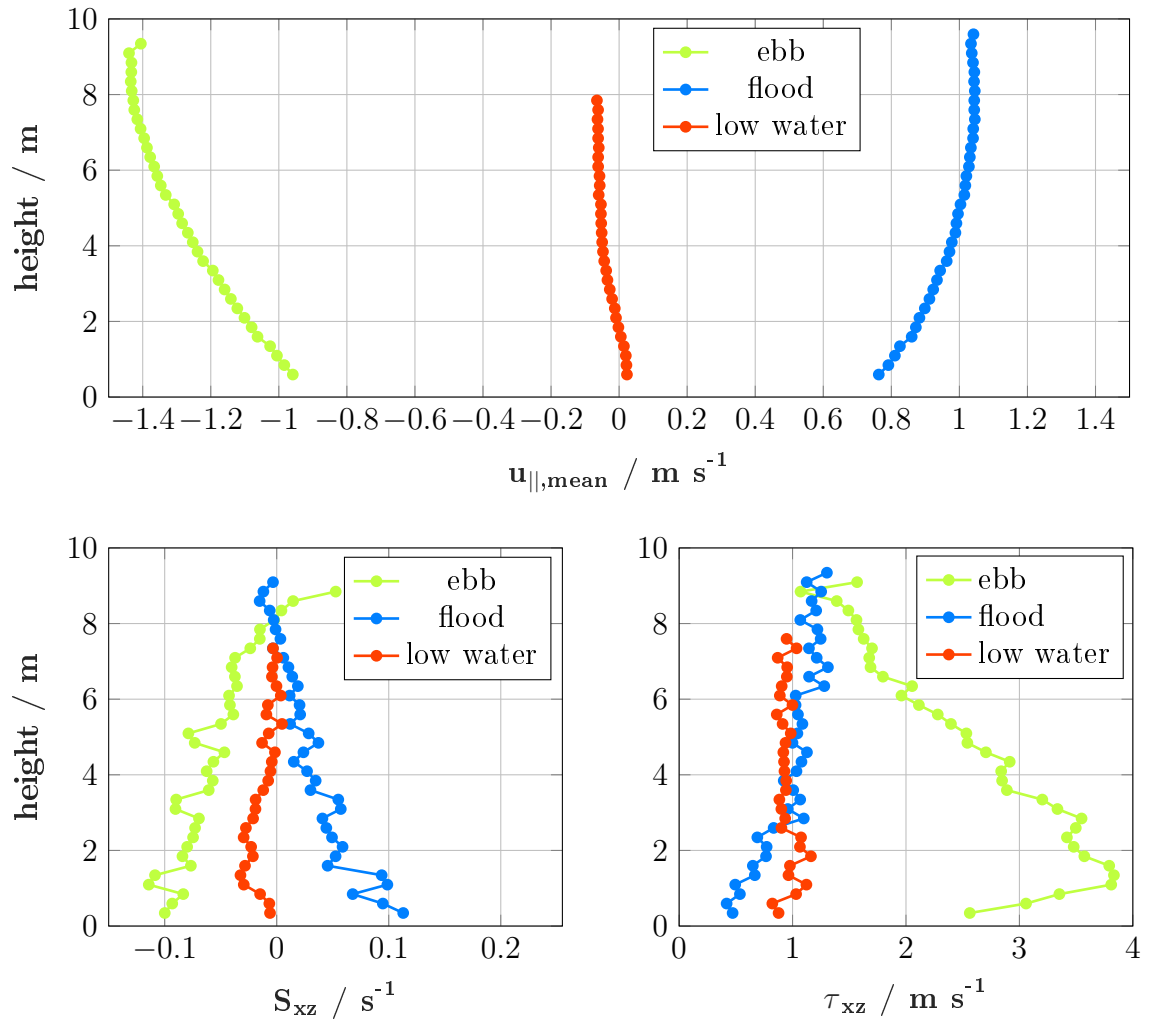

Figure 3.4: Exemplary hourly averaged profiles. Top: profiles of velocity component along channel $u_{\|}$ and corresponding shear S_{xz} (bottom left) and Reynolds Stress τ_{xz} profiles at ebb (green), flood (blue) and one at slack water (low water - red).
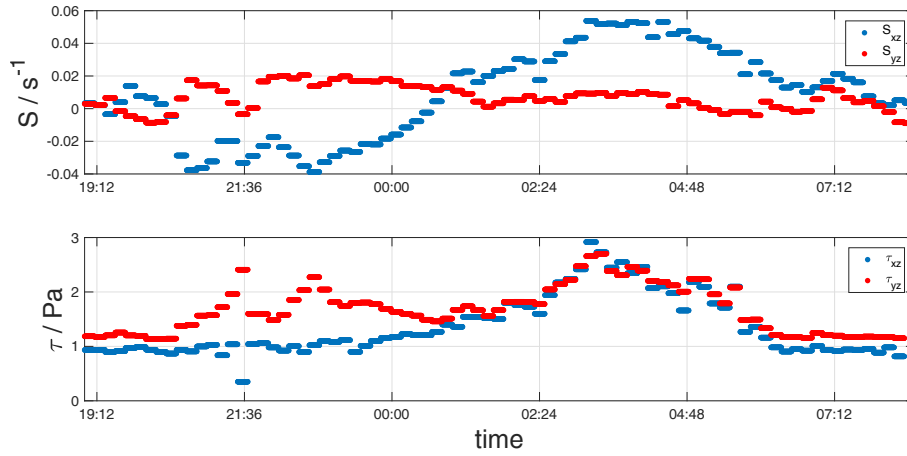
Figure 3.5: Comparison of the depth-averaged velocity shear S (top) and the depth-averaged Reynolds stress τ (bottom). In blue the along channel components and in red the across channel components of the variables.

3.5   Conclusion

There are differences between the across channel components of the Reynolds stress τ_{xz} and the velocity shear S_{xz}: the Reynolds stress shows also tidal course in time, while the velocity shear does not show this. A comparison between the along channel components of these variables shows similarities over the tidal cycle. Both reveal a period, which is related to the quarter-diurnal pattern M_4. The highest values were found near the seabed and in the middle of the water column, where the highest velocities and the highest gradients occur. Here, turbulence is generated by sheared currents at the bottom of the sea. Thus, shear acts to increase turbulent mixing. Due to the shallow water depth mixing occurs across the entire water column.

4 Assessment of turbulence patterns from non-high resolution data sets of current velocities

Abstract   Particularly in shallow water regions with high current velocities such as tidal channels, turbulence is important for mixing processes. To increase our understanding of coastal transport dynamics it is crucial to obtain a high number of field observations of turbulence parameters.

Here, we present a new method for analyzing turbulence patterns based on estimates of current speed and velocity shear. The data set used in this study was derived from high resolution Acoustic Doppler Current Profiler (ADCP) current measurements obtained during a single tidal cycle in November 2010 in the East Frisian Wadden Sea. The method was then applied to a long-term current data set obtained from a bottom-mounted, upward looking ADCP (1200 kHz) at the Time Series Station Spiekeroog.

Our method can reproduce the production rate P of turbulent kinetic energy based on velocity shear S with a goodness of fit of $R^2 = 0.76$ and based on current speed $|u|$ with $R^2 = 0.87$. Even parts of storm surges can be reproduced with $R^2 = 0.66$. The results give valuable insights into the turbulent processes within a tidal channel under various environmental conditions. The method is simple and can be easily applied to different data sets.

4.1   Introduction

Turbulence is important for mixing processes in aquatic ecosystems, particularly in shallow water regions with high current velocities such as tidal channels. Here, turbulence may be responsible for most of the exchange and transport processes, such as sediment transport and its dynamic. The dynamics of turbulent motion in

a fluid can be described by the equation of turbulent kinetic energy. To determine
the energy available for turbulent mixing of the water column one needs to know
the production rate of turbulent kinetic energy P (see e.g. Hinze (1975) and Rip-
peth et al. (2002)), which depends on several parameters. For example, Ralston and
Stacey (2006) show the relevance of shear for turbulence production in estuaries.
Others, like Lu et al. (2000), Rippeth et al. (2003, 2002) and Simpson et al. (2004,
2002), investigate the production rates P, dissipation rates ε of turbulent kinetic
energy (TKE), its relation (ε/P) and the corresponding Reynolds stress to analyse,
for example the tidal bore in an estuary. Kocsis et al. (1999) compare dissipation
rates ε of TKE estimated from shear and temperature microstructure probes (in a
lake). Turbulent kinetic energy can also be linked to other processes such as sedi-
ment dynamics in coastal seas (e.g. Bowers, 2003; Garaba et al., 2014; Schulz et al.,
2015).

In summary, these studies focus on those parameters, which are most suitable for
describing turbulence in natural environments. Besides, these studies primarily rely
on direct short-term measurements of turbulence. However, to increase our under-
standing of coastal hydrodynamics, such as tidal mixing, it is crucial to obtain a high
number of field observations of turbulence parameters. Previous modeling studies,
like Burchard (2009), Rippeth et al. (2001) and Stacey et al. (2001), motivated a
number of field studies in tidally dominated coastal seas under non-standard con-
ditions, dominant diurnal tides, or winds from various directions. But long-term
measurements of turbulence are difficult to obtain and thus only barely available.
For example, Orton and Visbeck (2009) provide merely a data set covering 100 days
restricted to battery and memory limitations. Opposed to that, measurements of
current velocity are much easier to perform and corresponding data sets are available
from a variety of coastal systems (e.g. Lu and Lueck, 1996, 1999a).

To close the gap between available short-term data of turbulence and the need for

long-term estimates of natural turbulence patterns, we developed a method that makes existing long-term data sets of current velocities available for turbulence investigations. Rather than investigating the fine structures of turbulence, this new method should serve to investigate the general patterns of turbulence in the system. The method presented in this paper, is based on measurements of speed and velocity shear. Additionally, no further environmental parameters are needed besides the estimates of speed (magnitude of current velocity), velocity shear and production rate of turbulent kinetic energy to investigate turbulence patterns.

4.2   Research area and measurements

The research area (figure 4.1, left) is located in the southern North Sea (German Bight). It is part of the UNESCO World Heritage Wadden Sea, which is the largest contiguous area of mud and sand flats in the world. A series of islands separate the Wadden Sea from the open North Sea. The natural strong dynamics of the tidal currents constantly change the appearance of the flats, particularly in the inlets between the islands (e.g. Stanev et al., 2003b). As part of the COSYNA (Coastal Observing System for Northern and Arctic Seas) project the Time Series Station Spiekeroog is deployed for automated observing and monitoring real-time conditions (Baschek et al., 2017; Schulz et al., 2016). At this Time Series Station, the magnitude of the current velocity reaches values up to $2\ m\ s^{-1}$ (Reuter et al., 2009). Here, a bottom-mounted, upward looking Acoustic Doppler Current Profiler (ADCP - Teledyne RD Instruments Workhorse Sentinel, 1200 kHz) is used to estimate the three dimensional current velocities. The ADCP is mounted to a boom at a distance of 12 m (figure 4.1, right), ensuring that turbulence induced by the station pole itself does not affect the ADCP measurements. Since 2006, ADCP data have been obtained at the Time Series Station in a measurement mode which is not

highly temporal and spacial resoluted because of compromises between scientific and technical issues; we name such mode as a non-high resolution measurement mode. Running the ADCP continuously in high resolution mode (in time and space) is not feasible because the set-up of the station does not allow storing, processing and transferring large volumes of data in real time. For a more comprehensive description of definitions of these measurement modes see table 4.1. In addition, measurements with high temporal resolution were conducted during one flood and one ebb tide from November 9 until November 10, 2010.
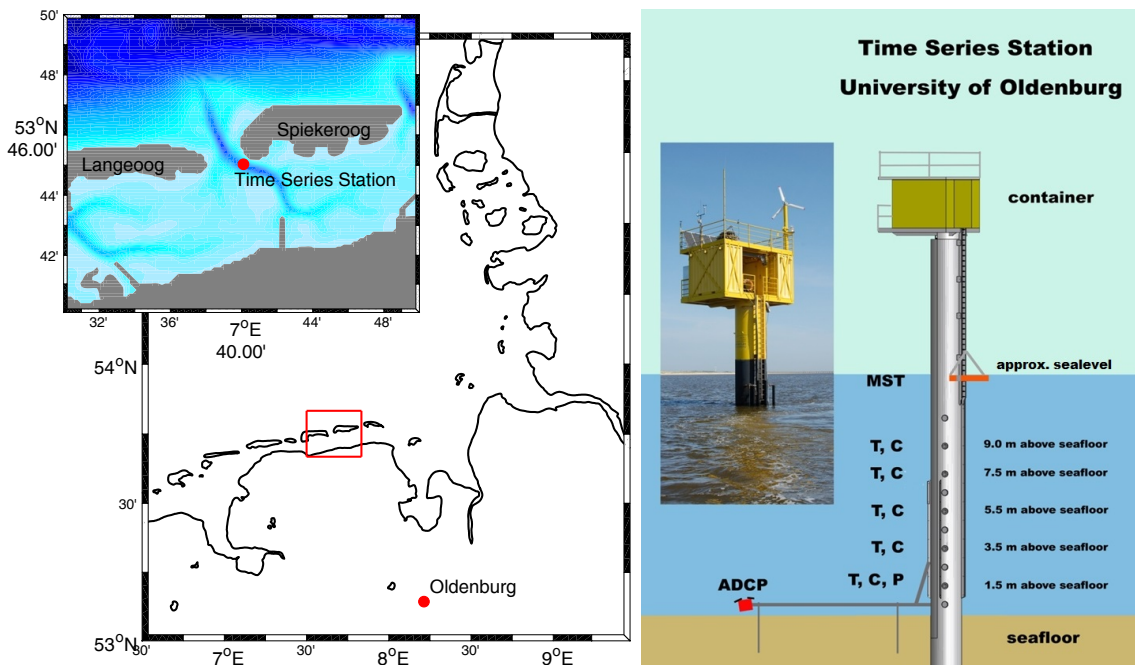
Figure 4.1: Left: Location of the Time Series Station (TSS) Spiekeroog in the southern North Sea. Right: Scheme of the TSS (modified after Badewien et al. (2009)).

Table 4.1: Definitions of ADCP measurement modes (regarding temporal resolution).

Measurement setup:	Description:
High resolution (HR)	Within this measurement mode the ADCP sends 5 acoustic pulses (pings). Using the Doppler effect, current velocities can be calculated from frequency shifts of transmitted pings. Spacial resolution of the data sets are given by travel time of pings. Averaging the results of these 5 single pings into different travel time periods provide velocity profiles over depth. The estimation of every current velocity profile (ensembles) is done every second (1 Hz).
Non-high resolution (NR)	The non-high resolution mode included 45 pings per ensemble (every 5 minutes).
Normal or common resolution	For example, 5 pings per ensemble every minute depending on scientific questions.

4.3   Methods

The aim of this work was to make non-high resolution long-term data sets of current velocities usable for turbulence investigations.

We used the production rate of turbulent kinetic energy P as a measure of turbulence, which is defined as:

$$P = \tau_{ij} S_{ij} = -\rho \overline{u_i' u_j'} \, \frac{\partial \overline{u_i}}{\partial x_j}, \qquad (4.1)$$

with the Reynolds stress τ_{ij}, the velocity shear S_{ij}, seawater density ρ and i, j relevant component (i.e. x, y or z) of the variable used. The velocity fluctuations

$u'_{i,j}$ and the spacial derivative x_j of the averaged velocity $\overline{u_i}$ in accordance to the Reynolds decomposition ($u_i = \overline{u_i} + u'_i$; with an averaging period of 10 minutes) were used to estimate the rate of production of turbulent kinetic energy P. These variables were estimated by high resolution measurements of current velocity components.

Our investigations of the turbulence producing processes showed that the production rate of turbulent kinetic energy P depends mainly on the velocity shear. Because velocity shear acts principally into the main direction of the flow, we assumed that the production rate of turbulent kinetic energy P can be predicted by velocity shear S_{xz} and the speed $|u|$. The velocity shear S_{xz} is calculated from horizontal velocities (east- and north-components), which are transformed into the main flow direction x (inflow 120° and outflow 300°; see figure 4.2) and the vertical velocity component z. We assumed that this simplified relationship can also be applied to estimate the production rate of turbulent kinetic energy P based on the velocity shear S_{xz} and the magnitude velocity $|u|$ from non-high resolution data sets of current velocities.
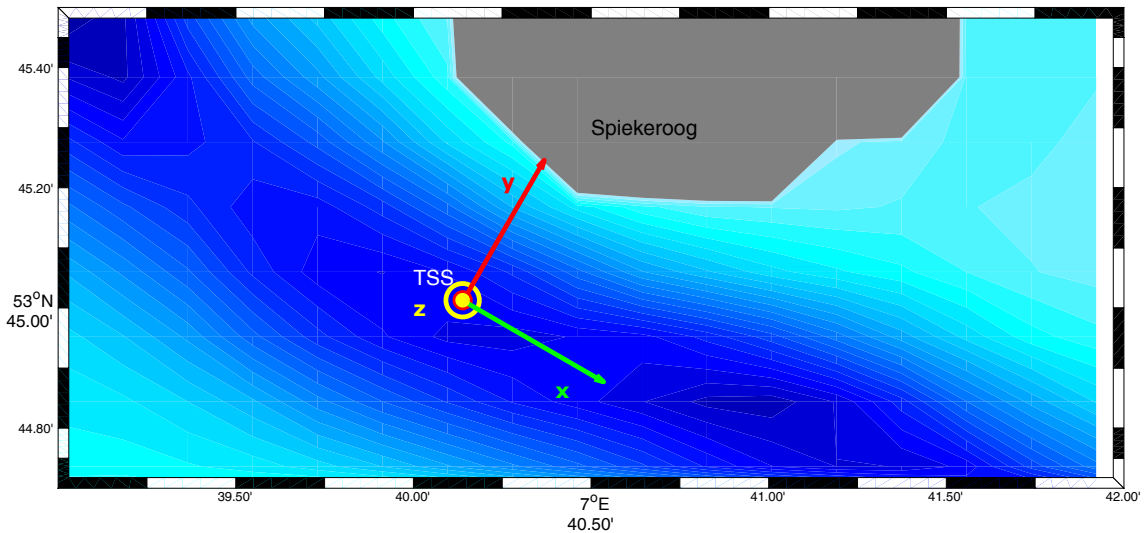
Figure 4.2: Resulting velocity components after coordinate rotation (main flow directions: inflow 120° and outflow 300°).

4.3.1   Approach

To develop the method in a first step we averaged the existing high resolution data set of velocity shear S_{xz} and production rate of turbulent kinetic energy P over the depth of the water column as a proxy for an averaged depth range. We investigated the relationship between the production rate P and the velocity shear S_{xz}. The results indicated an additional relation between the production rate P and the velocity speed $|u|$ (see figure 4.3).
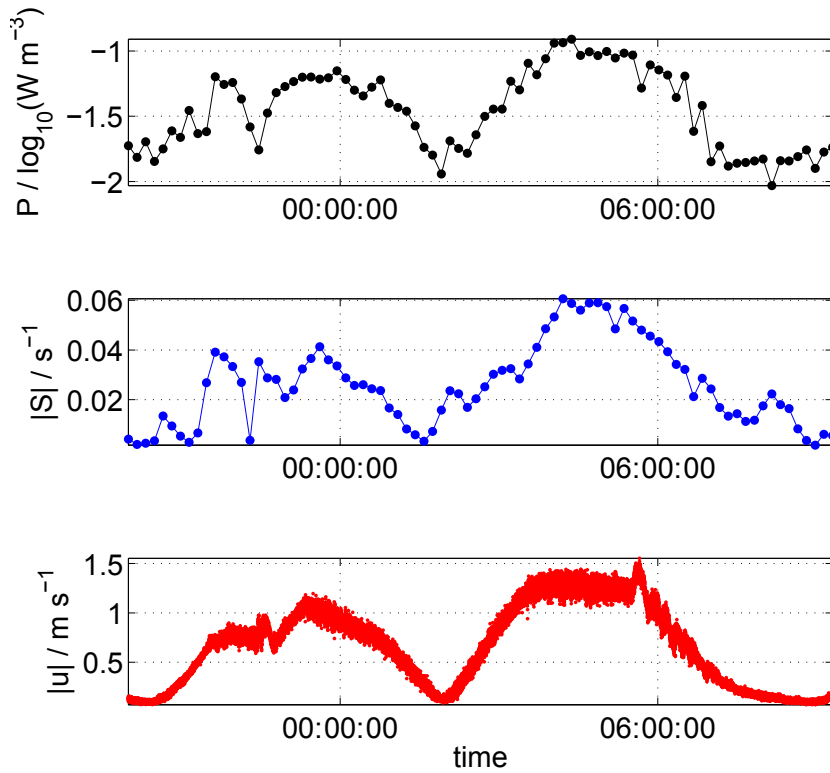

Figure 4.3: Depth averaged production rate of turbulent kinetic energy P in $log_{10}(W\ m^{-3)}$, absolute values of velocity shear $|S|$ in s^{-1} and current speed $|u|$ in $m\ s^{-1}$. Data sets were measured from November 9 until November 10, 2010.

Further we down-sampled the high resolution data set to a non-high resolution

data set (for details see table 4.1). With these down-sampled data sets of current velocities we estimated its magnitude, so speed $|u|_{NR}$, velocity shear $S_{xz,NR}$ and the production rate of turbulent kinetic energy P_{NR}.

Figure 4.4 shows the relationships between the production rate of turbulent kinetic
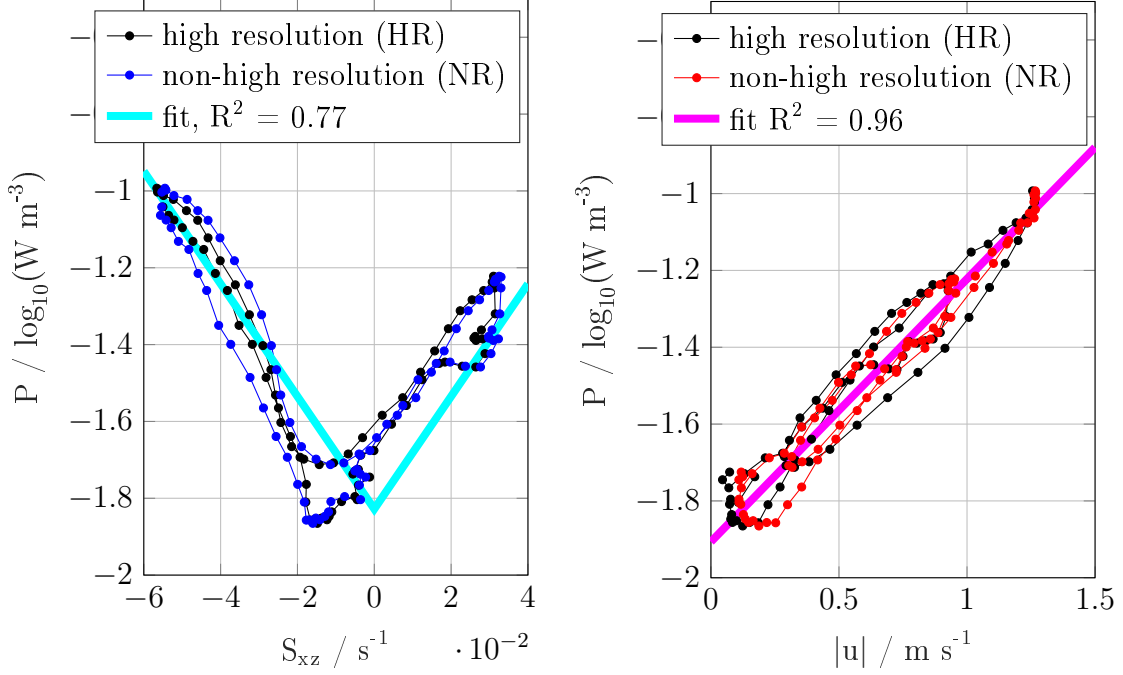
Figure 4.4: Depth averaged production rate P in $log_{10}(W\ m^{-3})$ vs. velocity shear S_{xz} in s^{-1} (left); and vs. speed $|u|$ in $m\ s^{-1}$ (right). High resolution (HR, black) and down-sampled (non-high resolution, NR, blue or red) data sets.

energy P and velocity shear S_{xz} (figure 4.4, left) and with speed $|u|$ (figure 4.4, right) over the entire tidal cycle. These plots depict the correlation over a complete tidal cycle, which can be described by

$$log(P_{rec,complete}) = a|x| + b, \tag{4.2}$$

at the right-hand-site of the equation is a linear fit function with $|x|$ the magnitude of the considered variable, a the slope or gradient and b the intercept point or threshold. These figures also show the fit (solid line) used to reconstruct P from

down-sampled data (non-high resolution data set). In addition, the graphs indicate that the turbulent processes differ between the tidal periods. We therefore plotted the data separately for the flood and ebb periods (figures 4.5 and 4.6), which improved the correlation. The data during ebb periods with decreasing water levels (dec.) are displayed on the left side of these figures. Accordingly the right side of these figures show the data during flood periods with increasing water levels (inc.). To reconstruct the production rate of turbulent kinetic energy P from both variables after separation into flood and ebb periods we used the following equation:

$$log(P_{rec,separation}) = p_1 x + p_2.$$ (4.3)

at the right-hand-site of the equation is again a linear fit function with x the considered variable, p_1 is the slope or gradient and p_2 the intercept point.

Table 4.2 shows the corresponding fit coefficients and the goodness of fit values R^2. Figure 4.5 depicts the shear correlations and figure 4.6 the speed correlations. Results from the corresponding tidal phase depending reconstructions of the production rate of turbulent kinetic energy are shown in figure 4.7. Here, the given production rate P is shown on a logarithmic scale. Thus, the correlation is logarithmic.

4.3.2 Reconstruction of production rate of turbulent kinetic energy

The approach worked excellent for reconstructing the production rate of turbulent kinetic energy based on the data set obtained in November 2010. However, when applying the approach to a control, nearly high resolution data set (e.g. September 15, October 21 and December 17, 2014), we found that the intercept points (thresholds) and slopes vary over time. At some times there were higher production rates and at other times the production rates were lower, implying that the turbulence varies over time. Hence, we adapted in the following these thresholds and slopes depending on the relevant variables shear and speed.
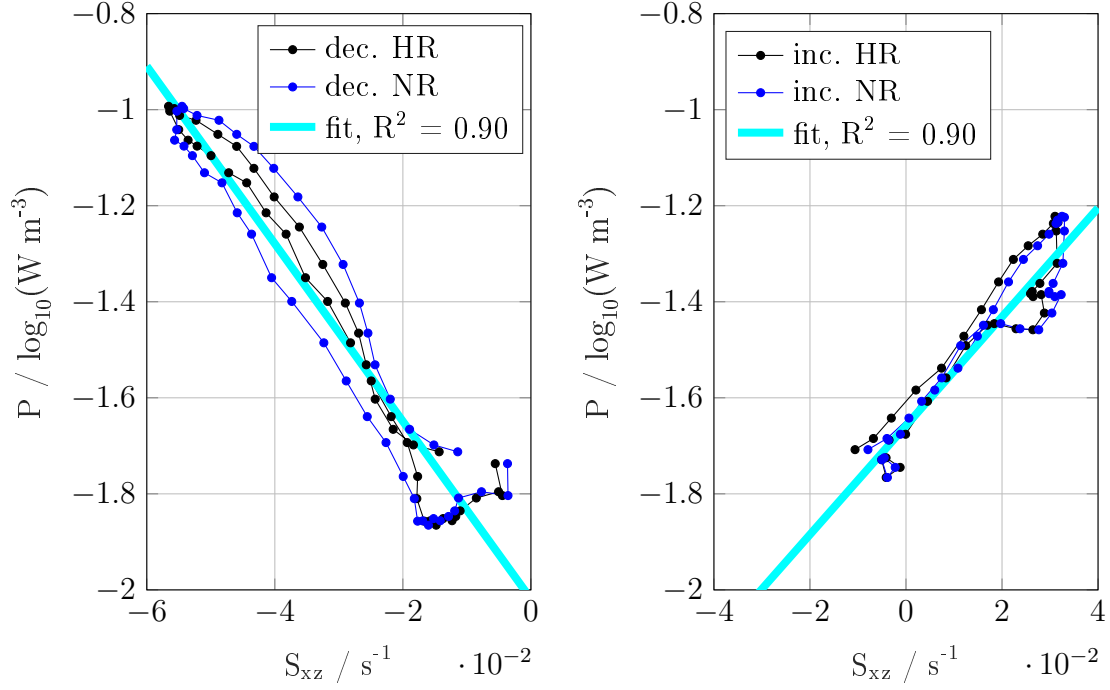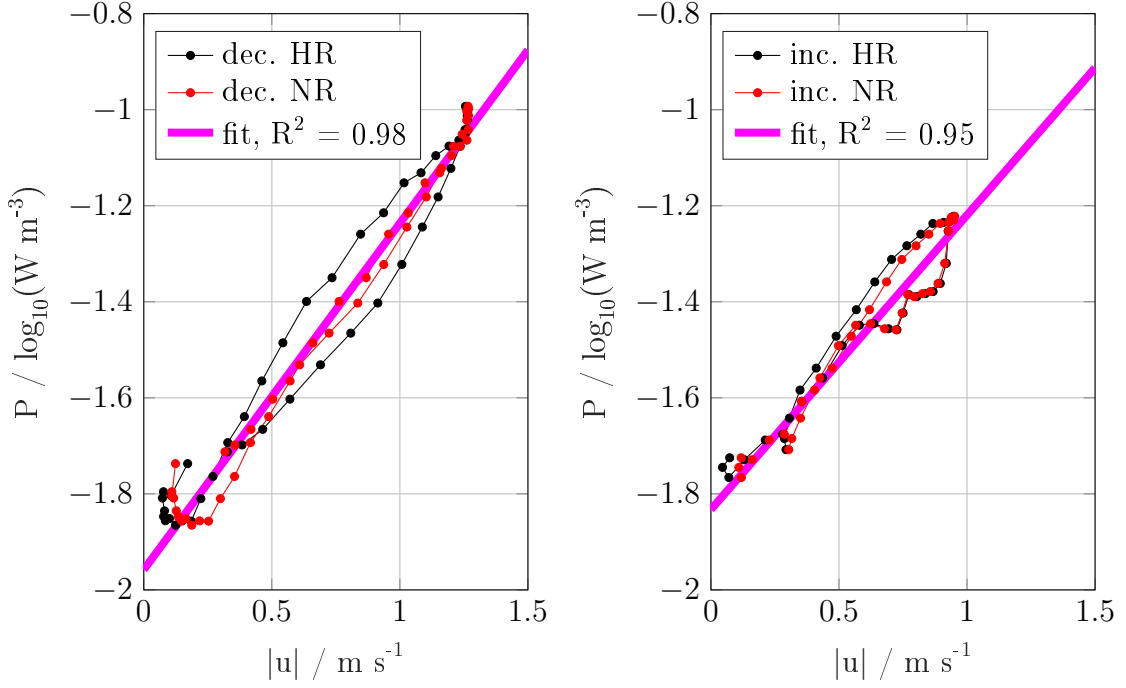
Figure 4.5: Depth averaged production rate P in $log_{10}(W\ m^{-3)}$ vs. velocity shear S_{xz} in s^{-1} - high resolution (HR, black) and down-sampled (non-high resolution, NR, blue). Separation into ebb (left) and flood period (right).

4.3.3   Threshold B

The threshold B can be described in the following way:

$$B = min(B_S, B_{|u|})$$ (4.4)

with the threshold depending on shear B_S being

$$B_S = -max(S_{xz}) + \Delta p,$$ (4.5)

the threshold depending on speed $B_{|u|}$ being

$$B_{|u|} = -max(|u|) \cdot 1.5$$ (4.6)

and the averaged tidal change Δp being

$$\Delta p = (\Delta p_{inc} + \Delta p_{dec})/2$$ (4.7)

Figure 4.6: Depth averaged production rate P in $log_{10}(W\ m^{-3)}$ vs. speed $|u|$ in $m\ s^{-1}$ - high resolution (HR, black) and down-sampled (non-high resolution, NR, red). Separation into ebb (left) and flood period (right).

(average of the difference of the increasing water level (flood) and decreasing water level (ebb)). In equation 4.3, $p2$ should be replaced by B as in equation 4.4.

4.3.4 Slope N

The magnitude of the slope N depended on the current tidal phase, so estimates differ between flood (inc.) and ebb (dec.) periods.

For estimating the slope based on shear data, we found the following relation:

$$N_{S,inc} = \Delta S_{inc} \cdot 300 \tag{4.8}$$

$$N_{S,dec} = -\Delta S_{dec} \cdot 1500; \tag{4.9}$$

Table 4.2: Fit coefficients and R^2-values of equations 4.2 and 4.3.

variable	complete tidal cycle	flood tide	ebb tide
shear	a = 14.6521	p1 = 11.3369	p1 = -18.4908
	b = -1.8279	p2 = -1.6581	p2 = -2.0188
	$R^2 = 0.7685$	$R^2 = 0.8989$	$R^2 = 0.9016$
speed	a = 0.6845	p1 = 0.6132	p1 = 0.7215
	b = -1.9064	p2 = -1.8328	p2 = -1.9580
	$R^2 = 0.9606$	$R^2 = 0.9457$	$R^2 = 0.9836$

and based on current speed:

$$N_{|u|,inc} = -max(|u|_{inc}) \cdot 0.3; \tag{4.10}$$

$$N_{|u|,dec} = -max(|u|_{dec}) \cdot 0.2; \tag{4.11}$$

These slopes (equations 4.8 until 4.11) should replace $p1$ in equation 4.3.

These equations for the threshold B and the slope N were estimated based on high resolution data sets of different months (September, October and December 2014; exemplified in figure 4.8). Based on the resulting values for the threshold B and the slope N, the following equation is used to reconstruct the production rate of turbulent kinetic energy:

$$log(P_{rec,separation}) = Nx + B. \tag{4.12}$$
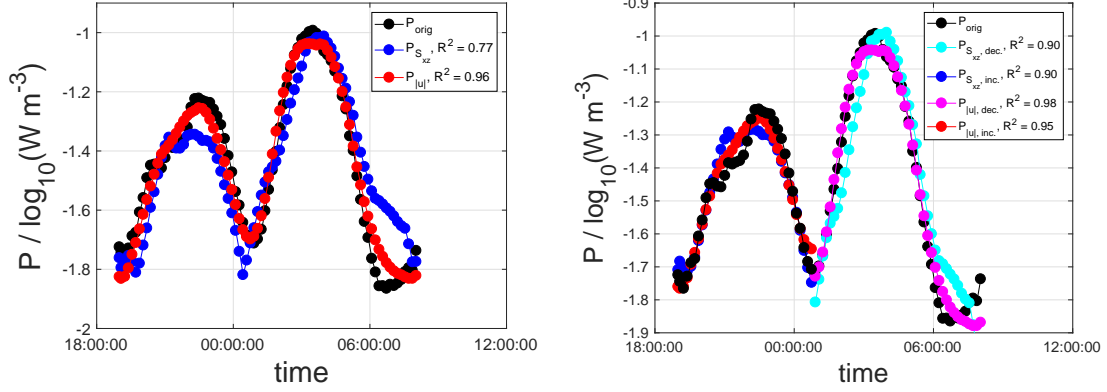
Figure 4.7: Comparison of originally estimated production rate P_{orig} of turbulent kinetic energy and the reconstructed ones from velocity shear $P_{S_{xz}}$ and speed $P_{|u|}$. Left: Reconstruction with equation 4.2 for the complete tidal cycle. Right: Reconstruction with equation 4.3 for ebb and flood separation.

4.4 Results

Relating the production rate of turbulent kinetic energy P to $P_{S_{xz}}$ based on estimates of velocity shear S_{xz} over the complete tidal cycle led to a correlation (quantity of goodness of fit) of $R^2_{Sxz} = 0.77$ (see figure 4.4, left). We found an additional relation between the production rate P and $P_{|u|}$ based on estimates of speed $|u|$ with $R^2_{|u|} = 0.96$ (see figure 4.4, right). Splitting the data into the flood period (increasing depth) and the ebb period (decreasing depth), improved the correlation to $R^2_{Sxz,inc,dec} = (0.90, 0.90)$ and $R^2_{|u|,inc,dec} = (0.95, 0.98)$ (see figure 4.5). Figure 4.7 shows the original estimates (black) and the reproduced production rates P (blue: reproduced values based on velocity shear $P_{S_{xz}}$, red: reproduced values based on speed of velocity $P_{|u|}$) from the down-sampled high resolution data set.

To evaluate whether this approach is suitable to estimate P based on data taken under varying environmental conditions, we applied our approach (equation 4.12) to other data sets. The results are shown in figure 4.8. The color-coding is the same as

in figure 4.7. The corresponding values of the quantity of goodness of fit are given
in table 4.3. R^2 was calculated with a linear regression function (poly1, MATLAB
R2013b). The R^2-values varied between $R^2_{min.} = 0.48$ and $R^2_{max.} = 0.87$. This
demonstrates that our approach is applicable for a variety of environmental condi-
tions.

Figure 4.8 shows also that the production rate of turbulent kinetic energy P varies
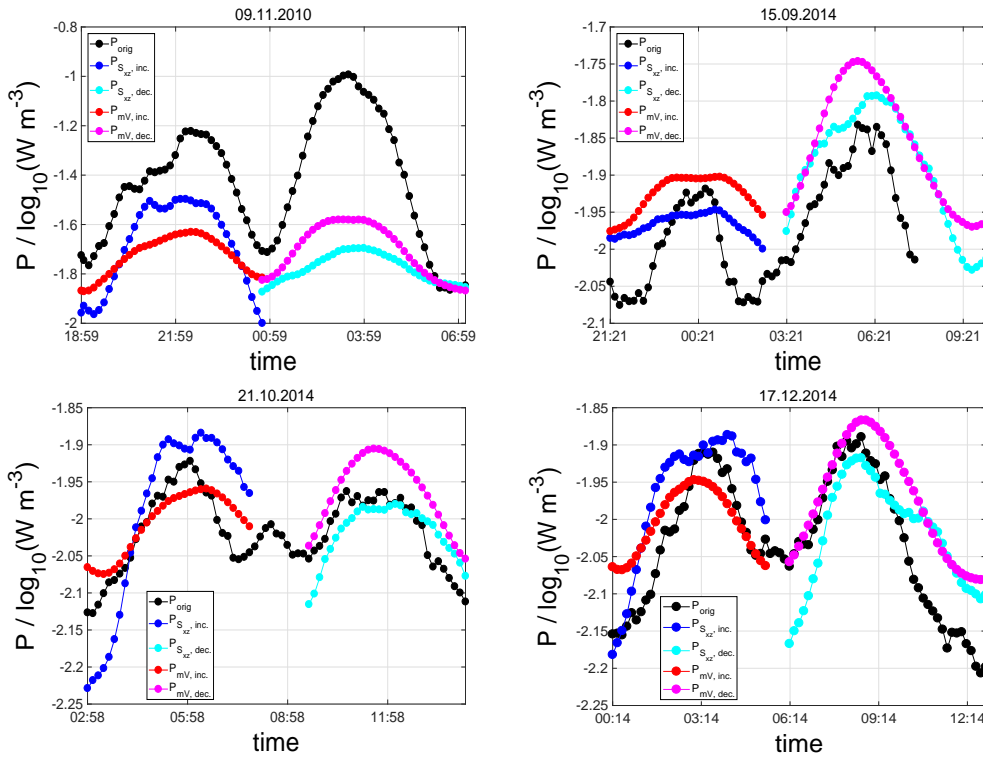

Figure 4.8: Reconstructed rates of production of turbulent kinetic energy. Top left:
HR data set from November 2010; top right: control data set from September 2014;
bottom left: control data set from October 2014; bottom right: control data set
from December 2014.

over time. Hence, the strength of the turbulence changes, too, both over different
time periods and over the tidal cycle. Using the control data sets, the reconstructed
and the originally estimated production rates correlate well (between $R^2_{min} = 0.48$
and $R^2_{max} = 0.99$). However, applying the method to the high resolution data

Table 4.3: Comparison between originally estimated production rates of turbulent kinetic energy and the predicted production rates of turbulent kinetic energy for different used reconstruction variables. R^2_{HR} derived from the HR data set (measured in November 2010) and R^2_{CD} estimated from the control data set (measured in 2014).

Reconstruction variable	R^2_{HR} (Nov. 2010)	R^2_{CD} (Sept. 2014)	R^2_{CD} (Oct. 2014)	R^2_{CD} (Dec. 2014)
S_{xz} inc	0.90	0.69	0.76	0.77
S_{xz} dec	0.90	0.64	0.50	0.48
$|u|$ inc	0.95	0.56	0.78	0.75
$|u|$ dec	0.99	0.80	0.87	0.85

set obtained in November 2010 leads to an underestimation of P (see figure 4.8 top left panel). For verification of the method different high resolution data set were used. First, the data sets were down-sampled. Afterwards, we applied the method to the control data sets obtained in September, October and December 2014. The reconstructed production rates varied over the tidal cycle within the same order of magnitude. Figure 4.8 presents the comparison of the originally estimated production rates P_{orig} (black) to the reconstructed production rate determined according to the different approaches.

Using the same approach to reconstruct P based on data obtained during a storm surge in October 2014 led to lower R^2-values between $R^2_{min,storm,2} = 0.18$ and $R^2_{max,storm,2} = 0.66$ (figure 4.9 left and table 4.4). We could not establish a correlation based on data obtained during the onset of the storm surge when water level stagnated during low tide (figure 4.10). However, the approach worked well ($R^2_{storm,2} = 0.66$) for data obtained during high tide, when the water level reached its maximum.
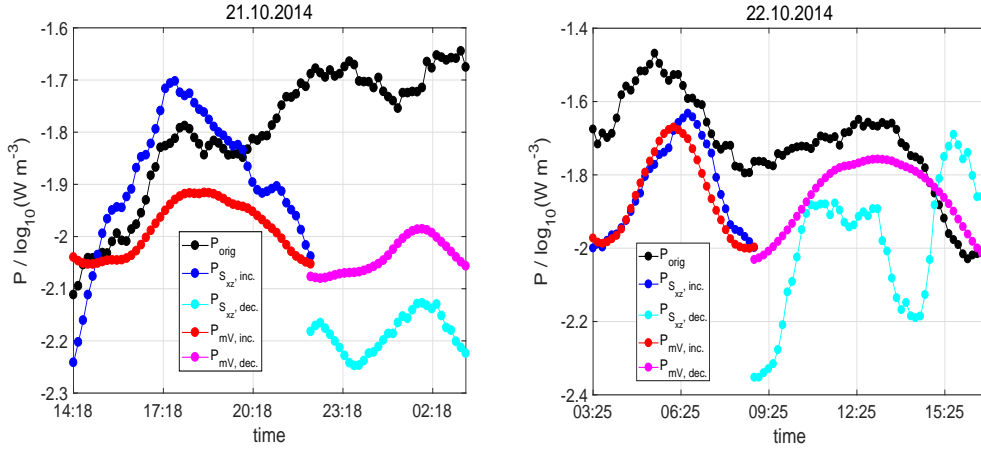
Figure 4.9: Reconstructed rates of production of turbulent kinetic energy during a storm surge at 21 and 22 October 2014. Figure 4.10 shows the corresponding water level from these two tides.

4.5   Discussion

The main goal of this work was to developed a method that makes existing long-term data sets of current velocities available for turbulence investigations. We find a robust relation between production rate of turbulent kinetic energy P and velocity shear S_{xz}. We were also able to establish a correlation between production rate P and speed $|u|$, which has not been described before. These correlations allow us to reconstruct the production rate of turbulent kinetic energy P from non-high resolution ADCP measurements of current speeds. This reconstruction is greatly improved by applying these additional correlation between P and $|u|$. Moreover, we showed that using different values for the threshold B and the slope N expands the applicability of our approach. In our view, the new method thus provides reliable and reasonable estimates of turbulence patterns from non-high resolution measurements of shear and speed velocities. This approach may prove particularly valuable when processing real-time data obtained from permanent stations or measurement platforms.
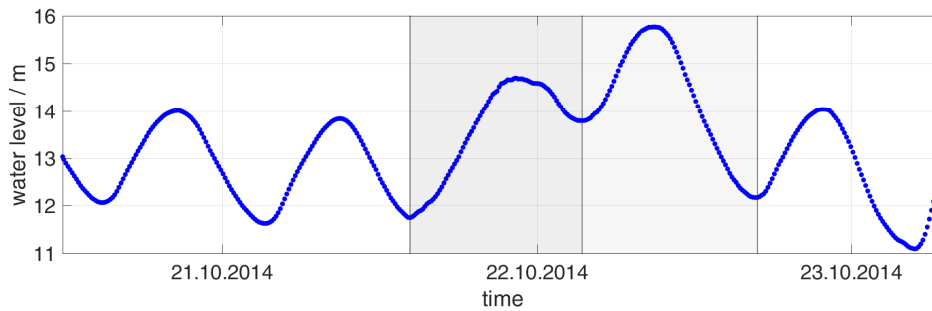
Figure 4.10: Water level in m during the storm surge in October 2014. Dark shaded: tidal cycle from 21 October 2014 (fig. 4.9, left); Light shaded: tidal cycle from 22 October 2014 (fig. 4.9, right).

Our findings also demonstrate that velocity shear has an important impact on the production rate of turbulent kinetic energy. This supports the results of previous studies, which have shown that shear over sub-tidal channels appears to be a significant mechanism for turbulence production (e.g. Ralston and Stacey, 2006). In addition, we present that the production rate can be predicted from the shear and current speed. According to equation 4.1, the production rate P should correlate to the cubed velocity value. However, we obtained the best results by using a linear regression with the velocity speed. Splitting the data into ebb and flood tides improved the correlation. This may be due to the ebb dominance in our research area, i.e. the tidal curves in the channels are steeper and the currents are faster during the ebb phase. For example, Stanev et al. (2003b) were able to demonstrate an asymmetry of the tidal phases in the research area.

However, our analysis also indicates that the approach is only applicable if each tidal cycle is treated separately. Certain environmental conditions, such as storm surges (at least parts of it), may further affect the correlation between the parameters. Even though we could only partly reconstruct special events such as storm surges, this approach provides first estimates of the turbulence.

Currently, our approach only takes into account the depth-averaged turbulent pro-

Table 4.4: Comparison between original production rate of turbulent kinetic energy
and the predicted production rate of turbulent kinetic energy for different used
reconstruction variables. R^2_{HR} derived from the HR data set (measured in November
2010) and R^2_{CD} estimated from the control data set (measured in 2014).

Reconstruction variable	$R^2_{storm,1}$ (Oct. 2014)	$R^2_{storm,2}$ (Oct. 2014)
S_{xz} inc	0.26	0.37
S_{xz} dec	0.02	0.18
$\lvert u \rvert$ inc	0.25	0.66
$\lvert u \rvert$ dec	0.05	0.37

cesses in the water column, so there could be other effects or influences distributed
over the water column. Therefore, we cannot evaluate the influence of factors that
act differently throughout the water column. Future studies may require a vertical
resolution of the relevant parameters.

Applying the approach to analyse extreme events such as storm surges also requires
further improvements, but may prove particularly helpful as turbulence patterns
are nearly impossible to measure under such harsh conditions. A model study by
Lettmann et al. (2009), focusing on the same research area as our study, indicated
that storm surges enhance the bottom shear stress through increased currents speeds
and dramatically increased wave activity. Consequently, turbulence should also
grow. A modeling study by Burchard (2009) suggests there is a stronger tendency
towards mixing in estuaries and coastal seas with prevailing onshore winds. In con-
trast, the tendency towards mixing decreases with prevailing offshore winds. For
future studies, it may thus be helpful to take wind speed and wind direction into
account.

4.6   Conclusions

We found correlations between velocity shear S, speed $|u|$ and production rate of turbulent kinetic energy P. Reliably estimating the thresholds B and slopes N was essential for the reconstruction of the rate of turbulent kinetic energy P. Unexpectedly, we were able to improve the reconstruction when using speed values instead of shear values.

Our results indicate that we can estimate turbulence from non-high resolution data sets of current velocity. Despite some shortcomings, such as the limited applicability for extreme events such as storm surges, our method can provide valuable insights into general patterns of turbulence under natural conditions. This is particularly helpful when studying turbulence in remote places or under environmental conditions where direct measurements of turbulence are not feasible.

In the future, we will apply the approach to other data sets of non-high resolution velocity data in coastal regions. We also plan to improve the method to make it better equipped for analyzing special events, such as storm surges, and for investigating the vertical patterns of turbulence in the water column. Additionally, we will take wind speed and wind direction into account. Such improvements would make it possible to analyze turbulence in coastal regions on seasonal scales.

5   Impact of currents and turbulence on turbidity dynamics at the Time Series Station Spiekeroog (Wadden Sea, southern North Sea)

Abstract   Shallow coastal areas with depths less than 20 m are high-energy regions where strong mixing processes occur mainly influenced by currents and turbulence. To investigate these mixing processes, it is necessary to obtain a high number of field observations of mixed variables as well as their interactions with other processes and dynamics.

In this context, our research platform (Time Series Station Spiekeroog) in the East Frisian Wadden Sea, southern North Sea, offers the opportunity to measure hydrodynamic and meteorological parameters over long time periods. This allows us to get insights into the natural processes of an intertidal ecosystem under various environmental conditions such as storm surges or algae blooms.

The objective of this paper was to investigate the impact of currents and turbulence on turbidity dynamics based on measurements at the Time Series Station Spiekeroog. Current velocities are continuously recorded in three dimensions from a bottom-mounted Acoustic Doppler Current Profiler (ADCP, RDI Workhorse Sentinel, 1200 kHz) with a high temporal and spacial resolution. These high resolution data sets are used to estimate turbulence using the production rate of turbulent kinetic energy. To determine turbidity, we used an ECO FLNTU sensor (WETlabs) which measured optical scattering at a wavelength of 700 nm while being mounted 12 m above the sea floor close to the sea surface.

Comparing the turbidity data set with the backscatter signal from the ADCP we could estimate the vertical structure of the turbidity. Further we compared the turbidity data set with current speed, production rate and velocity shear. Our results

showed a link between the production rate of turbulent kinetic energy and turbidity at slack water times. Although the research area is an ebb dominated system, we observed an opposite shaping of the turbidity and backscatter signals. Since current speeds, velocity shear and turbulence signals all show ebb dominance, we concluded that the production rate of turbulent kinetic energy holds the turbidity in the water column at high tides. At times with high current speeds the velocity shear and therefore the current velocities are responsible for the turbidity dynamics: At flood, the shear carries the turbidity up into the water column; In contrast, at ebb tide the shear prevents the transport to the sea surface.

5.1 Introduction

Turbidity is often used as an indicator for the quality of coastal waters. Turbidity reduces the visual range in water and light availability for photosynthesis (Davies-Colley and Smith (2001); Lemke et al. (2009)). It is defined as the reduction of transparency of a liquid caused by the presence of undissolved matter (ISO7027:1999, 2012). Hence, turbidity is the "cloudiness" of the water, which indicates the scattering capability of suspended particulate matter (SPM) in the water (Moore (1980); Garaba et al. (2014)). Especially in coastal regions with shallow water depths (less than 20 m) currents and turbulence lead to strong mixing processes. These high-energetic processes may lead to high turbidity in the water column, which affects the ecosystem at different levels.

The World Heritage Wadden Sea (southern North Sea) is the largest contiguous area of mud and sand flats in the world and offers a unique opportunity to study the influence of exchange and mixing processes on sediment transport and water turbidity. Here, the ICBM has been running a permanent research platform (Time Series Station Spiekeroog) in a tidal inlet of the East Frisian Wadden Sea since 2002.

Several sensors installed on this platform continuously record various hydrodynamic and meteorological parameters enabling insights into the natural processes of the intertidal ecosystem under various environmental conditions such as storm surges or algae blooms.

Several studies have previously dealt with the biogeochemistry of this dynamic ecosystem, above all the research group BioGeoChemistry of Tidal Flats (Rullkötter, 2009). Amongst others, the dynamics and budget of suspended particulate matter (SPM) and comparable parameters such as suspended sediment concentration (SSC) were investigated. The results revealed the impact of various environmental conditions, such as long-lasting strong winds and storm surges, and tidal currents on SPM and sediment transport (Cuneo and Flemming (2000); Bartholomä et al. (2009); Badewien et al. (2009)). Lettmann et al. (2009) modeled the impact of tidal currents, wind-enhanced currents and, wind-generated surface waves on SPM fluxes in the Wadden Sea area. Based on this approach they provided estimates of the total sediment budget of the region. Cuneo and Flemming (2000) inferred the concentration of SPM from the intensity of the backscatter signal of an Acoustic Doppler Current Profiler (ADCP). Bartholomä et al. (2009) showed a balanced budget of SSC during low energy (i.e. calm / fair weather) conditions and a remobilization of sediment by tidal current entrainment. During high-energy conditions (like strong wind events or storm surges), flow and transport of SSC are controlled by interference of wind/wave and tidal phase. The above mentioned studies applied different methods to estimate SPM, including water samples for SPM filtration and optical approaches (Laser-In-Situ-Scattering-and-Transmissometry (LISST), multispectral transmissometry (MST), Self-Contained Underwater Fluorescence Apparatus (SCUFA)). These data were analysed together with ADCP velocity and backscatter measurements and meteorological data sets (wind speed and direction).

While these studies have provided important insights into the large-scale dynamics

of SPM and sediment exchange processes, only few investigations focused on turbidity dynamics and the influencing factors on smaller spacial and temporal scales (Burchard et al., 2008). Moreover, considerable turbulent processes occur in the tidal flats due to the tidal currents even under calm weather conditions. It is therefore necessary to investigate the influence of turbulence on turbidity dynamics.

The aim of this paper is to investigate the influence of tidal currents and the resulting turbulent mixing on turbidity dynamics. Of special interest are the remobilization and the transport of substances in the water column. In a previous study, we developed a method to estimate the turbulence parameter P (production rate of turbulent kinetic energy, TKE) based on long-term ADCP measurements at the Time Series Station Spiekeroog (Schulz et al., 2018). In this paper, we analyze and discuss a subset of these long-term data. Our investigations provide new insights into the dynamics within a tidal channel and into the interaction between turbidity, currents and turbulence.

5.2   Methods

5.2.1   Research area & Time Series Station Spiekeroog

The natural strong dynamics of the tidal currents constantly change the appearance of the Wadden Sea, particularly in the inlets between the islands (e.g. Stanev et al., 2003a). The Time Series Station (TSS) is located in the tidal channel between the islands of Langeoog and Spiekeroog (53°45'01.0"N, 007°40'16.3"E) in the Southern North Sea (German Bight). At this Time Series Station, the mean sea level is 13 m with a tidal amplitude of about 3 m and the magnitude of the current velocity reaches values up to 2 $m\ s^{-1}$ (Reuter et al., 2009).
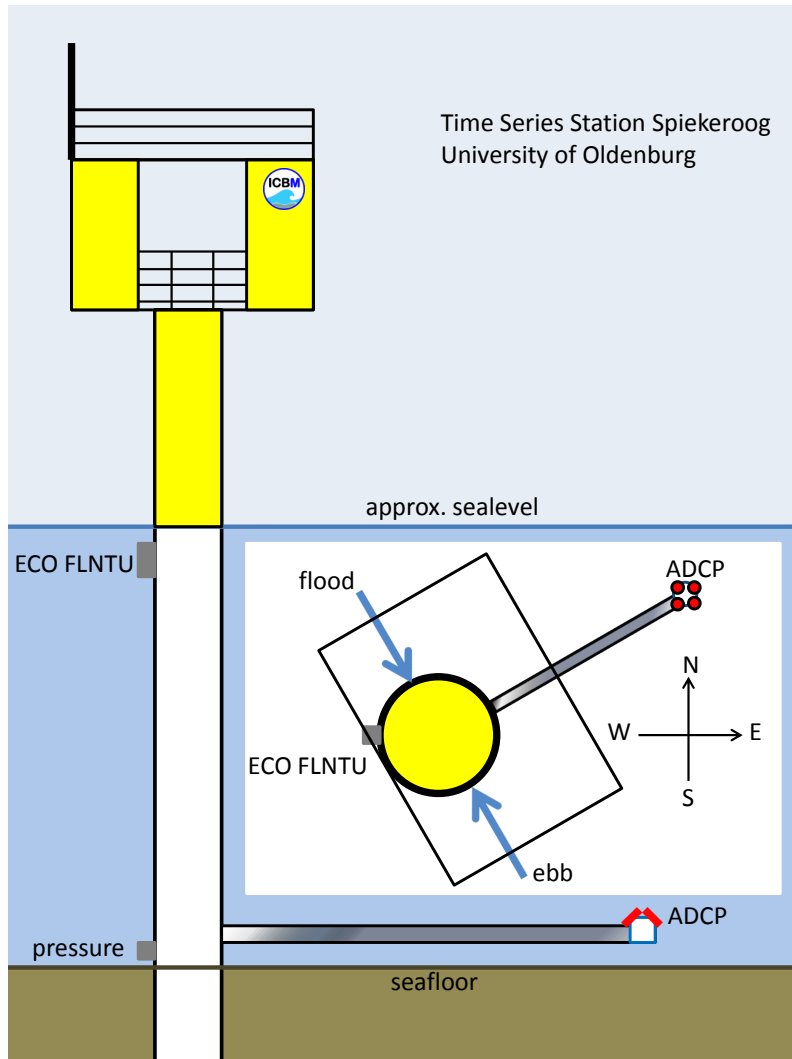
Figure 5.1: Sketch of the Time Series Station Spiekeroog (TSS) and the setup of the used measurement devices: ADCP, ECO FLNTU and pressure sensor. In small: the top view with the main flow directions (flood and ebb, 120° and 300°) and positions of the used measurement devices.

5.2.2   Experimental Setup

The TSS provides the opportunity to measure hydrodynamic and meteorological parameters over long time periods. In this study, we focus on the impact of currents

and turbulence on turbidity dynamics. This is achieved by using ADCP data sets of the current velocity and turbulence estimates deduced from the same ADCP data. This is added by an ECO FLNTU data set for turbidity.

Acoustic Doppler Current Profiler - ADCP   At the TSS, current velocities are continuously measured in three dimensions with a bottom-mounted Acoustic Doppler Current Profiler (ADCP, RDI Workhorse Sentinel, 1200 kHz) with a high temporal ($\Delta t_{ADCP} = 0.8\ s$) and vertical resolution ($\Delta z_{ADCP} = 0.20\ m$). The ADCP is fixed to a horizontal boom at a distance of about 12 m from the TSS. This means the station itself does not disturb the current measurements. The high-resolution data sets are used to estimate turbulence. We used the production rate of turbulent kinetic energy P as a measure of turbulence, which is defined as (e.g. Rippeth et al., 2003):

$$P = \tau_{ij} S_{ij} = -\rho \overline{u_i' u_j'} \frac{\partial \overline{u_i}}{\partial x_j} \tag{5.1}$$

with Reynolds s τ_{ij}, velocity shear S_{ij} and seawater density ρ The velocity fluctuations $u_{i,j}'$ and the spacial derivative x_j of the averaged velocity $\overline{u_i}$ in accordance to the Reynolds decomposition ($u = \overline{u} + u'$ - averaging period: 10 minutes) were used to estimate the production rate of turbulent kinetic energy P. Velocity shear S_{ij} is an important factor for estimating turbulence (e.g. Ralston and Stacey, 2006). Thus, velocity shear S_{ij} can be used as an indicator for turbulence, especially for the production rate of turbulent kinetic energy P. These variables were estimated by high resolution measurements of current velocity components.

Environmental Characterization Optics (ECO) FLNTU sensor   To determine turbidity, we used an ECO FLNTU sensor (WETlabs), which measures optical scattering at a wavelength of 700 nm. The sensor is mounted to the station 12 m above the sea floor and thus close to the sea surface. Since the tidal range is about

3 m at this side. At low tide, the sensor may occasionally be above the sea surface. In these cases, no reliable data sets can be obtained. These periods were removed from the data set by using water level data derived from a pressure sensor. The turbidity data set has a temporal resolution of 1 minute ($\Delta t_{FLNTU} = 60\ s$).

5.2.3 Data analyses

The data sets used were collected between 28 April 2014, 14:40 h and 30 April 2014 at 8:10 h. This period was chosen due to the following reasons: The weather conditions were calm with wind speeds between 2 $m\ s^{-1}$ and 6 $m\ s^{-1}$ from all wind directions. Moreover, as optical sensors are particularly affected by bio-fouling due to the high productivity in the area, we chose a period that yielded reliable data after cleaning of the sensor during a maintenance visit to the station.

While the turbidity (ECO FLNTU) data were measured at a fixed height above the seafloor, the ADCP data set covers the entire water column. To compare the data, we chose that part of the ADCP data set, which corresponds to the water depth of the turbidity data. Although the ECO FLNTU sensor is located 12 m above the seafloor and we chose ADCP data obtained from highest depth layer (9.60 m) which is lying (directly) under low tide water level with reliable ADCP data. Because of disturbances of the acoustic signal close to the sea surface, the data derived from near-surface measurements are less reliable.

Due to the different sampling rates, we developed a time vector with 1 minute time steps. Additionally, we smoothed the data sets over 10 minutes. The estimated production rate of the turbulent kinetic energy P has a sampling rate of 10 minutes (averaging period for Reynolds decomposition, see equation 5.1). We interpolate these values to the same time vector (with 1 minute time step) with linear interpolation.

Figure 5.2 show data sets of the turbidity (TRB / NTU), turbulence (produc-
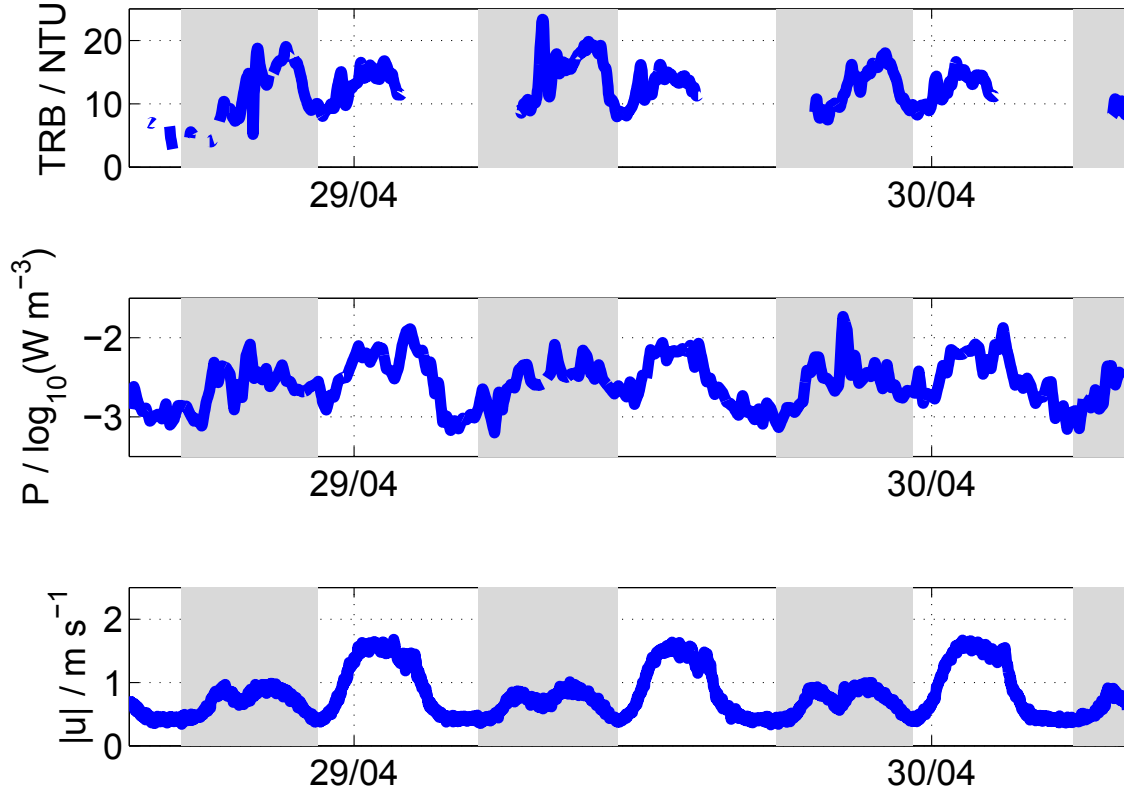
Figure 5.2: Time series of turbidity (TRB in Nephelometric Turbidity Unit NTU (Nephelometric Turbidity Unit); ECO FLNTU - top), production rate of TKE (P in $log_{10}(Wm^{-3})$; ADCP - middle) and speed of the current velocity ($|u|$ in ms^{-1}; ADCP - bottom) over the measurement period from 28 to 30 April 2014. Grey shaded: flood period and rest: ebb period.

tion rate P / $log_{10}(W\ m^{-3})$) and speed ($|u|$ / $m\ s^{-1}$) over the study period with a time vector with 1 minute time steps. The different signals correlate (see figure 5.3, $R^2_{P,TRB} = 0.5$ and $R^2_{|u|,TRB} = 0.36$), but there are differences between the flood (grey shaded) and ebb phases. We divided the signals into flood and ebb periods, based on the pressure data measured close to the seafloor at the station (a sketch of the Time Series Station and the setup of the measurement devices used are shown

in figure 5.1), and compared them to each other (figure 5.3).

Figure 5.2 shows that the production rate P and the turbidity TRB have minima during low tide. Both turbulence data and current speed shows an ebb dominated signal. Contrary to this, the turbidity signal shows a stronger flood signal (see figure 5.2). To simplify the correlation between backscatter signal BS and turbidity
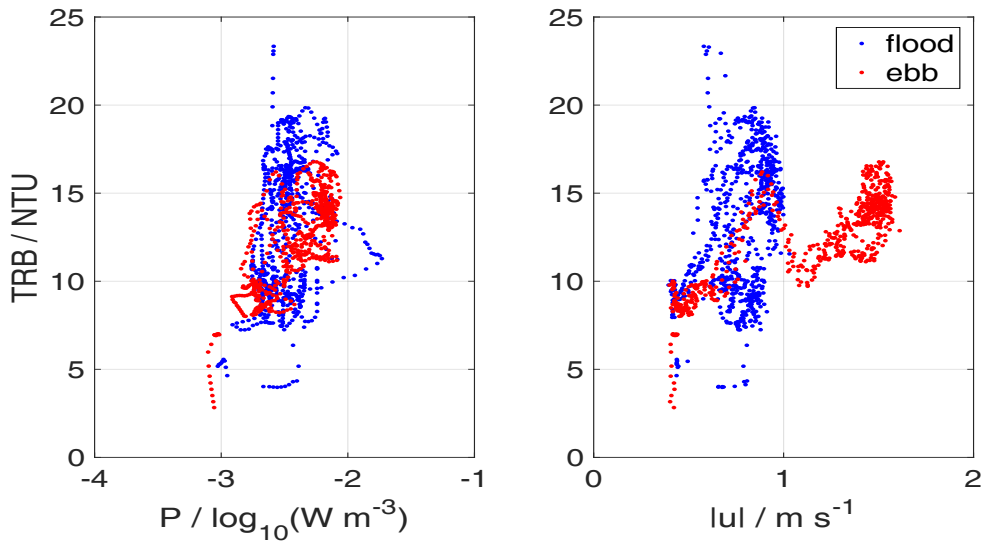
Figure 5.3: Graphic correlation between the production rate P in $log_{10}(Wm^{-3})$ TRB and speed of the current velocity $|u|$ in $m\ s^{-1}$ against turbidity TRB in NTU. Blue: correlation during flood and red: correlation during ebb.

TRB, we smoothed the data sets with an hourly (60 minutes) average. The results are shown in figure 5.3. This allows us to calculate turbidity based on fitting the backscatter ($BS\ /\ counts$) ADCP data to the ECO FLNTU data set using a quadratic polynomial function (see equation 5.2). The goodness of fit is $R^2\ =\ 0.74$. The regression function is fitted with a second degree polynomial ('poly2') function:

$$TRB = p_1 BS^2 + p_2 BS + p_3,\qquad(5.2)$$
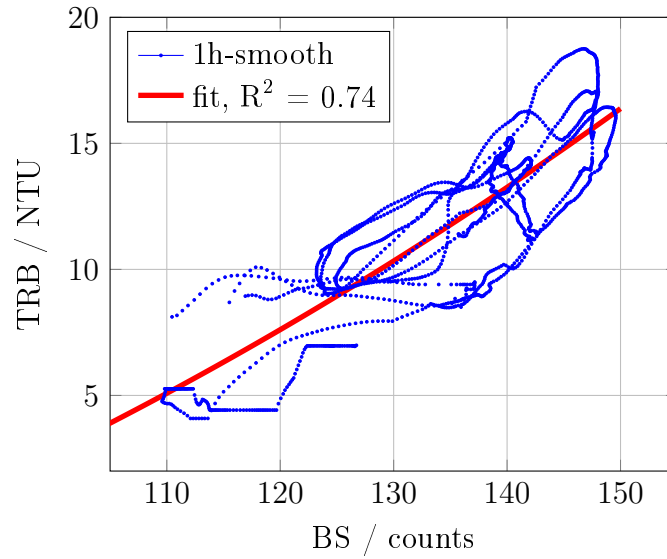
Figure 5.4: Correlation between backscatter signal BS in *counts* against the turbidity TRB in NTU. Red line: regression line with a quadratic polynomial function, goodness of fit $R^2 = 0.74$.

with coefficients $p_1 = 0.0010$, $p_2 = 0.0220$ and $p_3 = -9.4453$ (see figure 5.4). The turbidity data set TRB_{calc} derived from this calculation is shown in figure 5.5. The contour-plot shows the calculated turbidity versus depth. The red line depicts the turbidity data taken from the ECO FLNTU sensor. The green line depicts TRB_{calc} at the same depth. The calculated turbidity data show a good agreement with the original turbidity data. Figure 5.5 shows the vertical structure of the reconstructed turbidity over depth.

5.3   Results

The surface data of backscatter BS and turbidity TRB (figure 5.4) with 1 hour average correlate well ($R^2 = 0.74$). This implies, that estimating turbidity from the ADCP data yields reasonable results. Figure 5.5 shows the vertical structure of the turbidity derived from the ADCP data. The concentration of TRB_{calc} at 2 m
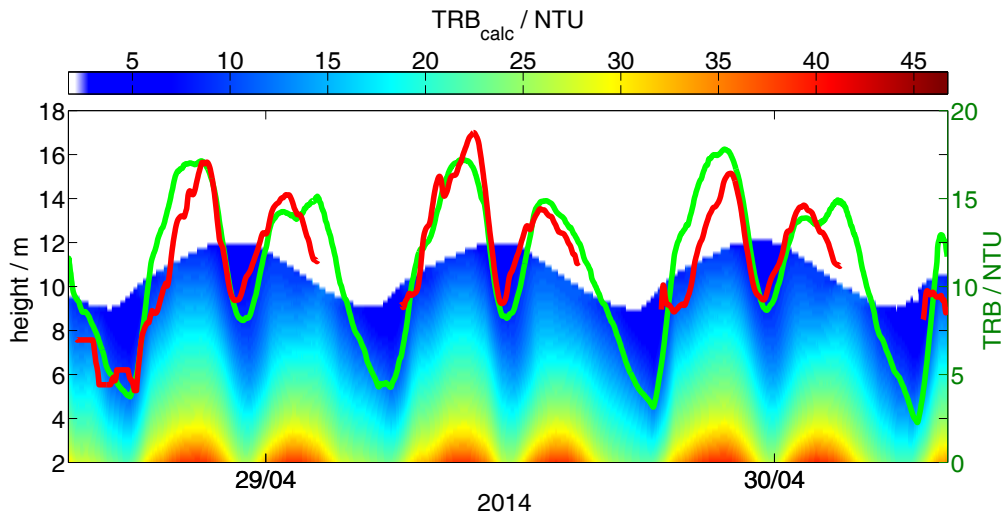
Figure 5.5: Calculated turbidity TRB_{calc} from backscatter signal BS, red: original turbidity TRB and green: calculated TRB_{calc}, both in NTU.

above the seafloor rises up to 43 NTU when current speed is at its maximum during flood and ebb (figure 5.8). About 8 m above the seafloor an asymmetry develops to a stronger flood signal (from 1 NTU up to 4 NTU differences between flood and ebb signals).

Figure 5.6 shows the production rate of turbulent kinetic energy P over time and depth. Here, we see different patterns throughout the water column. During flood, we see high production rates near the seafloor (up to -1.16 $log_{10}(Wm^{-3})$), which decreases towards the sea surface (down to -3.25 $log_{10}(Wm^{-3})$). During ebb, there are two areas with higher values of production rates. One is also near the seafloor (with values up to -1.12 $log_{10}(Wm^{-3})$). The other one is close to the sea surface during the beginning of the ebb period (up to -1.57 $log_{10}(Wm^{-3})$). During low water P has values of about -3.1 $log_{10}(Wm^{-3})$. During high water, P has values of about -2.8 $log_{10}(Wm^{-3})$. There is a difference in production rate at slack water, with higher production rates at high water than at low water.

The lowest turbidity values were observed during slack water (figures 5.6 and 5.7).

However, values were lower at slack water during low water (7.5 NTU) than during high water (8.5 NTU).

Figure 5.8 displays the current speed (magnitude of the current velocity $|u|$) with
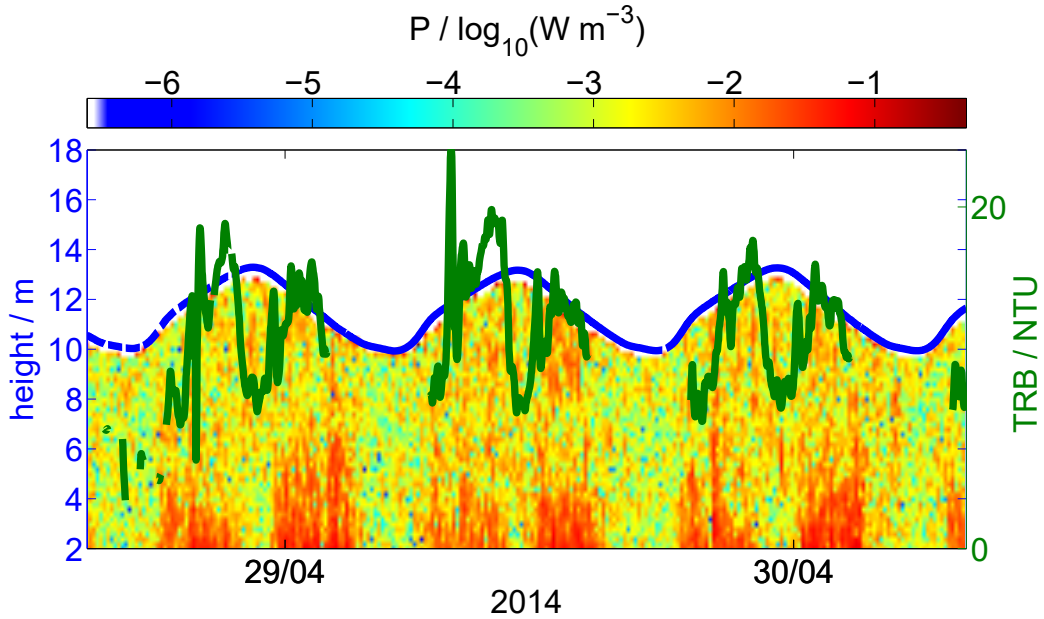
Figure 5.6: Comparison between production rate of turbulent kinetic energy P in $log_{10}(Wm^{-3})$ over time and depth (contour) and the turbidity TRB in NTU (green) near the sea surface. Blue: pressure (sea level) in m.

lower currents speeds during flood (up to 1.1 $m\ s^{-1}$) than during ebb tide (up to 1.7 $m\ s^{-1}$). During slack water times (both high and low water), values range from 0.3 $m\ s^{-1}$ to 0.4 $m\ s^{-1}$. This implies that current speed does not drop to zero during slack water. The current speed generally increases with increasing distance from the seafloor. While both current speed $|u|$ and turbidity TRB show a tidal signal, the maximum values do not correspond well. The speed signal peaks during ebb while the turbidity signal peaks during flood.

Figure 5.9 shows the velocity shear S_{xz} derived from the along channel (x) velocity
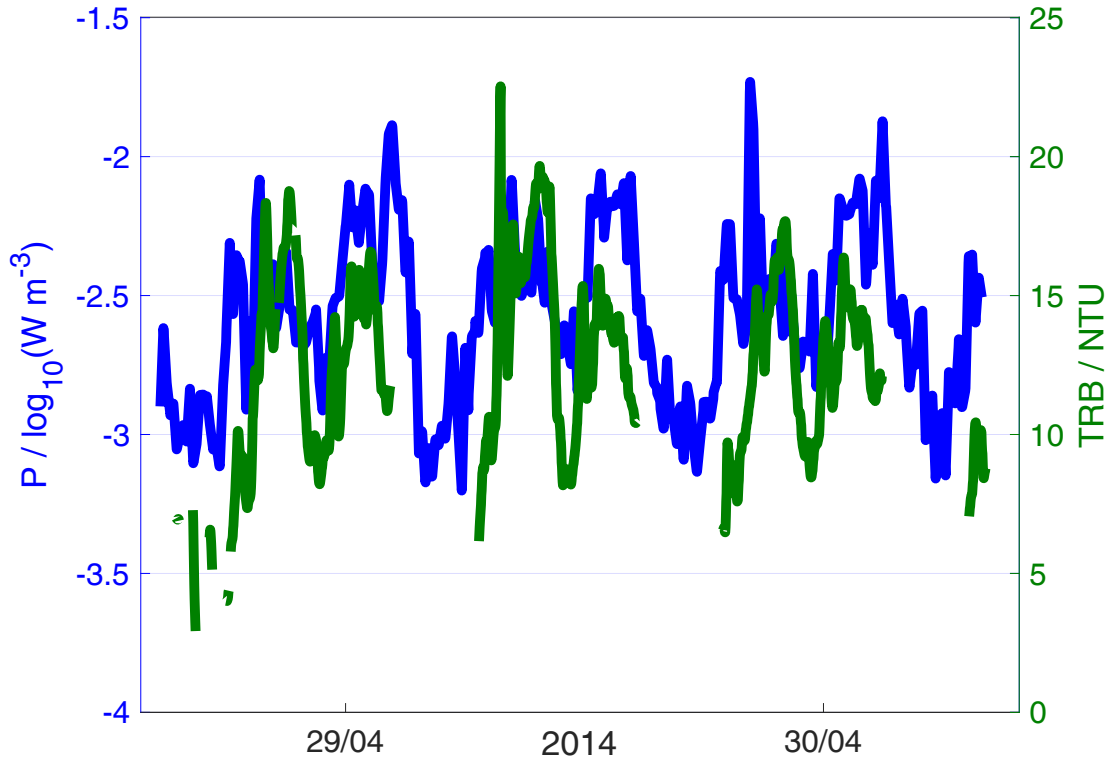
Figure 5.7: Time series of production rate P in $log_{10}(Wm^{-3})$ (blue) and the turbidity TRB in NTU (green).

$u_{\parallel}$ over depth (z) and the turbidity data set obtained close to the sea surface. The velocity shear signal shows different patterns near the seafloor and near the sea surface. The pattern near the seafloor shows at clear tidal cycle with values up to 0.1 s^{-1} at flood and values up to -0.11 s^{-1} at ebb. The sign of the shear indicates the direction in which the shear acts. A positive value indicates the along channel inflow direction (flood) and a negative value indicates the opposite direction (ebb). Velocity shear is highest near the sea surface during both flood and ebb. Here, the shear acts in the same direction. But the strength of the shear differs between flood (values about 0.05 s^{-1} with maximal values up to 0.06 s^{-1}) and ebb (values vary between 0.07 s^{-1} and 0.08 s^{-1}). These patterns of shear S_{xz} (figure 5.9) are similar
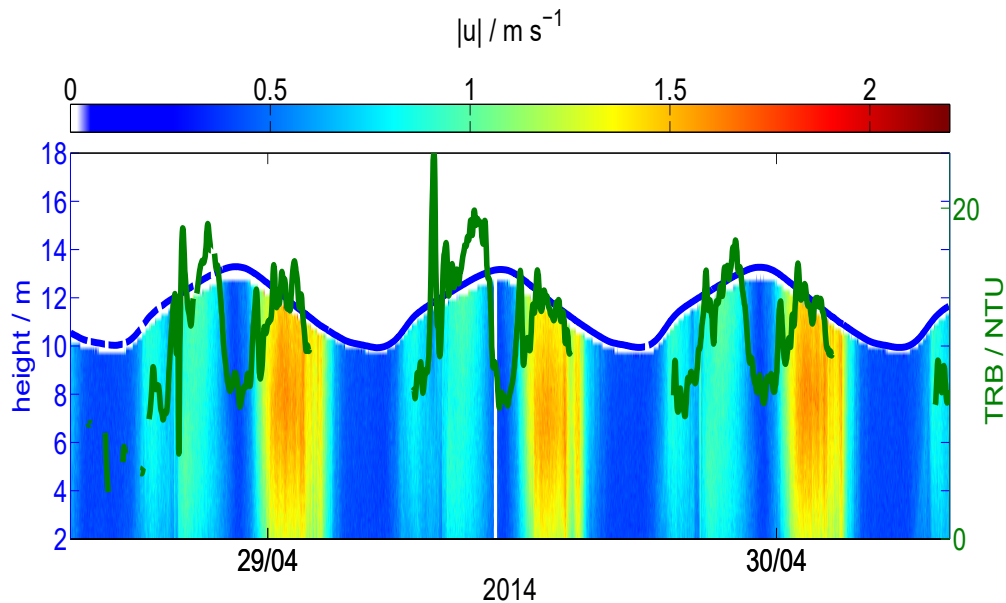
Figure 5.8: Comparison between speed of the current velocity $|u|$ in $m\ s^{-1}$ over time and depth (contour) and the turbidity TRB in NTU (green) near the sea surface. Blue: pressure (sea level) in m.

to patterns of production rate P (figure 5.6). Remarkably, during ebb the direction of the velocity shear differs between the sea surface and bottom.

Velocity profiles of the along channel component are shown in figure 5.10. Positive values indicate the inflow (flood) and negative values the outflow (ebb). The profiles obtained during flood (left) show a typical structure, with minimum values (between $0.6\ m\ s^{-1}$ and $0.7\ m\ s^{-1}$) near the seafloor and maximum values near the sea surface (between $0.88\ m\ s^{-1}$ and $0.9\ m\ s^{-1}$). The profiles obtained during ebb (right) show an overall slight increase of the velocity from around -1.2 $m\ s^{-1}$ near the seafloor to values ranging from -1.3 $m\ s^{-1}$ to -1.4 $m\ s^{-1}$ near the sea surface. However, there is a maximum of about -1.5 $m\ s^{-1}$ between 6 m to 7 m above the seafloor. The velocities (speed and along channel component) shows a stronger ebb than flood signal over the entire water column.
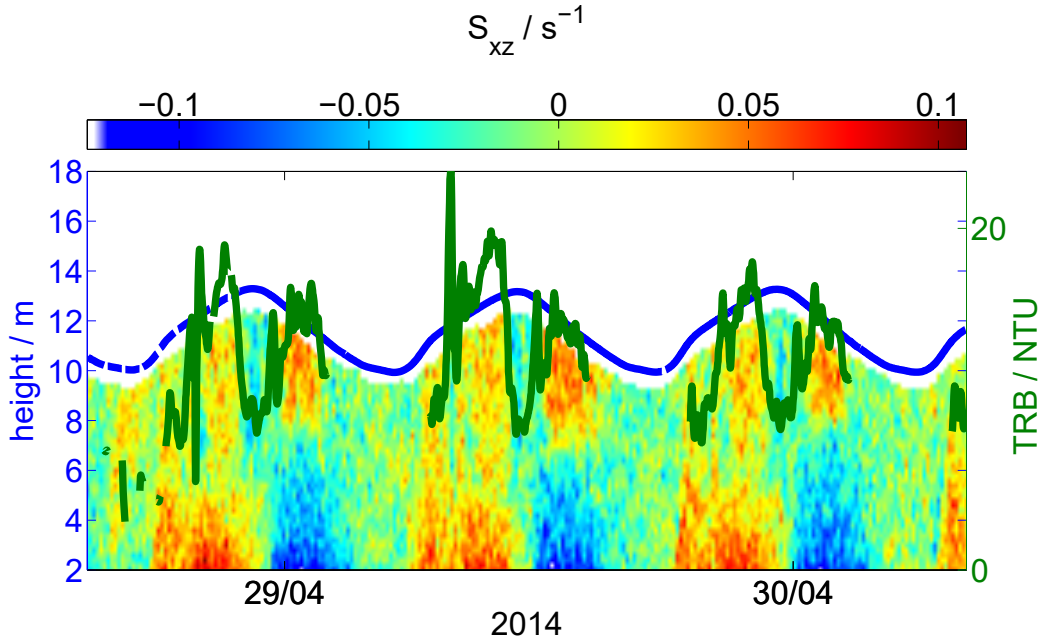
Figure 5.9: Comparison between velocity shear along the tidal channel S_{xz} in s^{-1} over time and depth (contour) and the turbidity TRB in NTU (green) near the sea surface. Blue: pressure (sea level) in m.

5.4   Discussion

In this study, we show that turbidity data TRB derived from optical methods correlate well with turbidity estimates derived from the backscatter signal BS of ADCP measurements ($R^2 = 0.74$, see figure 5.4). Both methods yield data that can be used as indicators for the amount of sediment in the water. However, only by using ADCP-derived estimates can the vertical distribution of turbidity be analyzed. Backscatter BS and turbidity TRB show similar patterns over the tidal cycle. This pattern, however, contrasts with the tidal course of the turbulence production rate P, current speed $|u|$ and velocity shear S_{xz}. We could therefore not establish a clear relation between the turbidity data and the turbulence parameters and current speed.
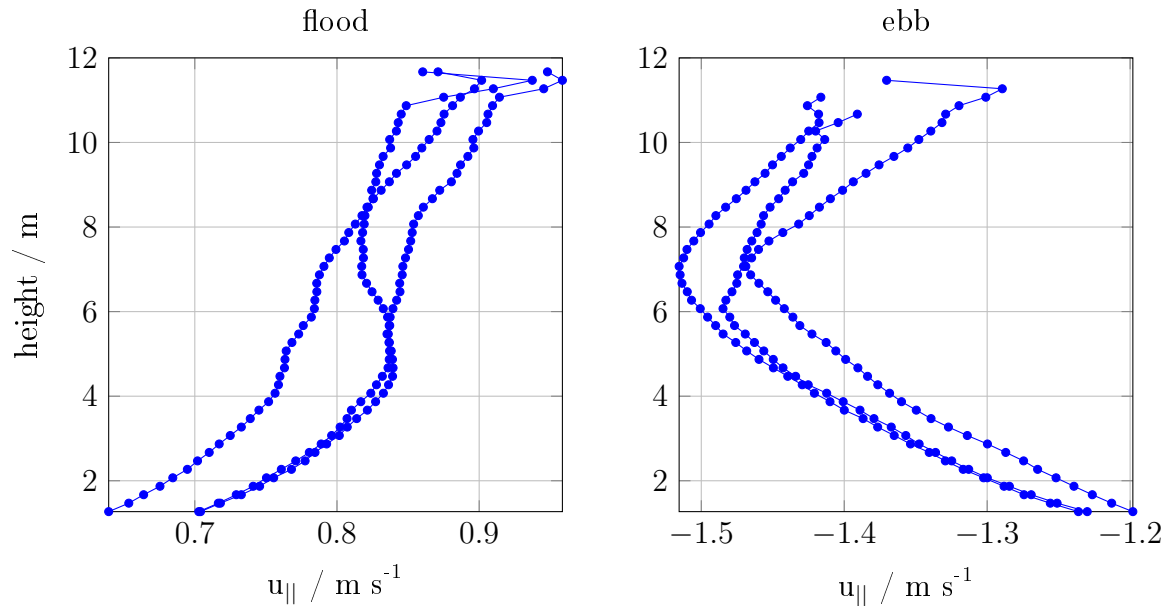
Figure 5.10: Hourly averaged profiles of along channel current velocity at maximum speeds - flood (left) and ebb (right) periods.

Stanev et al. (2003a) and Lettmann et al. (2009) showed in different modeling studies that the research area is ebb dominated. Our results for current speed, production rate, as a measure of turbulence, and velocity shear seem to support these modeling results.

The differences between the strength of the flood and ebb periods could result from the unusual velocities shear during ebb. Hence, the velocity shear may not be sufficiently high to induce turbidity upwards into the entire water column. To further support this assumption we would need additional measurements of turbidity in different water depths during ebb throughout several tidal cycles.

Also the location of the measurement devices at the station (see figure 5.1) may have influenced the turbidity measurements. While the ADCP signal is unaffected by the station, the turbidity sensor may have been influenced because it is mounted directly to the pole.

At this measurement period the environmental conditions have only a slight impact

on the results. On 29 April 2014 was new moon, so spring tide was three days later. The weather conditions were relatively calm with maximum wind speeds up to 6 $m\ s^{-1}$.

During slack water, the decreasing turbulence allows particles to settle down to the bottom. This can be seen in figures 5.6 and 5.7 that show that turbidity TRB and the turbulence production rate P decrease when current speed $|u|$ is at a minimum (figure 5.2 and 5.8). The minimum values of both production rate P and turbidity TRB are reached during low water. During the brief high water period, the production rate does not decrease to the same degree. Turbidity TRB is also higher than at low water times. This implies that the remaining production rate P is sufficient to keep particles floating (figures 5.2, 5.6 and 5.7).

During ebb tide, there are high values of production rate P near the sea surface and near the seafloor. This results from the velocity shear (relation between production rate and shear are shown in equation 5.1). Other investigations showed, that the velocity shear is the main influencing factor (Ralston and Stacey, 2006) for turbulence development and continuity. The contrasting velocity shear pattern during ebb tide results from the untypical distribution of current velocity during ebb.

Our results of production rate P show comparable results in strength (maximum values up to -1 $log_{10}(Wm^{-3})$ to -1.5 $log_{10}(Wm^{-3})$ and minimum values down to -4 $log_{10}(Wm^{-3})$ to -4.3 $log_{10}(Wm^{-3})$) to other investigations of the production rate (Rippeth et al. (2002, 2003); Wiles et al. (2006)) with nearly the same current speeds (between 1 $m\ s^{-1}$ and 1.7 $m\ s^{-1}$) in tidal channel.

5.5   Conclusion

We have shown that during slack water the remaining turbulence (production rate of turbulent kinetic energy P) is sufficiently strong to keep particles within the water

column. We observed two distinct high turbulent regions (high values of production rate P) during ebb tide (near the sea surface and near the seafloor). This probably results from contrary acting shear stress that weakens the transport of sediment particles to the surface (figure 5.9).

To validate ADCP-derived estimates of the vertical structure of turbidity, we have to conduct further measurements. It would also be useful to the study to have a variety of environmental conditions, such as storm surges, algal blooms and periods with sea ice.

In the future, high resolution turbidity data derived from ADCP measurements may be useful for interdisciplinary studies on biogeochemistry and sediment transport in the study area. We also plan to extend our research to other parameters such as oxygen and the influence of currents and turbulence on these.

6   Acoustic and optical methods to infer water transparency at the Time Series Station Spiekeroog, Wadden Sea

Abstract   Water transparency is a primary indicator of optical water quality that is driven by suspended particulate and dissolved material. A data set from the operational Time Series Station Spiekeroog located at a tidal inlet of the Wadden Sea was used to perform (i) an inter-comparison of observations related to water transparency, (ii) correlation tests among these measured parameters, and (iii) to explore the utility of both acoustic and optical tools in monitoring water transparency. An Acoustic Doppler Current Profiler was used to derive the backscatter signal in the water column. Optical observations were collected using above-water hyperspectral radiometers and a submerged turbidity meter. Bio-fouling on the turbidity sensors optical windows resulted in measurement drift and abnormal values during quality control steps. We observed significant correlations between turbidity collected by the submerged meter and that derived from above-water radiometer observations. Turbidity from these sensors was also associated with the backscatter signal derived from the acoustic measurements. These findings suggest that both optical and acoustic measurements can be reasonable proxies of water transparency with the potential to mitigate gaps and increase data quality in long-time observation of marine environments.

6.1   Introduction

Over the past decades, scientists, policy makers, and the public have become more aware of issues of environmental concern such as water quality (WFD, 2000; OECD,

1993; Borja et al., 2013). To better understand the dynamics of water quality, it is necessary to use different platforms and tools, which allow for collecting data over a broad range of temporal and spacial scales (Zielinski et al., 2009; Pearlman et al., 2014). The information from these different tools ought to be comparable for a comprehensive and reliable view of these dynamics. Water quality in general is the state of a water body parameterized according to predefined thresholds typically grouped according to ecological, chemical, optical or morphological properties. Water transparency is determined from optical observations that involve using the human eye as a tool or methods that replicate the human eye sensing approach (Moore et al., 2009). Optical water quality has been determined for decades as the tools needed are easy to use, fast, inexpensive and robust. Common optical observations provide information about the light availability in the water column, which can be translated into water transparency. Turbidity is one such measurement referring to a relative index of water cloudiness influenced by the inherent dissolved and particulate material (Kirk, 1985; Moore, 1980). Another parameter derived from ocean color remote sensing is remote sensing reflectance (R_{RS}) also known as an essential climate variable. R_{RS} is a proxy for the apparent color of water driven by optically active constituents of water (Garaba et al., 2015; Garaba and Zielinski, 2013; GCOS, 2011; Morel, 1980). The natural color of water, driven by the optically active constituents of water and environmental conditions, can be distinguished using a standard Forel-Ule comparator scale. The Forel-Ule color scale assigns numbers to the color of a natural water body, ranging from 1 (indigo-blue) to 21 (cola brown). This information can also be derived from R_{RS} information (Garaba et al., 2014; Wernand and van der Woerd, 2010).

Over the past decades, measurement methods based on acoustic backscatter have been increasingly used to estimate the abundance and distributional patterns of suspended matter (Deines, 1999; Thorne et al., 1991). Indeed, acoustics is one of

those technologies advancing our capabilities to probe sediment processes (Thorne
and Hanes, 2002; Voulgaris and Meyers, 2004). The acoustic backscatter signal is
used to quantitatively determine suspended matter and therefore relates to turbidity
(Deines, 1999; Lohrmann, 2001; Schulz et al., 2015). Therefore, acoustic backscatter
signals provide information about the suspended material in a given water body and
enable to record the changes over a long timescale. An Acoustic Doppler Current
Profiler (ADCP), for example, measures non-intrusively and three-dimensionally,
making it a very powerful tool for examining small-scale sediment transport pro-
cesses (Thorne and Hanes, 2002; Schulz et al., 2015).

The composition and concentration of suspended material is highly variable in
coastal and estuarine regions (Winter et al., 2007; Fugate and Friedrichs, 2002).
Fragile flocculants change their characteristics over short and over long timescales
due to hydrodynamic forcing such as currents, turbulence and tides (Vousdoukas
et al., 2011; Burchard and Badewien, 2015). Optical (White, 1998; Sutherland et al.,
2000) and acoustic methods (Voulgaris and Meyers, 2004; Fugate and Friedrichs,
2002) typically reveal different scattering properties of the sediment. Thus Winter
et al. (2007) concluded that the combination of different instruments reveal different
aspects of suspended particulate matter (SPM) dynamics.

The aim of this work is to find out whether measurements of acoustic backscatter
can be reliably related to optical water properties. As all these observations provide
information about the inherent suspended particulate and dissolved material, these
should also be suited as practical indicators of water transparency and thus qual-
ity. We also evaluate the utility of acoustic and optical technology in environmental
monitoring to gather qualitative and quantitative indicators of change within natural
waters taking advantage of operational long time series observatory platforms. The
goals of this study will be towards (i) inter-comparison of measurements from dif-
ferent tools, (ii) understanding correlations among the observed variables, and (iii)

developing methods geared to closing gaps in relevant information about variability in water transparency in the water column such as when individual instruments fail.

6.2   Materials and methods

6.2.1   Study area

Time Series Station Spiekeroog (TSS, figure 6.1) is a multidisciplinary, autonomously operating observatory located in a tidal channel between the islands of Langeoog and Spiekeroog at 53° 45.016' N, 007° 40.266' E (Reuter et al., 2009). These islands are part of an island barrier system in the East Frisian Wadden Sea, southern North Sea, which belongs to the UNESCO World Natural Heritage sites. The region is part of an extended North Sea tidal flat system with shallow water depths ranging from 0 to 20 m, with current velocities of up to 2 m s^{-1}. The tidal cycle is semi-diurnal. The water depth at the TSS Spiekeroog is about 13.5 m, with tidal range of about 2.7 m (Holinde et al., 2015). Here, the distribution of suspended particulate inorganic and organic material is strongly influenced by tidal currents as well as by wind-driven waves (Bartholomä et al., 2009; Badewien et al., 2009). Because of these strong and rapid dynamics, the area at the TSS is well suited for studying the biogeochemical and physical processes occurring at the transition from the coast to the open sea.

6.3   Sampling and analysis

Hyperspectral radiometers were used to collect and derive R$_{RS}$ data at 24 m above the seafloor at 5 min interval continuously. The reflectance measurements, corrected for environmental perturbations, were transformed into Forel-Ule color indices that
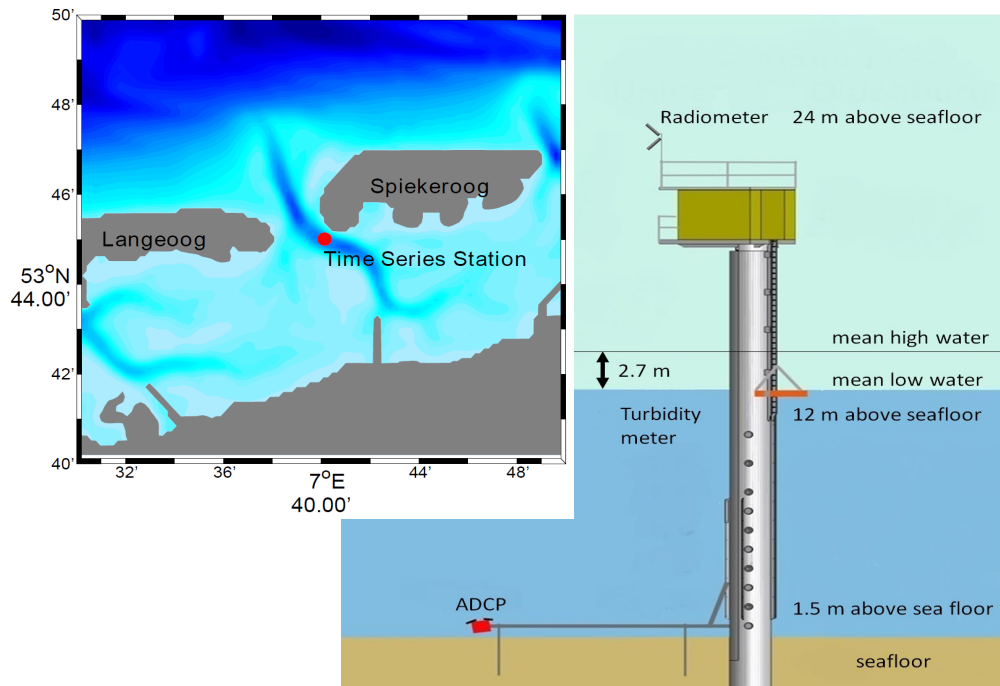
Figure 6.1: Schematic of the Time Series Station Spiekeroog showing the position of the radiometers (24 m), the turbidity meter (12 m), and the ADCP (1.5 m above the seafloor). The typical water depth is 13.5 m with tidal range of about 2.7 m between mean high and low water. The insert shows the location of the Time Series Station where the colors indicate the water depth at high water.

can be matched to the intrinsic color of water. A submerged WETlabs ECO FLNTU sensor measured turbidity at 12 m above the seafloor continuously at 1 min intervals. The ECO FLNTU sensor samples turbidity data with optical backscattering at a wavelength of 700 nm. Detailed information on the processing of these measurements is presented in an earlier study from Garaba et al. (2014).

A bottom-mounted (1.5 m above the seafloor), upward looking 1200 kHz ADCP (Teledyne RD Instruments Workhorse Sentinel, USA) was used to estimate the current velocity using the Doppler effect in three dimensions. The ADCP is installed

at a distance of 12 m north-north-west of the station's pole. We receive data over the entire water depth with a vertical resolution of 0.20 m (bin size) and a temporal resolution of 5 min (measurements are averaged over 45 pings in 5 min bursts). The shape of the depth profiles derived from the backscatter data (figure 6.2) vary depending on the tidal phase (flood, ebb, slack water). Those phases with similar current velocity also result in similar shapes of the backscatter profiles. Because the ADCP has a beam angle of 20° and a tilted orientation with a pitch of $\sim$ 19.39° and a roll of $\sim$ 17.96°, the maximum range R_{max} in meters of acceptable data is given by

$$R_{max} = D\cos(\phi) \tag{6.1}$$

where D is the distance between the ADCP and the surface in meters, and ϕ is the angle in degrees of the beam relative to the vertical. The resulting blank space near the surface reached values between 3.0 m to 3.5 m (see figure 6.3). To compare the data at nearly the same sampling target, we extrapolate the acoustic backscatter signal to the sea surface area (details of the sampling areas of the different sensors are shown in figure 6.4), using the acceptable acoustic backscatter data until R_{max} depth. To do so, we applied various curve fitting techniques using MATLAB R2015a, Curve Fitting Toolbox (MathWorks, USA). These methods were (i) the exponential fitting method ('exp', equation: $a \cdot exp(b \cdot x)$), (ii) the polynomial fitting method ('poly', equation: $p1 \cdot x + p2$, basically linear), (iii) the power fitting method ('power', equation: $a \cdot x^b$) and (iv) constant extrapolation (using the last reliable data value as the surface value). Applications of these methods are shown in figure 6.5. The top panels show profiles, which are exemplary for data obtained during low water and one during flood (violet and blue in figure 6.2) with different extrapolations to the surface layer. These panels also demonstrate the different ranges that were used for extrapolating; data were extrapolated using measurements obtained within the entire water column (left panel). In an alternative approach, extrapolation of data

67

was based solely on measurements not affected by bottom friction - that is data
derived in the near bottom range up to 4 m were excluded (right panel). In this
range, the impact of ebb- and flood-induced currents is strong. The bottom panel
shows the summary of all R^2 obtained from the different extrapolation methods on
the entire data set. We assume that the distribution of suspended matter near the
surface layer is nearly homogeneous (e.g. Badewien et al. (2009); van der Hout et al.
(2015)) because of turbulence and wind influence.
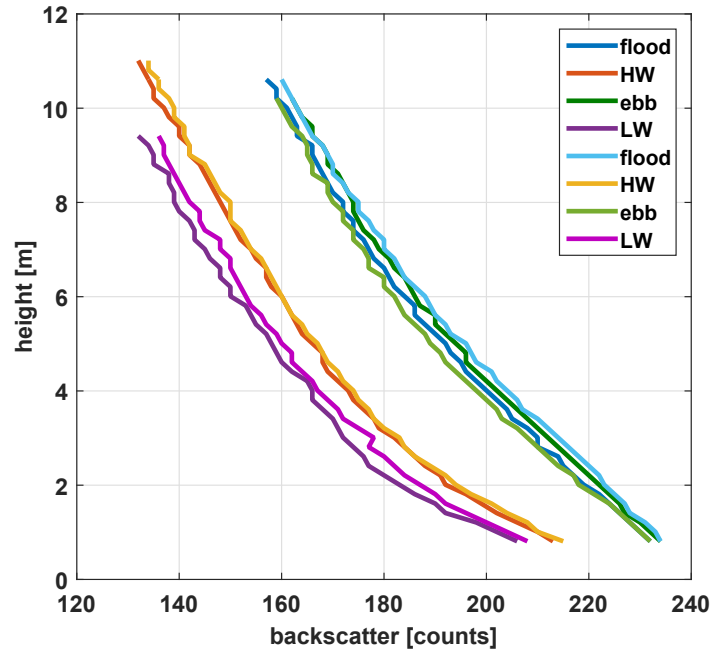
Figure 6.2: Example acoustic backscatter profiles measured from ADCP over height
in counts observed on 29 August 2013 at different tidal phases: flood, ebb, slack
water (high water (HW), low water (LW)).

The exponential extrapolation (exp) resulted in the best fits for all data sets and
extrapolation ranges. The R^2 values over the entire period are good with $R^2 > 0.99$
(see figure 6.5, bottom). Therefore, to compare acoustic backscatter data with
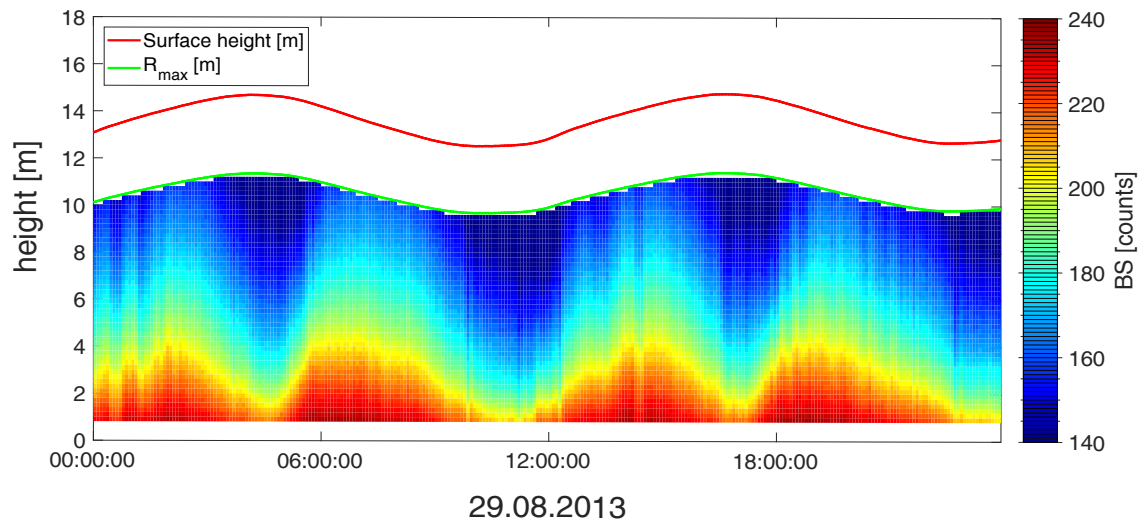
Figure 6.3: An example of acoustic backscatter signal in counts measured with the ADCP (from the seafloor upwards through the water column), acceptable backscatter data until R_{max}. Green line: R_{max} depth in meters; red line: sea level (height in meters) observed on 29 August 2013.

the other parameters, the exponential fitting method and the extrapolations with constant values ($BS_{Ex,exp}$ and $BS_{Ex,const}$) were used. The latter was based on the assumption of homogeneity in the top layer of the water column.

6.4 Results

The turbidity time series (figure 6.6 displayed data obtained from 29 August 2013 to 02 September 2013) shows a rapid response directly after cleaning of the ECO FLNTU sensor as expected in a highly bio-active season (summer). Even in this short time period of 5 days a strong increase and spreading of turbidity values is apparent. On 28 August 2013, the ECO FLNTU sensor was cleaned. Directly after cleaning, the values were below 5 NTU (nephelometric turbidity unit) with a range of 2.2 NTU. After 3 days, the values increased and reaching maximum values of up
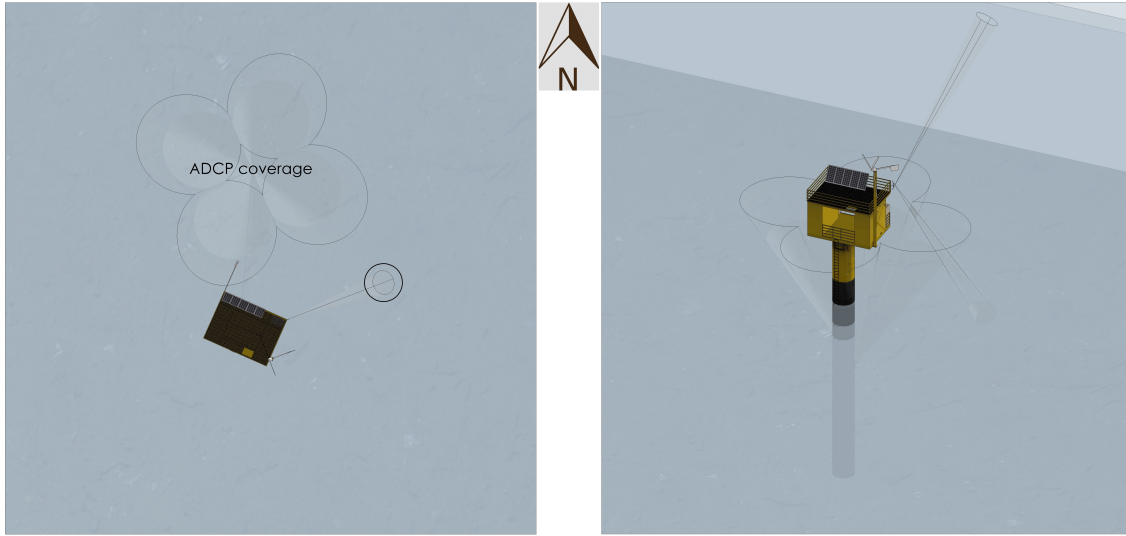
Figure 6.4: Schematic of the different measurement fields of view (FOV) of the sensors at the Time Series Station Spiekeroog at high water. Left panel: top view; right panel: perspective from south (provided by Nick Rüssmeier).

to 25 NTU with spreading out to 10 NTU at the end of the 5-day-period. These values indicate that the upper limit of reliable measurements had been reached. Figure 6.7 presents a closer look at the variables of the acoustic and optical measurements obtained on 29 August 2013. Visual inspection of data (Forel-Ule index, turbidity and the acoustic backscatter) suggested that there was a moderate correlation. As expected, the highest values of the variables investigated were during periods with high current speeds, i.e. when the water level rises or falls. Because of the measurement principle the Forel-Ule index was restricted to a time span between 06:00 and 18:00 resulting from daytime and the reflectance of the sunlight. The signals of both the Forel-Ule index FUI and the turbidity TRB were stronger during ebb tide than during flood tide. The acoustic backscatter signals, which were extrapolated using constant values $BS_{Ex,const}$, were nearly equal strength during ebb and flood tide, whereas $BS_{Ex,exp}$ exhibited stronger ebb signal. However, during slack water the values were slightly decreasing. Thus, the dynamics of all data sets corresponded

well to the observed tidal signal.

Results of the Spearman rank correlation for 1 day (29 August 2013, directly after sensor cleaning) and for a longer period (5 days) are shown in table 6.1. As described above, we extrapolated the acoustic backscatter signal towards the sea surface to be able to compare these acoustic measurements with the optical approaches. Two of these extrapolated variables ($BS_{Ex,const}$ and $BS_{Ex,exp}$) were used for the Spearman rank correlation test. The correlation coefficient between the data sets increased from moderate ($\rho_{Spearman} > 0.4$ and $\rho_{Spearman} < 0.6$) to strong ($\rho_{Spearman} > 0.6$ and $\rho_{Spearman} < 0.8$). In general, the correlation values of the shorter time periods were higher, than the values for the longer time period, especially for the comparison of the acoustic backscatter signal and the turbidity. The correlation between FUI and TRB was also very good ($\rho_{Spearman} > 0.8$). The comparison of the two different time periods showed nearly the same values. For further investigations, we used the constant extrapolated acoustic backscatter signal $BS_{Ex,const}$. For this approach, we assumed a homogenous surface layer (see above).

Table 6.2 shows a comparison between the constantly extrapolated ADCP backscatter signal $BS_{Ex,const}$ and the Forel-Ule index and the turbidity data separated into different tidal phases: ebb, flood, high waters, low waters. The data cover the time period from 29 August 2013 to 02 September 2013. The correlations between the acoustic backscatter data $BS_{Ex,const}$ and FUI ranged from a weak correlation of $\rho_{Spearman} = 0.34$ during high tide to a strong correlation during low tide of $\rho_{Spearman} = 0.81$. In between, the methods correlated mostly moderate ($\rho_{Spearman} > 0.4$ and $\rho_{Spearman} < 0.6$). The correlations between acoustic backscatter data $BS_{Ex,const}$ and TRB were weak at high tide and flood and otherwise strong ($\rho_{Spearman} > 0.6$ and $\rho_{Spearman} < 0.8$).

Table 6.1: Spearman rank correlation results of the backscatter data from the ADCP $BS_{EX,const}$ and $BS_{EX,exp}$ for 1 day and for a longer time period (29 August 2013-02 September 2013) as well as the estimated Forel-Ule index FUI and the turbidity TRB.

variables	$\rho_{Spearman}$ 1 day	$\rho_{Spearman}$ longer period	p-value 1 day	p-value longer period
$BS_{EX,const}$ vs. TRB	0.78	0.50	<0.001	<0.001
$BS_{EX,exp}$ vs. TRB	0.67	0.42	<0.001	<0.001
$BS_{EX,const}$ vs. FUI	0.58	0.52	<0.001	<0.001
$BS_{EX,exp}$ vs. FUI	0.48	0.44	<0.001	<0.001
FUI vs. TRB	0.88	0.85	<0.001	<0.001

6.5   Discussion

The time series of turbidity data shown in figure 6.6 indicate the strong influence of bio-fouling on the sensors during the bio-active seasons spring and summer even during shorter time periods of several days. Thus, it is vital to regularly check and, if necessary, clean sensors to reduce the impact of bio-fouling on data quality. The merely moderate correlation between the acoustic backscatter data $BS_{Ex,const}$ and the Forel-Ule index and turbidity (seen in figure 6.7 and table 6.1) presumably results from the fact that the sensors had different positions, namely, above the sea surface, submerged near the sea surface and submerged near the seafloor (an overview of the fields of view is shown in figure 6.4). Additionally, the lack of a strong correlation may be due to different scattering characteristics of suspended sediment (White, 1998; Sutherland et al., 2000; Voulgaris and Meyers, 2004; Fugate and Friedrichs, 2002) depending on whether optical or acoustic methods are applied. Comparisons

of acoustic and optical sensors for measurements of suspended sediment concentrations performed under laboratory conditions showed that most in-water sensors have a linear response under bimodal and randomly sorted suspended sediments (Vousdoukas et al., 2011). Optical measurements are more sensitive to fine sediment and are wavelength dependent, while acoustic measurements are more sensitive to coarser material, depending on the operating frequency (Gartner, 2004). Both depend on the amount of suspended sediment in the water column. Badewien et al. (2009) measured a range of particle sizes from 1.25 to 26.9 μm (radius) at the same site. Therefore, mainly fine sediment concentrations are expected. A modeling study by Stanev et al. (2007) showed different sediment concentrations and dynamics for fine SPM (mud, $d_{mud} = 63\ \mu m$; d: diameter) and sand ($d_{sand} = 200\ \mu m$) for this Wadden Sea area. Depending on the specific location, the dynamics of the different sediment types (fine or coarse) act differently dependent on the tidal signal. Concentrations of coarser material usually clearly peak at maximum flow velocities (flood and ebb). The concentration of fine sediments is highest during ebb, although the peak is broader. The peak during flood is less pronounced. In this study, the dynamics observed in all data sets correspond well to the observed tidal signal (figure 6.7). As shown in Schulz et al. (2015) the remaining shear currents in the surface layer kept particles within the water column at slack water times. Thus, we assume that the instruments used in this study provide reasonable proxies for suspended material which is comparable in size.

To be able to compare the data obtained by different methods at about the same sampling site, we had to extrapolate the acoustic backscatter signal towards the sea surface as described above. Two of these extrapolated variables ($BS_{Ex,const}$ and $BS_{Ex,exp}$) were used for the Spearman rank correlation test as shown in table 6.1 and 6.2. The correlation coefficient between the data sets increased from moderate to strong. These differences may result from the different scattering characteristics

Table 6.2: Spearman rank correlation results of the backscatter data from the ADCP $BS_{EX,const}$, the estimated Forel-Ule index FUI and the turbidity TRB with separation into tidal phases.

variables	tide phase	$\rho_{Spearman}$	p-value
$BS_{Ex,const}$ vs. FUI	ebb	0.45	<0.001
	flood	0.52	<0.001
	high tide	0.34	0.06
	low tide	0.81	<0.001
$BS_{Ex,const}$ vs. TRB	ebb	0.71	<0.001
	flood	-0.34	<0.001
	high tide	0.40	0.0014
	low tide	0.77	<0.001

and dynamics of the kinds of sediment, which occur in this location.

The bio-fouling influence started already in the short 5-day time period. Therefore, correlation values derived from the data of the shorter 1-day time period directly after cleaning the ECO FLNTU sensor were stronger than the values for the entire time period of 5 days. Even the correlation between FUI and the TRB was very good and the comparison of the two different time periods showed nearly the same values. This indicates that both optical measurements (above and in-water) detect the same type of sediment. In a previous study it was shown that the Forel-Ule index can be used to accurately derive turbidity (Garaba et al., 2014). We therefore evaluated its potential in providing information about suspended material, which in turn can be compared to information derived from acoustic backscatter signals. Our results regarding the correlation between the acoustic backscatter signal and turbidity agree well with investigations of Schulz et al. (2015). The data sets of the in-water sensors correlated moderately to strongly. In particular, the counter

wise strengths of the signals during the tidal cycle could be identified. In summary, our results on the correlation of the different sensor types agree well with previous results from laboratory investigations (Vousdoukas et al., 2011).

6.6   Conclusions

The goals of this study were to perform an inter-comparison of measurements from different tools, to understand correlations among the observed variables, and to develop methods geared to closing gaps in relevant information about variability in water transparency in the water column when individual instruments fail.

The results of this study show that bio-fouling decreases the data quality of in-water optical measurements of turbidity within short time periods. Hence, it is important to find an approach to improve the monitoring over time and increase the robustness of the turbidity results. This study demonstrates that bottom-mounted ADCP measurements, which are hardly influenced by bio-fouling, can be a suitable alternative to overcome the problem. We found that using the acoustic backscatter signal and the Forel-Ule index both yield reliable results, thus broadening the work of Garaba et al. (2014). On a qualitative level, using the Forel-Ule index, as derived from radiometer measurements, is a powerful tool for exchangeable estimations of water transparency as much as data sets derived from ADCP measurements.

We have shown that data sets from different measurement principles (optical and acoustic) are comparable and complementary. This is even though the different sensors reveal different scattering properties of particles and are positioned in different ways, i.e. above the sea surface, submerged near the sea surface and submerged near the seafloor.

Thus, our study strongly suggests that combining these methods can be an effective tool to monitor environmental processes as a part of long time series observatories.
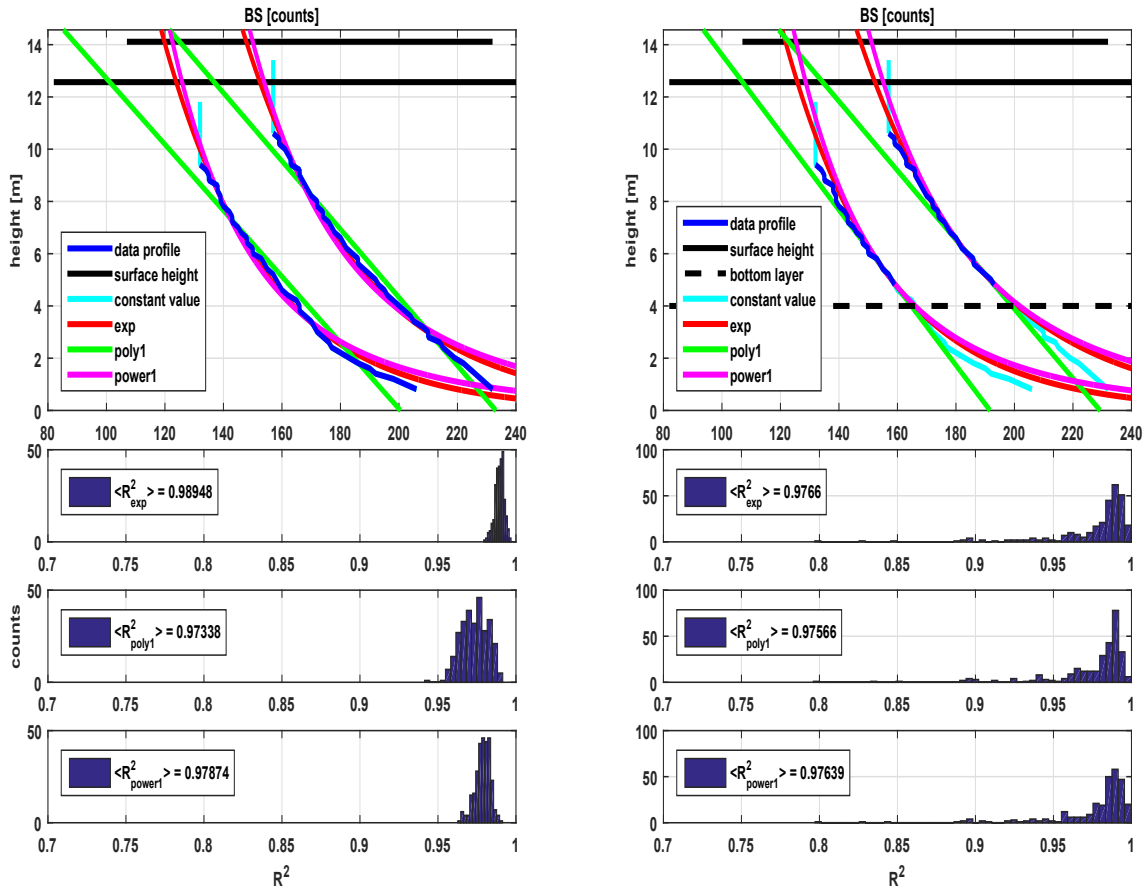
Figure 6.5: Selected acoustic backscatter profiles during low water and during flood; top left: extrapolation through the whole water column; top right: extrapolation through the reduced water column. The colored profiles show the results of the different extrapolation methods (cyan: constant extrapolation; red: exponential extrapolation; green: polynomial extrapolation; magenta: power extrapolation). Black line: surface layer and black dotted line: lower layer. Bottom panels: histograms of the corresponding R^2 values (from every profile) for the entire period; left: for the whole water column, right: for the reduced water column.
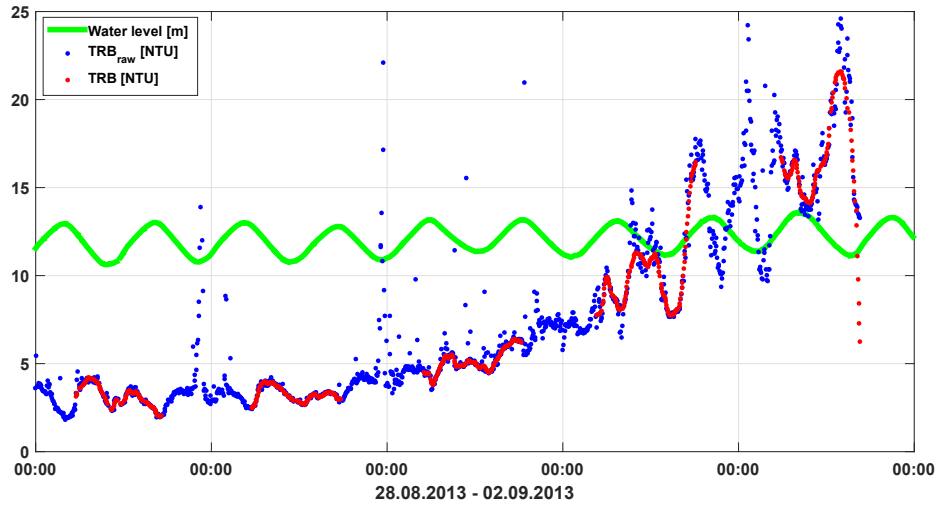
Figure 6.6: Turbidity data in *NTU* from 29 August 2013 to 02 September 2013, limited in range (0-25 *NTU*), blue: raw data, red: quality checked data and green: water level in meters.
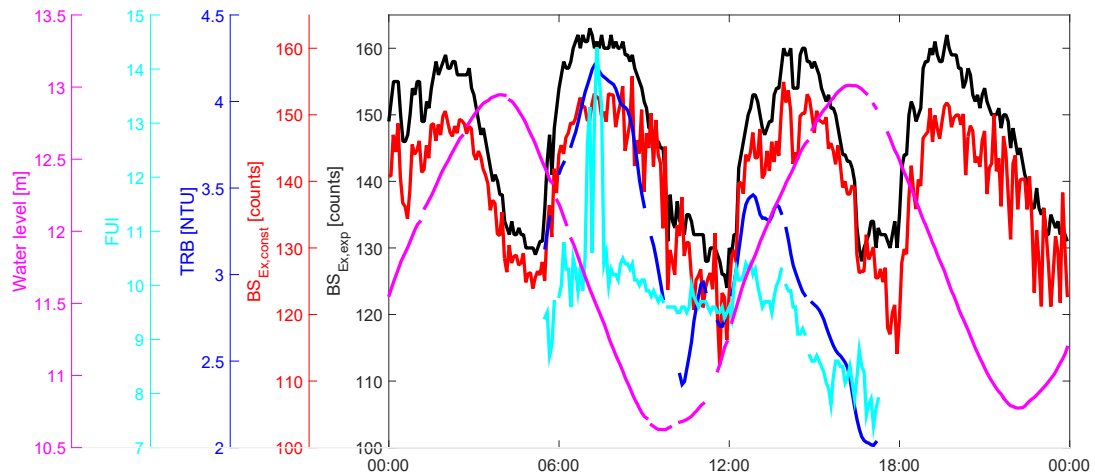
Figure 6.7: Time series observations on 29 August 2013 of Forel-Ule color index (*FUI*, cyan), backscatter signal (*BS*, constant extrapolation: red, exponential extrapolation: black), turbidity (blue) and water level (magenta).

7   Synopsis

Summary   The aim of this dissertation was the characterization and quantification of hydrodynamic exchange processes in one of the inlets between two islands (tidal channel) within the Wadden Sea area. This topic was dealt with the incipiently mentioned research questions in chapter 1.3. My investigations revealed that it was possible to measure long-term data sets of current velocities and even estimate turbulence (chapter 2) with for example an autonomous continuous operating measurement station such as the Time Series Station Spiekeroog of the ICBM, together with a suitable measurement device like an ADCP and an appropriate measurement setup. Natural flows are exclusively turbulent, but the producing processes could differ or have different influencing effects. Chapter 3 showed that turbulence is generated by sheared currents at the bottom of the sea. Thus, shear increases turbulent mixing. Due to the shallow water depth mixing occurs across the entire water column. Because of the importance and the influence of current velocities and the resulting turbulence to a coastal ecosystem like the Wadden Sea area, it is crucial to collect data over long time periods to investigate e.g. seasonal processes or dynamics at extreme events. Unfortunately, data sets over long time periods like several months or even years are not available. To overcome this problem, I developed an approach to make already existing data sets of current velocities available for turbulence research. Results presented in chapter 4 gave a first starting point to apply this approach. An essential point here was that no further environmental parameter besides the current velocity itself, the corresponding velocity shear and the water level was needed to obtain an assessment of turbulence patterns within the water column. Despite some shortcomings, such as the limited applicability for extreme events such as storm surges, the method can provide valuable insights into general patterns of turbulence under natural conditions. This is particularly help-

ful when studying turbulence in remote places or under environmental conditions where direct measurements of turbulence are not feasible. However, further research is needed to expand the developed methods to the boundary layers of the water column, so towards the sea surface and towards the bottom area.

The enormous number of measurement equipment at the Time Series Station Spiekeroog and the wide range of measurement device applications provided the opportunity to study the interactions across disciplines like physics and bio-optics. Because of the relevance of physical and bio-optical dynamics and its relation to each other, the impact of measured currents and turbulence on turbidity dynamics was explored (chapter 5). Results showed a link between the production rate and turbidity at slack water times. Remaining turbulence is sufficiently strong to keep particles within the water column. Although the research area is an ebb dominated system, an opposite behavior of the turbidity and backscatter signals was observed. Since current speeds, velocity shear and turbulence signals all show ebb dominance, it has been concluded that the production rate holds the turbidity in the water column at high tides. At times with high current speeds the velocity shear and, therefore, the current velocities are responsible for the turbidity dynamics: At flood, the shear carries the turbidity up into the water column; In contrast, at ebb tide the shear prevents the transport to the sea surface area.

A further step was the comparison of water transparencies received from sensors with totally different measurement principles. Chapter 6 showed data from acoustical and optical operating and from submerged and above-water mounted sensors. The findings suggest that both optical and acoustic measurements can be reasonable proxies of water transparency with the potential to mitigate gaps and increase data quality of long-time observations of marine environments. In general, it is possible to measure interactions of different environmental parameters, exchange processes and quantify them. Especially for sensitive principles or sensors (e.g. easily affected

by bio-fouling) a validation or verification of measured data to comparable data which are more stable is a crucial benefit of this study.

In all operational studies or field campaigns the research location influences the results in a certain manner. However, this is mostly the objective of the investigations. The UNESCO World Heritage Wadden Sea is no exception. The investigations of this thesis were conducted within a tidal channel, which shows the typical structure of the tidal-inlet / backbarrier-basin system described in chapter 1.1. Because of the typical characterization of the investigated tidal channel, all findings could be transferred to other tidal inlets of the Wadden Sea system. Especially, if tidal currents are the dominant physical process at these tidal inlets. Processes like sediment transport and its dynamics could act differently in regions with strong influences of freshwater. These influencing freshwater entries are usual rivers (estuaries). At the coastline of the German Wadden Sea area are a lot sluices or sewers. These sluices supply freshwater in distinct time frames into the backbarrier-basin of the system. Hence, estuarine circulation (interplay of freshwater and oceanic saltwater) also exists. During estuarine circulation saline water flows near the bottom into the estuary and freshwater flows near the surface towards the sea. Density gradients occur in both the horizontal and vertical plane. During freshwater is supplied and estuarine circulation predominates, the results of this thesis could not be fully transferred.

Outlook   In the future, the developed methods for analyzing turbulence patterns from non-high resolution velocity data sets presented in chapter 4 should be extended to the vertical component of the relevant parameters. This will improve the method especially for analyzing special events, such as storm surges, and for investigating the vertical patterns of turbulence in the water column. Additionally, wind speed and wind direction should be taken into account. Such improvements would

make it possible to analyze turbulence in coastal regions on seasonal scales.

Further measurements should be conducted to validate estimates of the vertical structure of turbidity derived by ADCP measurements. Validated and high resolution turbidity data derived from ADCP measurements will be useful for interdisciplinary studies on the biogeochemistry and sediment transport in the study area. Additionally, other parameters such as oxygen and the influence of currents and turbulence on these could be considered. It would also be useful to study a variety of environmental conditions, such as storm surges, algal blooms and periods with sea ice.

In general, future work should investigate interactions with more multidisciplinary parameters. These relationships are probably more complex than shown in this thesis. For these purposes more operational measurements over longer time periods with higher resolutions in time and space are necessary. The continuous operation of the Time Series Station Spiekeroog with its always expanding measurement equipment and its further growing potential for deepening the knowledge of such special environment is a powerful tool for future work.

Apprendix

A   Publications and conference contributions

A.1   Publications and manuscripts

- **A.-C. Schulz**, T. H. Badewien and O. Zielinski, 2018. Assessment of turbulence patterns from non-high resolution data sets of current velocities. Ocean Dynamics, submitted.

- B. Friedhoff, D. Abma, P. van Mensch, R. Verbeek, **A.-C. Schulz** and A. Lutz, 2018. Digital solutions for environmental performance and energy efficient navigation using on-board monitoring and river modeling. Proceedings of 7th Transport Research Arena TRA 2018, April 16-19, 2018, Vienna, Austria.

- A. Orlovius and **A.-C. Schulz**, 2017. Das Binnenschiff als Messplattform - Automatisierte Erfassung von Sohlhöhen und Strömungsgeschwindigkeiten im laufenden Schiffsbetrieb. Hydrographische Nachrichten, 106, p. 14-19.

- J. Schweighofer, R. Verbeek, D. Abma, P. van Mensch, S. Creten, K. van Mullen, B. Friedhoff, **A.-C. Schulz**, A. Orlovius, S. Blagoci, I. Roman, R. Rafael, B. Kruyt, T. Jongkind, R. van Reem, M. Quisel, E. Jung and L.-M. Putz, 2017. PROMINENT D6.2 Mid-term pilot evaluation report.

- J. Schweighofer, R. Verbeek, D. Abma, M. Seitz, R. Rafael, B. Friedhoff, A. Orlovius and **A.-C. Schulz**, 2016. PROMINENT - D5.6 Land based tool for evaluation of ship efficiency and navigation performance.

- **A.-C. Schulz**, T. H. Badewien, S. P. Garaba and O. Zielinski, 2016. Acoustic and optical methods to infer water transparency at Time Series Station

Spiekeroog, Wadden Sea. Ocean Sci., 12(6): 1155-1163. DOI: 10.5194/os-12-1155-2016.

- **A.-C. Schulz**, T. H. Badewien and O. Zielinski, 2015. Impact of currents and turbulence on turbidity dynamics at the Time Series Station Spiekeroog (Wadden Sea, southern North Sea). 2015 IEEE/OES Eleventh Current, Waves and Turbulence Measurement (CWTM). DOI: 10.1109/CWTM.2015.7098095.

- S. P. Garaba, T. H. Badewien, A. Braun, **A.-C. Schulz** and O. Zielinski, 2014. Using ocean colour remote sensing products to estimate turbidity at the Wadden Sea time series station Spiekeroog. J. Europ. Opt. Soc. Rap. Public., 9, 14020, DOI: http://dx.doi.org/10.2971/jeos.2014.14020.

- M.H. Einsporn, J. Wiedling, S. Beilfuss (Hrsg.), 2013. Recent Impulses to Marine Science and Engineering - From coast to deep sea: multiscale approaches to marine sciences (RIMSE 2013). Hamburg, Deutsche Gesellschaft für Meeresforschung, S. 132 - 142. ISBN-13: 978-3-00-043157-9. L. Holinde, **A.-C. Schulz**: Chapter 11 - Operational Oceanography.

A.2   Conference contributions

- **Talk**: A.-C. Schulz, T. H. Badewien and O. Zielinski, 2015. Impact of currents and turbulence on turbidity dynamics at the Time Series Station Spiekeroog (Wadden Sea, southern North Sea). Current, Waves and Turbulence Measurement Workshop (CWTM), St. Petersburg, Florida, USA.

- **Talk**: A.-C. Schulz, T. H. Badewien and O. Zielinski, 2014. An approach to estimate turbulence based on long-term non-high resolution data sets of current velocities. Physics of Estuaries and Coastal Seas (PECS), Porto de Galinhas, Pernambuco State, Brasilien.

- **Session Chairman**: Operational Oceanography, YouMaRes 4, 2013, Oldenburg, Deutschland.

- **Talk**: A.-C. Schulz, T. H. Badewien and O. Zielinski, 2013. Turbulence Producing Processes in a Tidal Channel. Warnemünde Turbulence Days (WTD), Vilm, Deutschland.

- Poster presentation: A.-C. Schulz, T. H. Badewien and O. Zielinski, 2013. Turbulence Producing Processes in a Tidal Channel. European Geosciences Union (EGU), Wien, Deutschland.

- **Talk**: A.-C. Schulz, T. H. Badewien and O. Zielinski, 2012. Estimation of Turbulence in an East Frisian Tidal Channel. YouMaRes 3, Lübeck, Deutschland.

- Poster presentation: A.-C. Schulz, T. H. Badewien and O. Zielinski, 2012. Estimation of Turbulence in an East Frisian Tidal Channel. European Geosciences Union (EGU), Wien, Deutschland.

- Poster presentation: A.-C. Schulz and T. H. Badewien, 2011. Measurements of the rate of dissipation of turbulent kinetic energy in the Wadden Sea. YouMaRes 2, Bremerhaven, Deutschland.

- Poster presentation: A.-C. Schulz and T. H. Badewien, 2010. Estimation of Reynolds Stress by current measurements with an Acoustic Doppler Current Profiler. YouMaRes 1, Hamburg, Deutschland

B Curriculum Vitae

Berufserfahrung

12/2015 –
31.10.2017
Wissenschaftliche Mitarbeiterin, Bundesanstalt für Wasserbau, Kußmaulstr. 17, 76187 Karlsruhe, www.baw.de.
Referat: Schiff / Wasserstraße, Naturuntersuchungen, Abteilung: Wasserbau im Binnenbereich.
Ausrüstung von Großgütermotorschiffen mit Sensorik zur autonomen Erfassung von Umweltbedingungen (z.B. Strömungsgeschwindigkeiten, Flottwassertiefen und Sohlhöhen), sowie Schiffs- und Maschinendaten. Datenanalyse und Bewertung des Aufwandes der Installation und des Betriebs für das EU-Projekt PROMINENT (www.prominent-iwt.eu; Ziel: Förderung der energie-effizienten Navigation in der Binnenschifffahrt).

08/2015 –
11/2015
Wissenschaftliche Hilfskraft, Carl-von-Ossietzky Universität Oldenburg, Ammerländer Heerstr. 114-118, 26129 Oldenburg, www.icbm.de.
Arbeitsgruppe: Marine Sensorsysteme, Institut für Chemie und Biologie des Meeres.
Charakterisierung und Quantifizierung von hydrodynamischen Austauschprozessen in einem Gezeitenkanal.

01/2012 –
07/2015
Wissenschaftliche Mitarbeiterin, Carl-von-Ossietzky Universität Oldenburg, Ammerländer Heerstr. 114-118, 26129 Oldenburg, www.icbm.de.
Arbeitsgruppe: Marine Sensorsysteme, Institut für Chemie und Biologie des Meeres.
Charakterisierung und Quantifizierung von hydrodynamischen Austauschprozessen in einem Gezeitenkanal bzw. Seegatt:
- Durchführung und Planung von ozeanographischen Messkampagnen auf verschiedenen Forschungsbooten und -schiffen.
- Datenerhebung und Wartungsarbeiten der Messstation Spiekeroog des ICBM im Seegatt Otzumer Balje.
- Erfassung physikalischer, hydrographischer und meteorologischer Parameter.
- Lehre:
  ○ Übung zur Vorlesung Meereskunde I, Studiengang Meerestechnik, Jade Hochschule in Wilhelmshaven.
  ○ Betreuung von ozeanographischer Praktika, Studiengang Umweltwissenschaften, Universität Oldenburg.

2009 – 2011
Studentische Hilfskraft, Carl-von-Ossietzky Universität Oldenburg, Ammerländer Heerstr. 114-118, 26129 Oldenburg, www.icbm.de.
Arbeitsgruppe: Marine Sensorsysteme, Institut für Chemie und Biologie des Meeres.
Strömungsdatenerhebung, -prozessierung, -analyse und Vergleich mit modellierten Daten. Betreuung von Studenten auf Messkampagnen auf dem Forschungsschiff Heincke.

2006 – 2008
Werkstudent, Airbus Deutschland GmbH, Riesweg 155, 26316 Varel.
Sekretariat des Betriebsrates.

2000 – 2003
Ausbildung zur Verwaltungsfachangestellten, Kommunalverwaltung Stadt Varel, Windallee 4, 26316 Varel.
Fachrichtung: Landes- und Kommunalverwaltung.

Akademische Abschlüsse

Master of Science, Physik

Titel — *Bestimmung der Turbulenz im ostfriesischen Seegatt (Otzumer Balje).*

Gutachter — Professor Jörg-Olaf Wolff & Dr. Thomas H. Badewien

Carl-von-Ossietzky Universität Oldenburg, Institut für Chemie und Biologie des Meeres, Arbeitsgruppe Marine Sensorsysteme.

Entwicklung und Durchführung eines Messkonzeptes zur Turbulenzbestimmung in Meeresströmungen im Küstenbereich mit akustischen Messgeräten (Acoustic Doppler Current Profiler). Vergleich der Ergebnisse verschiedener Messmethoden.

Bachelor of Science, Physik

Titel — *Zeitlich hoch auflösende Widerstandsmessungen an einem Zylinder mittels druckmessenden Sensoren.*

Gutachter — Professor Joachim Peinke & Dr. Michael Hölling

Carl-von-Ossietzky Universität Oldenburg, Institut für Physik, Arbeitsgruppe Turbulenz, Windenergie und Stochastik.

Bestückung von Platinen mit Elektronik und Drucksensoren, Kalibrierung der Sensoren und Durchführung der Messungen in einem Windkanal. Bestimmung der Ablösefrequenz der durch den Zylinder entstehenden Wirbel (Kármánsche Wirbelstraße) in der Strömung.

Studium und Ausbildung

Promotion

01/2012 – heute — **Promotion, Fach: Marine Umweltwissenschaften**, Carl-von-Ossietzky Universität Oldenburg, Oldenburg, Arbeitsgruppe: Marine Sensorsysteme, Institut für Chemie und Biologie des Meeres.
Charakterisierung und Quantifizierung von hydrodynamischen Austauschprozessen in einem Gezeitenkanal.

Graduiertenschule "Naturwissenschaft und Technik" OLTECH, Carl-von-Ossietzky Universität Oldenburg, Oldenburg, Fakultät V: Mathematik und Naturwissenschaften.
PhD programme Environmental Sciences and Biodiversity.

Fach-Master Physik

04/2009 – 09/2011 — **Master of Science Physik**, Carl-von-Ossietzky Universität Oldenburg, Oldenburg, Institut für Physik.

Fach-Bachelor Physik

10/2005 – 03/2009 — **Bachelor of Science Physik**, Carl-von-Ossietzky Universität Oldenburg, Oldenburg, Institut für Physik.

Ausbildung

08/2000 – 07/2003 — **Ausbildung zur Verwaltungsfachangestellten**, Kommunalverwaltung Stadt Varel.

C List of abbreviations

ADCP	Acoustic Doppler Current Profiler
BS	(acoustic) backscatter
CD	control data
COSYNA	Coastal Observing System for Northern and Arctic Seas
CTD	Conductivity-Temperature-Depth probe
dec.	decreasing (water level); at ebb tide
ECO FLNTU	fluorometer
FOV	field of view
FUI	Forel-Ule-Index
HR	high resolution
ICBM	Institute for Chemistry and Biology of the Marine Environment
inc.	increasing (water level); at flood tide
LISST	Laser-In-Situ-Scattering-and-Transmissometry
MST	multispectral transmissometry
NR	non-high resolution
NTU	Nephelometric Turbidity Unit
	Nephelometry: optical analysis methods for determining turbidity within a water sample by measuring the effect of this turbidity upon the transmission and scattering of light.
RVS	Research Vessel Senckenberg
SCUFA	Self-Contained Underwater Fluorescence

		Apparatus
SPM		Suspended particulate matter
SSC		Suspended sediment concentration
TKE		turbulent kinetic energy
TRB		turbidity
TSS		Time Series Station
UNESCO		United Nations Educational, Scientific and
		Cultural Organization
UTC		Coordinated Universal Time

a		any variable
$\overline{a}$		average of variable a
a'		fluctuating part of variable a
c_l	-	proportionality factor
d	nm	diameter
D	m	distance between ADCP and sea surface
E	J	turbulent kinetic energy
E^*	J/m^3	kinetic energy density
i	-	i-component of variable
j	-	j-component of variable
L	m	characteristic length
L_T	m	Thorpe-Scale
M_4		quarter-diurnal tidal pattern
N	$1/s$	buoyancy frequency, Brunt-Väisälä-frequency
p_i	-	coefficient (of fitting function)
q^2	Pa^2	trace of Reynolds stress tensor
R^2	-	goodness of fit

R_{max}	m	maximum measurement range of ADCP
Re	-	Reynolds number
R_{RS}	-	remote sensing reflectance
S	psu	salinity
S_{ij}	$1/s$	velocity shear in ij-plane
t	s	time
T	°C	temperature
P	W/m^3	production rate of TKE
p	Pa	pressure
$\vec{u}$	m/s	current velocity
$\overline{\vec{u}}$	m/s	averaged current velocity
$\vec{u}'$	m/s	fluctuating part of current velocity
$|u|$	m/s	magnitude of current velocity
u	m/s	x-component of current velocity
$u_{\parallel}$	m/s	component of current velocity along (parallel) to main flow direction
$u_{\perp}$	m/s	component of current velocity across (perpendicular) to main flow direction
v	m/s	y-component of current velocity
w	m/s	z-component of current velocity
x	m	east-coordinate
y	m	north-coordinate
z	m	vertical coordinate (up-direction)
ε	W/m^3	dissipation rate of TKE
μ	$Pa\ s$	dynamic viscosity
ν	m^2/s	kinematic viscosity

ρ	kg/m^3	density
τ_{ij}	Pa	Reynolds stress in ij-plane
ϕ	$^\circ$	angle between ADCP transducer to vertical

Units and their conversion:

$N = kg \ m \ s^{-2}$

$Pa = N \ m^{-2} = kg \ m^{-1} \ s^{-2}$

$J = N \ m = kg \ m^2 \ s^{-2}$

$W = J \ s^{-1} = kg \ m^2 \ s^{-3}$

Instrument specifications Table C.1 points out the main specifications of the used instrument. Detailed information are available on the manufacturers websites:
- Acoustic Doppler Current Profiler, 1200 kHz, Workhorse Sentinel, Teledyne RD Instruments (nd),
- Conductivity-Temperature-Depth-probe, CTD48M, Sea & Sun Technology (nd),
- the radiometers RAMSES-ACC hyperspectral cosine irradiance meter and RAMSES-ARC hyperspectral radiance meters, TriOS (nd), and
- the turbidity sensor, ECO FLNTU sensor, WETlabs, Sea-Bird Scientific (nd).

Table C.1: Small overview of used instruments specifications.

Instrument	Range	Resolution	Accuracy
ADCP	$\pm$ 5 $m\ s^{-1}$	0.1 $cm\ s^{-1}$	$\pm$ 3 $cm\ s^{-1}$
- velocity			(default)
CTD			
- pressure	< 6000 $dbar$	$\pm$ 0.1 %	0.002 %
(piezo-resistive)		full scale	full scale
- temperature	-2 - 36 $°C$	$\pm$ 0.002 $°C$	0.0001 $°C$
(pt 100)			
- conductivity	0 - 70 $mS\ cm^{-1}$	$\pm$ 0.003 $mS\ cm^{-1}$	0.001 $mS\ cm^{-1}$
(7-pole-cell)			
RAMSES			
-ACC	320 - 950 nm	0.3 nm	< 6 - 10%
-ARC	320 - 950 nm	0.3 nm	< 5%
Turbidity sensor	0-25 NTU	0.013 NTU	-

List of Figures

List of Tables

References

Badewien, T. H., E. Zimmer, A. Bartholomä, and R. Reuter

2009. Towards continuous long-term measurements of suspended particulate matter (SPM) in turbid coastal waters. *Ocean Dynamics*, 59:227–238. doi: 10.1007/s10236-009-0183-8.

Bartholomä, A., A. Kubicki, T. H. Badewien, and B. W. Flemming

2009. Suspended sediment transport in the German Wadden Sea-seasonal variations and extreme events. *Ocean Dynamics*, 59(2):213–225. doi: 10.1007/s10236-009-0193-6.

Baschek, B., F. Schroeder, H. Brix, R. Riethmüller, T. H. Badewien, G. Breitbach, B. Brügge, F. Colijn, R. Doerffer, C. Eschenbach, J. Friedrich, P. Fischer, S. Garthe, J. Horstmann, H. Krasemann, K. Metfies, L. Merckelbach, N. Ohle, W. Petersen, D. Pröfrock, R. Röttgers, M. Schlüter, J. Schulz, J. Schulz-Stellenfleth, E. Stanev, J. Staneva, C. Winter, K. Wirtz, J. Wollschläger, O. Zielinski, and F. Ziemer

2017. The Coastal Observing System for Northern and Arctic Seas (COSYNA). *Ocean Science*, 13(3):379–410. doi: 10.5194/os-13-379-2017.

Borja, A., M. Elliott, J. H. Andersen, A. C. Cardoso, J. Carstensen, J. G. Ferreira, A.-S. Heiskanen, J. C. Marques, J. M. Neto, H. Teixeira, L. Uusitalo, M. C. Uyarra, and N. Zampoukas

2013. Good Environmental Status of marine ecosystems: What is it and how do we know when we have attained it? *Marine Pollution Bulletin*, 76:16–27. doi: 10.1016/j.marpolbul.2013.08.042.

Bowers, D. G.

2003. A simple turbulent energy-based model of fine suspended sedi-

ments in the Irish Sea. *Continental Shelf Research*, 23(16):1495–1505. doi: 10.1016/j.csr.2003.08.006.

Burchard, H.
2009. Combined Effects of Wind, Tide, and Horizontal Density Gradients on Stratification in Estuaries and Coastal Seas. *Journal of Physical Oceanography*, 39:2117–2136. doi: 10.1175/2009JPO4142.1.

Burchard, H. and T. H. Badewien
2015. Thermohaline residual circulation of the Wadden Sea. *Ocean Dynamics*, 65:1717–1730. doi: 10.1007/s10236-015-0895-x.

Burchard, H., G. Flöser, J. V. Staneva, T. H. Badewien, and R. Riethmüller
2008. Impact of Density Gradients on Net Sediment Transport into the Wadden Sea. *Journal of Physical Oceanography*, 38(3):566–587. doi: 10.1175/2007JPO3796.1.

Cournot, A.-A.
1847. *De l' origine et des limites de la correspondance entre l' algèbre et la géométrie.* Hachette, Paris/Algier.

Cuneo, P. S. and B. W. Flemming
2000. Quantifying concentration and flux of suspended particulate matter through a tidal inlet of the East Frisian Wadden sea by acoustic doppler current profiling. *Muddy Coast Dynamics and Resource Management*, 2:39–52. 10.1016/S1568-2692(00)80005-4.

Davies-Colley, R. J. and D. G. Smith
2001. Turbidity, Suspended Sediment, and Water Clarity: A Review. *Journal of the American Water Resources Association*, 37(5):1085–1101. doi: 10.1111/j.1752-1688.2001.tb03624.x.

de Swart, H. and J. T. F. Zimmerman

2009. Morphodynamics of tidal inlet systems. *Annual Review of Fluid Mechanics*, 41(1):203–229. doi: 10.1146/annurev.fluid.010908.165159.

Deines, K. L.

1999. Backscatter Estimation Using Broadband Acoustic Doppler Current Profilers. In *Current Measurement, 1999. Proceedings of the IEEE Sixth Working Conference on*, Pp. 249–253. doi: 10.1109/CCM.1999.755249.

Dilthey, W.

1894. Die Autonomie des Denkens, der konstruktive Rationalismus und der pantheistische Monismus nach ihrem Zusammenhang im 17. Jahrhundert. *Archiv für Geschichte der Philosophie*, 8:28–91.

Eurimage

2008. *Mosaik aus Satellitenbildern aus dem Zeitraum 2000-2002*. Gemeinsames Wattenmeersekretariat und Brockmann Consult.

Ferron, B., H. Mercier, K. Speer, A. Gargett, and K. Polzin

1998. Mixing in the Romanche Fracture Zone. *Journal of Physical Oceanography*, 28:1929–1945. doi: 10.1175/1520-0485(1998)028<1929:MITRFZ>2.0.CO;2.

Fugate, D. C. and C. T. Friedrichs

2002. Determining concentration and fall velocity of estuarine particle populations using ADV, OBS and LISST. *Continental Shelf Research*, 22:1867–1886. doi: 10.1016/S0278-4343(02)00043-2.

Garaba, S. P., T. H. Badewien, A. Braun, A.-C. Schulz, and O. Zielinski

2014. Using ocean colour products to estimate turbidity at the Wadden Sea time series station Spiekeroog. *Journal of the European Optical Society*, 9(14020):1–6. doi: 10.2971/jeos.2014.14020.

REFERENCES

Garaba, S. P., D. Voß, J. Wollschläger, and O. Zielinski

2015. Modern approaches to shipborne ocean color remote sensing. *Applied Optics*, 54(12):3602–3612. doi: 10.1364/AO.54.003602.

Garaba, S. P. and O. Zielinski

2013. Comparison of remote sensing reflectance from above-water and in-water measurements west of Greenland, Labrador Sea, Denmark Strait, and west of Iceland. *Optics Express*, 21(13):15938–15950. doi: 10.1364/OE.21.015938.

Gartner, J. W.

2004. Estimating suspended solids concentrations from backscatter intensity measured by acoustic Doppler current profiler in San Francisco Bay, California. *Marine Geology*, 211:169–187. doi: 10.1016/j.margeo.2004.07.001.

GCOS

2011. *The Global Climate Observing System - Systematic Observation Requirements for Satellite-based Data Products for Climate: 2011 Update GCOS-154.*

Hinze, J. O.

1975. *Turbulence.* McGraw-Hill series in mechanical engineering.

Holinde, L., T. H. Badewien, J. A. Freund, E. V. Stanev, and O. Zielinski

2015. Processing of water level derived from water pressure data at the Time Series Station Spiekeroog. *Earth System Science Data*, 7:289–297. doi: 10.5194/essd-7-289-2015.

ISO7027:1999

2012. Water quality – Determination of turbidity (This standard was last reviewed in 2010.). Published Stage: 90.92 (2012-09-17) TC/SC: ISO/TC 147/SC 2 Number of Pages: 10.

Ivey, G. N. and J. Imberger

1990. On the Nature of Turbulence in a Stratified Fluid. Part I: The Energetics of Mixing. *Journal of Physical Oceanography*, 21:650–658. doi: 10.1175/1520-0485(1991)021<0650:OTNOTI>2.0.CO;2.

Kirk, J. T. O.

1985. Effects of suspensoids (turbidity) on penetration of solar radiation in aquatic ecosystems. *Hydrobiologia*, 125(1):195–208. doi: 10.1007/BF00045935.

Kocsis, O., H. Prandke, A. Stips, A. Simon, and A. Wüest

1999. Comparison of dissipation of turbulent kinetic energy determined from shear and temperature microstructure. *Journal of Marine Systems*, 21:67–84. doi: 10.1016/S0924-7963(99)00006-8.

Lemke, A., M. Lunau, J. Stone, O. Dellwig, and M. Simon

2009. Spatio-temporal dynamics of suspended matter properties and bacterial communities in the back-barrier tidal flat system of Spiekeroog Island. *Ocean Dynamics*, 59:277–290. doi: 10.1007/s10236-009-0190-9.

Lettmann, K. A., J.-O. Wolff, and T. H. Badewien

2009. Modeling the impact of wind and waves on suspended particulate matter fluxes in the East Frisian Wadden Sea (southern North Sea). *Ocean Dynamics*, 59:239–262. doi: 10.1007/s10236-009-0194-5.

Lohrmann, A.

2001. Monitoring Sediment Concentration with acoustic backscattering instruments. Nortek technical notes/October15, 2001/Document No. N4000-712.

Lu, Y. and R. G. Lueck

1996. Flow Measurements in a Tidal Channel using an Acoustic Current Profiler. *CEOR Report*, 96-2.

REFERENCES

Lu, Y. and R. G. Lueck

1999a. Using a Broadband ADCP in a Tidal Channel. Part I: Mean Flow and Shear. *Journal of Atmospheric and Oceanic Technology*, 161:1556–1567. doi: 10.1175/1520-0426(1999)016<1556:UABAIA>2.0.CO;2.

Lu, Y. and R. G. Lueck

1999b. Using a Broadband ADCP in a Tidal Channel. Part II: Turbulence. *Journal of Atmospheric and Oceanic Technology*, 161:1568–1579. doi: 10.1175/1520-0426(1999)016<1568:UABAIA>2.0.CO;2.

Lu, Y., R. G. Lueck, and D. Huang

2000. Turbulence Characteristics in a Tidal Channel. *Journal of Physical Oceanography*, 30:855–867. doi: 10.1175/1520-0485(2000)030<0855:TCIATC>2.0.CO;2.

Martin, T. H.

1868. *Galilée. Les droits de la science et la méthode des sciences physiques.* Didier, Paris.

Moore, C., A. Barnard, P. Fietzek, M. R. Lewis, H. M. Sosik, S. White, and O. Zielinski

2009. Optical tools for ocean monitoring and research. *Ocean Science*, 5:661–684. doi: 10.5194/os-5-661-2009.

Moore, G. K.

1980. Satellite remote sensing of water turbidity / Sonde de télémesure par satellite de la turbidité de l'eau. *Journal of the European Optical Society - Rapid Publications*, 5:407–421.

Morel, A.

1980. In-water and remote measurements of ocean color. *Boundary-Layer Meteorology*, 18(2):177–201. doi: 10.1007/bf00121323.

OECD

1993. Core set of indicators for environmental performance reviews - a synthesis report by the group on the state of the environment. Organisation for Economic Co-operation and Development, Paris.

Orton, P. M. and M. Visbeck

2009. Variability of internally generated turbulence in an estuary, from 100 days of continuous observations. *Journal of Physical Oceanography*, 29:61–77. doi:10.1016/j.csr.2007.07.008.

Pearlman, J., R. Garello, E. Delory, A. Castro, J. del Rio, D. M. Toma, J. F. Rolin, C. Waldmann, and O. Zielinski

2014. Requirements and approaches for a more cost-efficient assessment of ocean waters and ecosystems, and fisheries management. In *2014 Oceans - St. John's*, Pp. 1–9. doi: 10.1109/OCEANS.2014.7003144.

Ralston, D. K. and M. T. Stacey

2006. Shear and turbulence production across subtidal channels. *Journal of Marine Research*, 64:147–171. doi: 10.1357/002224006776412359.

Reuter, R., T. H. Badewien, A. Bartholomä, A. Braun, A. Lübben, and J. Rullkötter

2009. A hydrographic time series station in the Wadden Sea (southern North Sea). *Ocean Dynamics*, 59:195–211. doi: 10.1007/s10236-009-0196-3.

Rippeth, T. P., N. R. Fisher, and J. H. Simpson

2001. The Cycle of Turbulent Dissipation in the Presence of Tidal Straining. *Journal of Physical Oceanography*, 31:2458–2471. doi: 10.1175/1520-0485(2001)031<2458:TCOTDI>2.0.CO;2.

Rippeth, T. P., J. H. Simpson, E. Williams, and M. E. Inall

2003. Measurement of the Rates of Production and Dissipation of Turbu-

lent Kinetic Energy in an Energetic Tidal Flow: Red Wharf Bay Revisited. *Journal of Physical Oceanography*, 33:1889–1901. doi: 10.1175/1520-0485(2003)033<1889:MOTROP>2.0.CO;2.

Rippeth, T. P., E. Williams, and J. H. Simpson
2002. Reynolds Stress and Turbulent Energy Production in a Tidal Channel. *Journal of Physical Oceanography*, 32:1242–1251. doi: 10.1175/1520-0485(2002)032<1242:RSATEP>2.0.CO;2.

Rullkötter, J.
2009. The back-barrier tidal flats in the southern North Sea - a multidisciplinary approach to reveal the main driving forces shaping the system. *Ocean Dynamics*, 59:157–165. doi: 10.1007/s10236-009-0197-2.

Schulz, A.-C., T. H. Badewien, S. P. Garaba, and O. Zielinski
2016. Acoustic and optical methods to infer water transparency at time series station spiekeroog, wadden sea. *Ocean Science*, 12(6):1155–1163. doi: 10.5194/os-12-1155-2016.

Schulz, A.-C., T. H. Badewien, and O. Zielinski
2015. Impact of currents and turbulence on turbidity dynamics at the time series station spiekeroog (wadden sea, southern north sea). In *2015 IEEE/OES Eleveth Current, Waves and Turbulence Measurement (CWTM)*, Pp. 1–6. doi: 10.1109/CWTM.2015.7098095.

Schulz, A.-C., T. H. Badewien, and O. Zielinski
2018. Assessment of turbulence patterns from non-high resolution data sets of current velocities. *Ocean Dynamics*. Submitted.

Sea & Sun Technology

n.d. CTD 48 | CTD 48 M, Online and Memory Probe. `http://www.sea-sun-tech.com/fileadmin/img/pdf_sea/CTD48.pdf`, state: 27.02.2018.

Sea-Bird Scientific
n.d. ECO FLNTU, Fluorometer and Scattering Meter (WET labs). `http://www.seabird.com/sites/default/files/documents/datasheet_ECO-FLNTU.pdf`, state: 27.02.2018.

Simpson, J. H., H. Burchard, N. R. Fisher, and T. P. Rippeth
2002. The semi-diurnal cycle of dissipation in a ROFI: model-measurement comparisons. *Continental Shelf Research*, 22:1615–1628. doi: 10.1016/S0278-4343(02)00025-0.

Simpson, J. H., N. R. Fisher, and P. Wiles
2004. Reynolds stress and TKE production in an estuary with a tidal bore. *Estuarine, Coastal and Shelf Science*, 60:619–627. doi: 10.1016/j.ecss.2004.03.006.

Stacey, M., J. R. Burau, and S. G. Monismith
2001. Creation of residual flows in a partially stratified estuary. *Journal of Geophysical Research: Oceans*, 106(C8):17013–17037. doi: 10.1029/2000JC000576.

Stanev, E. V., G. Brink-Spalink, and J.-O. Wolff
2007. Sediment dynamics in tidally dominated environments controlled by transport and turbulence: A case study for the East Frisian Wadden Sea. *Journal of Geophysical Research: Oceans*, 112:1–20. doi: 10.1029/2005JC003045.

Stanev, E. V., G. Flöser, and J.-O. Wolff
2003a. First- and higher-order dynamical controls on water exchanges between tidal basins and the open ocean. A case study in the East Frisian Wadden Sea. *Ocean Dynamics*, 53:146–165. doi: 10.1007/s10236-003-0029-8.

Stanev, E. V., G. Flöser, and J.-O. Wolff

2003b. On the circulation in the East Frisian Wadden Sea: numerical modeling and data analysis. *Ocean Dynamics*, 53:27–51. doi: 10.1007/s10236-002-0022-7.

Sutherland, T., P. Lane, C. Amos, and J. Downing

2000. The calibration of optical backscatter sensors for suspended sediment of varying darkness levels. *Marine Geology*, 162:587–597. doi: 10.1016/S0025-3227(99)00080-8.

Teledyne RD Instruments

n.d. Workhorse Sentinel, Self-Contained 1200, 600, 300kHz ADCP. `http://www.teledynemarine.com/Lists/Downloads/sentinel_datasheet_lr.pdf`, state: 27.02.2018.

Tennekes, H. and J. L. Lumley

1972. *A first course in Turbulence*. The MIT Press.

Thorne, P. D. and D. M. Hanes

2002. A review of acoustic measurement of small-scale sediment processes. *Continental Shelf Research*, 22:603–632. doi: 10.1016/S0278-4343(01)00101-7.

Thorne, P. D., C. E. Vincent, P. J. Hardcastle, S. Rehmann, and N. Pearson

1991. Measuring suspended sediment concentrations using acoustic backscatter devices. *Marine Geology*, 98:7–16. doi: 10.1016/0025-3227(91)90031-X.

TriOS

n.d. RAMSES, 40SXXX010. `http://www.trios.de/index.php?eID=tx_nawsecuredl&u=0&g=0&t=1519856767&hash=9f9f1133801a9be9d77dbdee0bf230b80c31fc6b&file=uploads/tx_cccascatalog/files/d02-010en201704_brochure_ramses.pdf`, state: 27.02.2018.

UNESCO World Heritage Center

2009. Description: Wadden sea. http://whc.unesco.org/en/list/1314, state: 23.02.2018.

van der Hout, C. M., T. Gerkema, J. J. Nauw, and H. Ridderinkhof

2015. Observations of a narrow zone of high suspended particulate matter (spm) concentrations along the dutch coast. *Continental Shelf Research*, 95:27 – 38. doi: 10.1016/j.csr.2015.01.002.

Voulgaris, G. and S. T. Meyers

2004. Temporal variability of hydrodynamics, sediment concentration and sediment settling velocity in a tidal creek. *Continental Shelf Research*, 24:1659–1683. doi: 10.1016/j.csr.2004.05.006.

Vousdoukas, M., S. Aleksiadis, C. Grenz, and R. Verney

2011. Comparisons of acoustic and optical sensors for suspended sediment concentration measurements under non-homogeneous solutions. *Journal of Coastal Research*, 64:160–164.

Wernand, M. R. and H. J. van der Woerd

2010. Spectral analysis of the Forel-Ule Ocean colour comparator scale. *Journal of the European Optical Society - Rapid Publications*, 5:10014s. doi: 10.2971/jeos.2010.10014s.

WFD

2000. European Water Framework Directive, Directive 2000/60/EC of the european parliament and of the council. *Official Journal of the European Union*, L327:1–72.

White, T. E.

1998. Status of measurement techniques for coastal sediment transport. *Coastal Engineering*, 35:17–45. doi: 10.1016/S0378-3839(98)00033-7.

Wiles, P. J., T. P. Rippeth, J. H. Simpson, and P. J. Hendricks
2006. A novel technique for measuring the rate of turbulent dissipation in the marine environment. *Geophysical Research Letters*, 33. doi: 10.1029/2006GL027050.

Winter, C., M. Becker, V. B. Ernstsen, D. Hebbeln, A. Port, A. Bartholomä, B. Flemming, and M. Lunau
2007. In-situ observation of aggregate dynamics in a tidal channel using acoustics, laser diffraction and optics. *Journal of Coastal Research*, 50:1173–1177. doi: 10013/epic.27648.

Zielinski, O., J. A. Busch, A. D. Cembella, K. L. Daly, J. Engelbrektsson, A. K. Hannides, and H. Schmidt
2009. Detecting marine hazardous substances and organisms: sensors for pollutants, toxins, and pathogens. *Ocean Science*, 5(3):329–349. doi: 10.5194/os-5-329-2009.

Acknowledgments